ABSTRACT

Studies on the neural networks and genes critical for feeding behaviors in *Drosophila melanogaster*

Soohong Min

Department of Biological Sciences

The Graduate School

Seoul National University

Although feeding is affected by multiple extrinsic and intrinsic stimuli, this behavior is primarily shaped by the two hard-wired motivational states – hunger and satiety. To expand our current understanding on the neuromolecular mechanism governing the states, I performed a genetic screen using a straightforward high-throughput feeding assay to identify novel genes and neurons critical for feeding regulation in *Drosophila*. By analyzing a library of 224 neuron-specific GAL4 drivers and 250 RNAi lines, I discovered two groups of anorexigenic neurons that showed striking

elevation of feeding when silenced, and identified a gene that affected feeding when knocked down. Silencing Myoinhibitory peptide (MIP) neurons and the corresponding gene, *mip*, elicited significant increases in body weight (BW) which could be completely restored by restriction of food intake, showing the tight correlation of BW and food intake regulated by MIP neurons. By contrast, activating MIP neurons markedly decreased food intake and BW, and the loss of food intake and BW was fully rescued shortly after termination of the neural activation indicating the switch-like role of MIP neurons in food intake BW regulation. By quantifying the levels of satiety using two behavioral paradigms upon silencing or activating MIP neurons, I revealed that indeed MIP neurons induce satiety to regulate food intake and ultimately BW. Another anorexigenic neuronal population marked by *48899-GAL4* displayed a series of hunger responses when silenced; indicating 48899 neurons normally induce satiety. Consistently, activating 48899 neurons reduced food intake. Among the neural structures labeled by *48899-GAL4*, the ellipsoid body (EB) subsets appeared to be critical for 48899-mediated feeding regulation. By analyzing the role of five serotonin receptors present in *Drosophila*, I found that the potential inhibitory role of 5-HT1A in 48899 neurons to regulate food intake. Lastly, I showed that the RNAi knockdown of *misato (mst)* elicited a dramatic hypophagia. Particularly, the intestine of the flies with the muscle-specific *mst* RNAi

knockdown showed characteristic enlargement followed by severe damages on the visceral muscle. However, these phenotypes were fully rescued by exogenous expression of *mst,* indicating the specificity of *mst* in the tight linkage between food intake and visceral muscle fidelity. Altogether these results demonstrated that feeding behaviors can be targeted by multiple neuromolecular entry points, and provided new insights into the understanding of animal feeding behaviors especially through satiety.

Keywords: feeding behavior, satiety/anorexigenic, MIP, BW, the EB, 5-HT receptors, Misato, visceral muscle

Student Number: 2012-30083

TABLE OF CONTENTS

List of Figures

List of Tables

Background

Background

I have always been fascinated by the diverse animal behaviors such as social interactions, reproduction, decision-making, sleeping and feeding behaviors and by that these behaviors are the ultimate outcome from the networking of genes and neurons' function which means we can identify sets of genes and neurons dedicated for these behaviors. With the recent technical advances in manipulating neuronal activity, researchers have shown that a defined neuronal pathway dictates a behavior such as the avoidance behavior elicited by the optogenetic activation of a group of olfactory receptor neurons expressing a member of G protein-coupled receptors (GPCRs) specialized for sensing carbon dioxide in *Drosophila* and mice (Hu et al., 2007; Suh et al., 2007; Suh et al., 2004). More strikingly, motivation-driven behaviors could be evoked by the activation of a subpopulation of D2 dopamine receptor-expressing neurons in mice (Soares-Cunha et al., 2016), suggesting the pools of hard-wired circuits involving the genes and neurons dedicated for certain behaviors. Among the behaviors, the feeding behaviors have particularly been interesting to me because they are primarily controlled by the two hard-wired motivational states, hunger and satiety, even though the behaviors are diverse and complex needing the appropriate coordination of various sensory modalities and motor outputs toward food source.

Clinically, hunger and satiety are profoundly related to feeding-related disorders such as hyperphagia and anorexia and often associated with metabolic syndromes including the obesity when these motivational states are abnormally controlled. The worldwide prevalence of the obesity further alarms us to be comprehensive in the understanding of the neuromolecular mechanisms underlying hunger and satiety.

The turning point for studying hunger and satiety is the finding of the nuclei and corresponding genes that control appetite in the brain. The arcuate nucleus of the hypothalamus (ARH) is comprised of the orexigenic agouti-related peptide (AgRP)/ neuropeptide Y (NPY) neurons and the anorexigenic pro-opiomelanocortin (POMC) neurons **(Fig. 1)**. Stimulation of AgRP/NPY neurons provokes hunger to increase feeding (Kaushik et al., 2011; Ren et al., 2012). Ghrelin, another orexigenic hormone produced from the gastrointestinal tract is known to stimulate the AgRP/NPY neurons to promote feeding (Gillard et al., 2016; Rezaie et al., 2015; Shrestha et al., 2006). By contrast, the pro-opiomelanocortin (POMC)-expressing neurons suppress feeding stimulated by the anorexigenic hormones such as leptin (Yaswen et al., 1999). Genetic ablation of POMC neurons markedly elevates both food intake and body weight (Mineur et al., 2011; Zhan et al., 2013). Especially, Leptin produced from the adipose tissue acting on the ARH

inhibits the AgRP neurons, but activates the POMC neurons to suppress Feeding (Baver et al., 2014; Cowley et al., 2001; Morrison et al., 2005; Ren et al., 2015; Swart et al., 2002). Genetic disruption of the gene encoding Leptin/Obese in mice produced the well-known *ob/ob* phenotype associated with profoundly increased food intake (Friedman, 2014, 2015; Friedman and Halaas, 1998; Zhang et al., 1994).

To further expand our understanding on feeding regulation in animals, we need to choose the appropriate model system for studying the behavior. *Drosophila* is an amenable model organism to study feeding behaviors benefit from its simplicity of neural system. Taking advantage of plenty of genetic tools available, manipulation of individual subset of neurons that may be related to feeding behavior could be easily achieved. For example, using GAL4-UAS system where GAL4 binds to UAS sequence to express the downstream neural silencer or activator, I could control the activity of a specific neuron by combining a neuron-specific GAL4 driver with the UAS transgene in the flies (Klueg et al., 2002). Not only the simplicity of neural system but also the conservation of various aspects of neuromolecular, anatomical and behavioral components in feeding behaviors makes this model organism attractive for studying feeding behaviors.

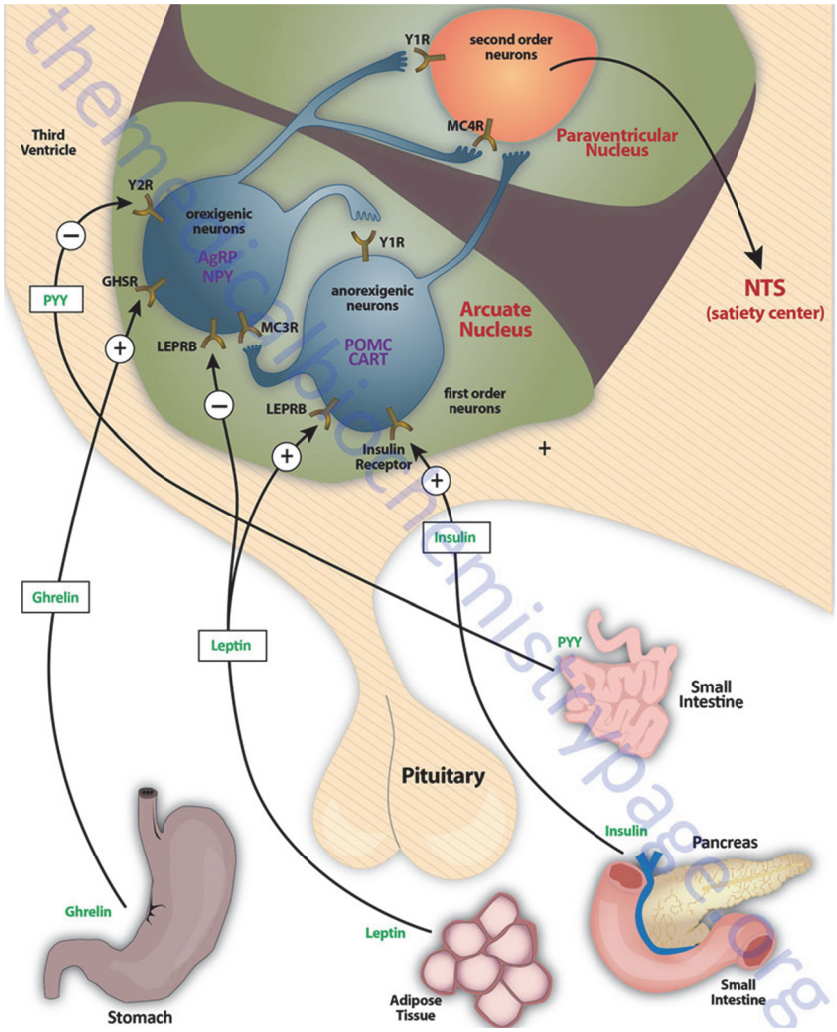

Figure 1. The hypothalamic control of the hunger and satiety (image adopted from http://themedicalbiochemistrypage.org/gut-brain.php). The orexigenic AgRP neurons are positively stimulated by Ghrelin and inhibited by PYY and Leptin, in contrast to the anorexigenic POMC neurons stimulated by Leptin and Insulin from the peripheral tissues such as adipose tissue, small intestine, pancreas and the stomach to regulate food intake.

In *Drosophila*, several feeding regulators have been identified including the vertebrate NPY homologs, neuropeptide F (NPF) and short neuropeptide F (sNPF), the key players for orexigenic control in feeding (Hong et al., 2012; Lee et al., 2004; Wu et al., 2003). Overexpression of NPF prolonged larval feeding and the expression level of NPF showed a positive correlation with the feeding behavior (Wu et al., 2003). Likewise, upregulation of sNPF pathway in the adult promoted food intake, but downregulation of it decreased food intake (Lee et al., 2004). Recently, a subpopulation of serotonergic neurons in the brain has been shown to elicit a series of hunger-driven behaviors in *Drosophila* (Albin et al., 2015). Despite the clear structural and functional parallel observed between the vertebrate NPY and the insect NPF signaling systems, a system analogous to the vertebrate POMC system has yet to be identified in insect models such as *Drosophila*.

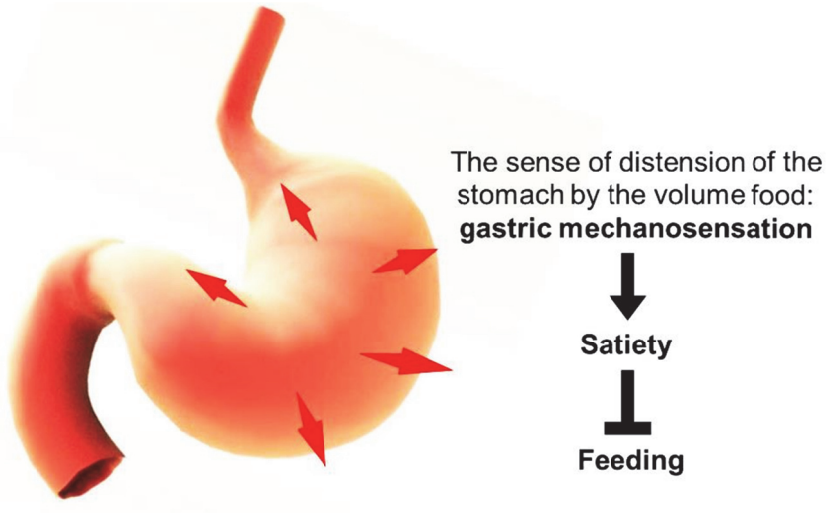

Figure 2. The illustration of satiety induced by gastric mechanosensation. The distention of the stomach by the ingested food induces mechanical force that is conveyed as "satiety", and thus this satiety signal inhibits feeding.

From this ground, I decided to dedicate my Ph.D. study on the identification of such system critical for regulation of feeding behaviors – especially on satiety using *Drosophila*. People have believed that satiety signal originates from the mechanical distention of the stomach after a meal, called "gastric mechanosensation" **(Fig. 2)**. To test the theory, they performed interesting experiments where a balloon was inserted in the stomach of animals for the artificial distention to examine whether the artificial distention induces satiety via the gastric mechanosensation. Remarkably, they indeed observed the increased mechanical responses in the sensory nerves innervating the stomach and enhanced physiological responses in the hypothalamus upon the artificial distension of the stomach (Anand and Pillai, 1967; Paintal, 1954). In consistence with the observations, the sham feeding condition where a dog with the esophagus disconnected from the stomach by the surgery allowing ingested food to bypass the stomach still elicited decreased food intake upon the artificial distention of the stomach using the inserted balloon (Towbin, 1949) **(Fig. 3)**. Supporting this, the amputation of the sensory nerve innervating the stomach eliminated the decrease of food intake (Towbin, 1949). Likewise, Dethier et al. showed that the section of the recurrent nerve coming from the foregut produced hyperphagic symptom in the blow fly (Dethier, 1967). These data suggest the potential role of gastric mechanosenstion in signaling satiety.

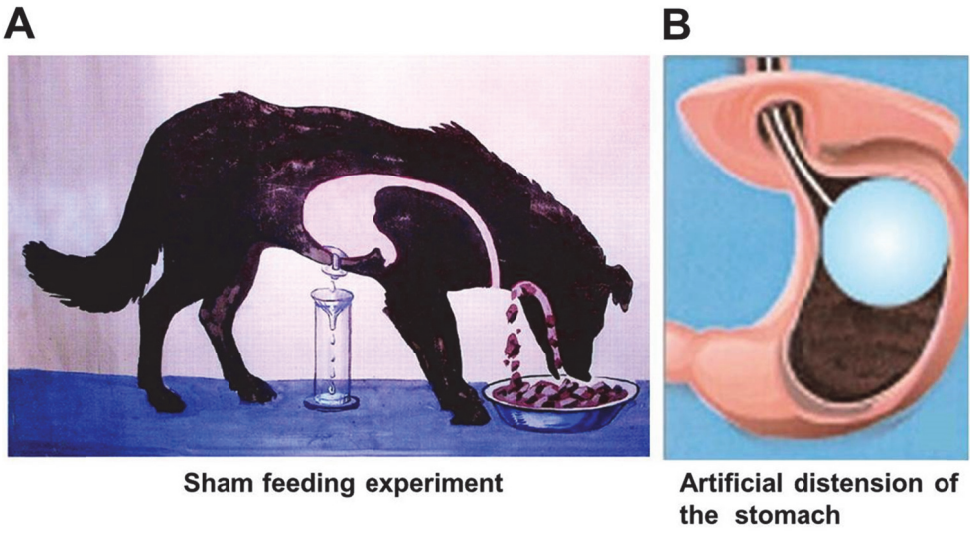

Figure 3. The illustration of sham feeding condition and artificial distention of the stomach using a balloon (Images adopted from the ref. (Wood, 2004) and https://www.weightlosssurgerydubai.com/gastric-balloon-dubai/). (A) The dog with the esophagus disconnected from the stomach and exposed to outside by a surgical operation consumes the food, but it cannot enter the stomach. This experiment uncouples the effect by the distention of the stomach from that by ingestion of food. **(B)** A balloon is inserted into the stomach to achieve the mimicry of the distention of the stomach by food.

Initially, to find such satiety signaling system conserved in *Drosophila*, I sought to identify the recurrent nerves and indeed found a pair of nerves innervating the stomach of *Drosophila* **(Fig. 4)**. Remarkably, however, section of these nerves did not affect the voluntary movement of the stomach, implicating the role of these nerves other than the stomach movement **(Fig. 5)**. To further characterize the molecular identity of the neurons, I paid first attention to the ion channels that are known to detect mechanical stimuli such as the transient receptor potential (TRP) and degenerin/epithelial sodium channels (DEG/ENaC) (Geffeney and Goodman, 2012). Thus, I examined their expression patterns in the stomach or recurrent nerves, and checked the alteration of food intake upon manipulation of the activity of the genes and the corresponding neurons.

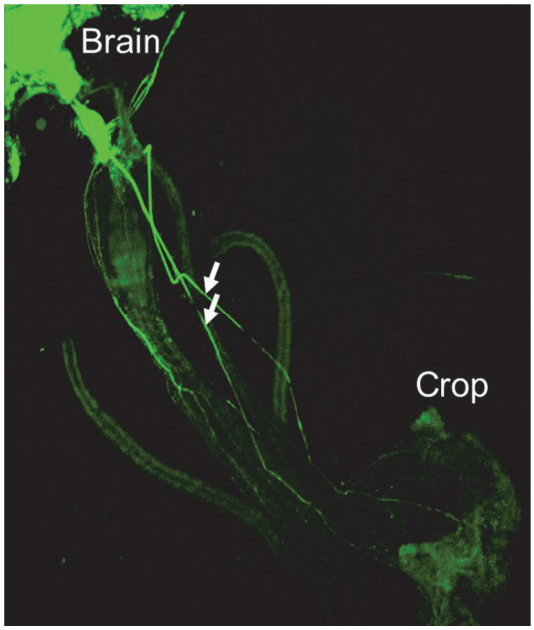

Figure 4. The recurrent nerves innervating the fly stomach. The recurrent nerves are visualized by mCD8GFP expression driven by *Appl-GAL4* driver. Arrows indicate the recurrent nerve innervating the fly stomach (crop).

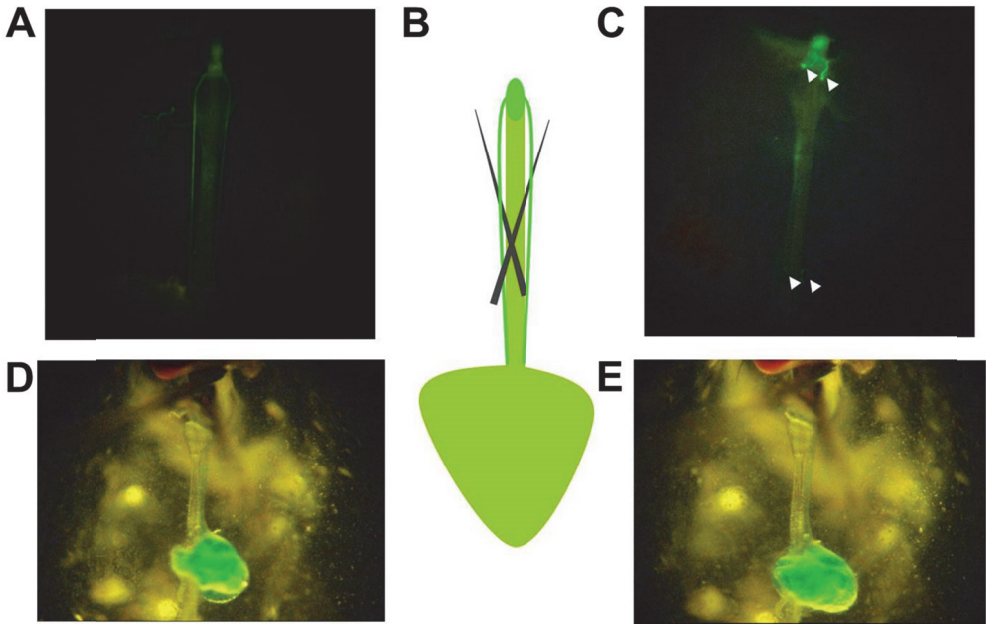

Figure 5. The section of the recurrent nerves innervating the fly stomach did not affect the movement of the stomach. (A) The recurrent nerves were visualized by mCD8GFP expression driven by *Appl-GAL4* driver. **(B)** The nerves were surgically cut by the forceps as illustrated in the middle. **(C)** Arrowheads indicate the remnants of the recurrent nerve cut by the surgery. **(D, E)** The voluntary movement of the fly stomach was observed *in vivo* before and after the surgery.

Although I failed to find a strong correlation between these ion channels and food intake based on the results from these functional studies on them, there is still a possibility that other types of sensors are involved in regulation of food intake by the gastric mechanosensation. For example, a group of peptidergic cells secretes a satiety factor in response to gastric distention or a population of mechanosensory neurons innervating elsewhere in the gastrointestinal tract other than the stomach signals satiety. Indeed, a recent study demonstrated that PPK1 (Pickpocket 1), a member of the epithelial sodium channel family in *Drosophila*, functions in the posterior enteric neurons to negatively control the level of food intake (Olds and Xu, 2014). Taken lessons from these preliminary experiments, I decided to perform a large scale feeding screen to identify candidate genes and neurons involved in regulation of food intake especially through controlling satiety.

In my Ph.D. study, I developed a reliable high-throughput feeding assay and performed a genetic screen on a collection of GAL4 driver and RNAi lines. From the screen, I identified two neuronal GAL4 lines that elicited dramatic hyperphagic phenotypes when silenced and an RNAi line that showed severe hypophagic symptom appeared to be associated with disrupted intestine homeostasis. In Part 1 of my Ph.D. dissertation, I describe

the identification of candidate neurons and genes that affect feeding from a genetic screen using a high-throughput feeding assay. In Part 2, I describe the characterization of myoinhibitory peptide-expressing neurons in regulation of satiety to maintain body weight. In Part 3, I describe the characterization of neurophysiological and molecular mechanism underlying 48899 neuron-mediated feeding control. In Part 4, I describe the identification and characterization of the role of *misato* in the *Drosophila* intestine.

Materials and Methods

Materials and Methods

Fly Stocks

All the fly stocks were maintained on a standard cornmeal agar food containing dextrose 1,260 g, cornmeal 635 g, agar 91 g, yeast 900 g, propionic acid 84 ml, and tegosept 132 ml in 18 L of food manufactured by KAIST *Drosophila* Library Facility, Korea. Detailed information on the JF-GAL4 lines in the study can be found in the database of Bloomington *Drosophila* Stock Center (BDSC). Other fly lines used in this study were following: *UAS-TNT* (Sweeney et al., 1995), *UAS-impTNT* (Sweeney et al., 1995), *nSyb-GAL80* (Julie Simpson, Janelia Farm, USA), *UAS-mCD8GFP* (BDSC No. 5137), *nSyb-GAL80* (Julie Simpson, Janelia Farm, USA), *Cha-GAL80* (Sakai et al., 2009), *UAS-TRPA1* (Hamada et al., 2008), EB-subset specific GAL4 line (Renn et al., 1999). Fly lines used in this study were following: *Tub-GAL80^{ts}* (Ron Davis, Scripps research institute, USA), *UAS-TNT* (Sweeney et al., 1995), *UAS-impTNT* (Sweeney et al., 1995), *nSyb-GAL80* (Julie Simpson, Janelia Farm, USA). SPR mutant (*spr$^{-/-}$*) (Yapici et al., 2008). Among 24 neuromodulator specific-*GAL4* lines used in the initial screening, 16 *GAL4* lines are generated in this study. Unless stated otherwise, *GAL4* transgenes generated in this study were prepared in pAGAL4, and

inserted into a specific site of second chromosome (VIE-72A, a gift from B. J. Dickson, Janelia Farm, USA) using ΦC31 system (Groth et al., 2004). pAGAL4 is prepared by inserting a site-specific integration site (attB) into 7-74 site of pPTGAL4(+) vector (Sharma et al., 2002). *MIP-GAL4* and *Kinin-GAL4* were prepared in pPTGAL4(+) and inserted into the second chromosome using conventional p-element transgenesis. Following neuropeptide-GAL4 lines are obtained from either published or unpublished sources; *Akh-GAL4* (Lee and Park, 2004), *Burs-GAL4* (a gift from J. H. Park, University of Tennessee, USA), *Crz-GAL4* (Choi et al., 2006), *Ilp2-GAL4* (Rulifson et al., 2002), *Hugin-GAL4* (Melcher and Pankratz, 2005), *Npf-GAL4* (Wu et al., 2003), *Pdf-GAL4* (Renn et al., 1999), *SIFa-GAL4* (Terhzaz et al., 2007), and *FMRF-GAL4* (Suster and Sung et al., 2003). *ETH-GAL4* crossed to *UAS-TNT* produced lethal phenotype.

Generation of *mip* mutant

To generate mip^1, I employed ends-out homologous recombination. Briefly, PCR-amplified homology arms were cloned into pw35 vector (Gong and Golic, 2003). Primers listed below are used for amplification of homology arms; left homology arm (5'-gcggccgcaaaattgcgattgatatattaatc-3', 5'-gcatgcagctgtggaaatgttaaattaaaaa-3'), right homology arm (5'-

ggtacctcgcagagaatcgccgtagcac-3', -ggtaccttaatcagttcccgcctatttagc-3'). Targeting construct was integrated into genome by germ-line transformation. The targeting construct was excised by crossing transformants with *FLP*, *I-SceI* flies (Bloomington stock No. 6934). Individual mosaic eyed flies (F1) were collected and crossed with w^{1118}. Each red eyed flies (F2) was crossed to Df(3L)BSC432 (Bloomington stock No. 24936). F3 progenies were subjected to PCR analysis to confirm the deletion using the following primer pairs (5'-TCCACAGCTATGGCTCACAC-3' and 5'- GCCTGCGAGATCAT CGAAAT-3').

Measurement of body weight

F1 flies were 5-10 males bearing a neuropeptide-GAL4 transgene and less than 30 virgin females carrying *UAS-TNT* crossed in a fly bottle. They were transferred into a new bottle every 3-4 day depending on the status of crowdedness. This step is critical for the analysis, because the body size of the progenies (F2) vary upon crowdedness. It is important to keep the number of the parents similar in the bottle for control and experimental groups. F2 flies were collected after eclosion. F2 males and females were sorted into vials in groups of 15 individuals under CO_2 anesthesia. The flies were then aged until 5-8 days. For measuring BW, I used a precision

weighing balance (Satorius, BP221S). 3-5 flies were put in a 1.5 ml microtube and measured the weight of the tube containing the flies following the blanking the weight of tube. The BW of a single fly was calculated by the equation: The weight of flies in the tube/ the number of flies in the tube.

Food intake assay

Prior to testing, twelve flies in a vial were starved for 18 hours with water and on the next day the starved flies were fed on food consisting of 10% sucrose + 5% active yeast in 0.5% green dye solution for 30 minutes. The fed flies were anesthetized on ice to immediately cease feeding and their colored-stomach was imaged using a digital camera through the optical lens of common light microscope. The amount of feeding was scored by the visual inspection of the volume of colored-food ingested in flies' stomach. The score was as the following: 0ul (no-feeding)/ 0.1ul/ 0.25ul/ 0.5ul/ 1ul (excessive feeding). Satiated flies in this study refer to the flies that were provided with *ad libitum* on the standard cornmeal agar food. The fly instant food was made by the following: food powder (66-117, Genesee Scientific) 0.8g in 3ml water.

For measuring food intake for 12 or 24 hours, the CAFÉ assay was used as previously described (Ja et al., 2007). with some modifications: Two

capillaries filled with 5 μl of food solution (5% sucrose + 1% yeast extract (REF#212750, Becton, Dickinson and Company) were provided to 4 flies housed in a vial. For water supply, 1% agar medium was placed on the bottom of vial. Flies were put into the tube with an oral aspirator without CO_2 anesthetization.

For measuring the % flies fed, twenty flies housed in a group were put in a vial containing colored food and provided given time of period for feeding: 1/5/10/20/30 minutes. After each period, the % of flies that ate was calculated by the equation, the number of fed flies/ total number of flies.

For assaying food intake on D-glucose versus L-glucose, 10% D-glucose (G8270, Sigma) and L-glucose (G5500, Sigma) mixed with 0.5% green dye solution were provided for 30 minutes. Before comparing the levels of food intake on these sugars, I measured the frequencies of PER by WT flies to D-glucose and L-glucose to make sure that flies sense these sugars with the same degree of sweetness. To ensure that D-glucose is metabolizable and thus produces energy to survive the starvation conditions, but L-glucose is a non-metabolizable sugar that yields no energy to survive the starvation conditions, I measured survival rate of WT flies in the presence of water only, L-glucose, D-glucose ad sucrose (All the sugars were 10%). flies supplied with sucrose and D-glucose indeed survived the periods

of starvation in contrast the flies provided with water or L-glucose died earlier at similar rate.

Survival rate was measured by calculating the fraction of the dead flies over total number of flies at each time point in the presence of the solutions.

Video recording of food intake

A fly was put into a 200 μl tip using an oral aspirator and its head and proboscis were exposed by notching the tip end. The tip containing the fly was immobilized on an array of clay and placed under a light microscope. To record the video, a digital camera (Canon Powershot, A450) was fixed on the optical lens of the microscope. Immediately before the recording, food solution was dropped by its proboscis without drowning it. The recorded video was edited using Camtasia Studio (TechSmith) program.

Behavioral testing for preference to food odors

Twenty-five flies aged 10-14 days were sorted into a fly vial with food under CO_2 anesthesia. Prior to testing, the flies were starved for 18 hours in the presence of water provided by wet paper. Food odor was prepared as the

following: 10% sucrose + 5% active yeast in water. The food odor and water as control were absorbed into a piece of 0.5 cm X 0.5 cm filter paper and placed in testing tubes (The common 14 ml round-bottom bacteria culture tube). The tubes containing food odors were tightly sealed with parafilm and let stand for 10 minutes for pervading of odors in the tube before testing. The starved flies were let accommodated in the testing room for 1 hour. For testing, flies were tapped into a T-maze and trapped in an elevator. The tubes containing food odors and water were armed into each side of the T-maze and by pushing down the elevator flies were given a choice between the two tubes containing food odors and water for 2 minutes. The side of the armed tubes was changed for every trial to control possible positional biases. For the activation experiment using TRPA1, the testing room was set at 30-32°C with 40% humidity. Attraction (preference) index was calculated by the equation: (the number of flies in the food odor side – the number of flies in the water side) / the total number of flies in the both sides.

PER assay

The assay was performed as previously described (Dus et al., 2011) with some modifications. Food solution was 2% yeast extract in 10% sucrose solution with 0.5% green dye (McCormick). Before testing, all the flies were

kept at 18°C and either *ad libitum*-fed on the standard fly food for satiated condition or starved for 18 hours for starved condition. Starvation was achieved by providing only water to the flies in a fly vial containing wet kimwipe. For neuronal activation using TRPA1, the testing room was set at 30-32°C with 40% humidity.

Nile red staining on abdomens

Whole flies were fixed in a fixative (4% paraformaldehyde in 0.1% PBST) on an orbital mixer at room temperature (RT) for 3 hours. Flies were then washed 3 times in 1X PBS for 5 minutes. Abdomens were carefully dissected in 1X PBS to keep fat tissue intact with the gut and reproductive organs eliminated. If necessary, the dissected abdomens were fixed again for 20 minutes in 4% paraformaldehyde solution and washed 3 times in 1X PBS for 5 minutes. Nile red solution (0.5 mg/ml, Sigma) was added to the tube containing abdomens at 1:500 dilutions, and the abdomens were incubated in the solution for 30 minutes. Abdomens were washed 3 times in 1X PBS for 5 minutes and then mounted on a slide glass with 80% PBG (80% glycerol in 1X PBS).

Fly crop dissection

Flies subjected to the *ad libitum* feeding condition on fly instant food were under CO_2 anesthetization. Briefly, a fly was immobilized on a silicon plate using insect pins (Fine Science Tools; #26002–10) and its legs and wings were removed under a dissecting microscope. The cuticle of the thorax and abdomen was peeled off in PBS using fine tweezers (Fine Science Tools; #11251–20) to expose the crop. Images were taken with the digital camera.

Immunohistochemistry on the fly tissues

Flies aged 4-5 days were fixed by 4% paraformaldehyde (PFA) in 0.1 % PBST for 3 hours at room temperature (RT) and the fixed whole fly was then dissected for the tissues out in PBS. The dissected tissues were incubated in 0.5% PBST for 5 minutes at RT for permeablization for the efficient antibody absorption and washed in 0.1% PBST 3 times for 5 minutes at RT. As a blocking step, the brains were incubated in 3% bovine serum albumin (BSA) in 0.1% PBST for 20 minutes at RT. The primary antibodies were treated directly in the blocking solution and the brains with the antibodies were incubated overnight at 4**°C**. The primary antibodies were as the following: rabbit anti-GFP (1:1000; A11122, Invitrogen) and mouse anti-DH44 (kind gift from Jan A. Veenstra, Bordeaux University, France). On

the next day, the brains were washed in 0.1% PBST 3 times for 5 minutes and the secondary antibodies were treated to the brains in 3% BSA in 0.1% PBST. Secondary antibodies were as the following: Alexa 488-conjugated goat anti-rabbit (A11008, Invitrogen), anti-mouse TRITC (115-026-062, Jackson ImmunoResearch).

Statistical analysis

The statistical analysis was performed for all the BW and feeding experiments using Graphpad prism program. P values were calculated either by the unpaired *t*-test for comparison of two columns of data or ANOVA test for comparisons of multiple columns of data and groups of data. Asterisks indicate following: *, $p < 0.05$; **, $p < 0.005$; ***, $p < 0.0005$. All the experiments were performed more than three times at least.

Bromodeoxyuridine (BrDU) staining

~30 newly-born flies were collected and reared in a vial containing a piece of filter paper at the bottom wet with BrdU solution at the concentration of 0.1mg/ml in 5% glucose. After 3 days of feeding, the intestine of the flies were dissected in PBS and fixed in 4% PFA at RT for

30 minutes. The fixed intestine was washed 3 times with 0.1% PBST (0.1% triton X-100 in PBS) and incubated in 200 µl of DNAse I solution containing 20µl of 10X DNase I buffer, 20 µl of DNase I (1 unit), 160 µl of PBS at 37°C for 2 hours. The solution containing the intestine was tapped several times during incubation. After incubation, the tissue was washed 2 times by 0.1% PBST and permeabilized in 0.5% PBST for 5minutes followed by washing by 0.1% PBST a time. The intestine was blocked with 3% bovine serum albumin (BSA) in 0.1% PBST for 1 hour at RT and incubated with the primary antibody against BrdU (1:100, anti-rat, Abcam, ab6326) at 4°C overnight. On the next day, the tissue was washed 3 times by 0.1% PBST and incubated with the secondary antibody (anti-rat FITC Alexa Fluor, 1:200) for 2 hours at RT. The tissue then was washed 3 times with 0.1% PBST and 2 times with PBS, and mounted for imaging.

TUNEL assay

Fly intestines were dissected in PBS and fixed with 4% PFA for 30 minutes at RT. The fixed intestines were washed and permeabilized by 0.5% PBST 2 times for 10 minutes and washed 1 time by 0.1% PBST for 10 minutes. The tissues were incubated in 0.1 % sodium citrate in 0.1% PBST for 30 minutes at 65°C. After washing by PBS 2 times for 10 minutes, the

tissues were incubated in the TUNEL reaction (2 μl of TUNEL enzyme + 10 μl of 10X TUNEL buffer) for 2 hours at 37°C. After incubation, the tissues were blocked in 3 % BSA in 0.1% PBST for 30 minutes and incubated with phalloidin-TRITC at 1:200 and Hoechst at 1:200 for 2 hours at RT. After 3 times of washing by 0.1% PBST for 5 minutes and 2 times by PBS for 5 minutes, the stained tissues were mounted for imaging.

Results

PART 1

A genetic screen identified candidate neurons and genes critical for food intake using a high-throughput feeding assay

Introduction

In 2008, Gerald Rubin and his coworkers in Janelia Farm (JF) claimed to generate GAL4 driver lines that cover all the neural system in *Drosophila* and analyzed their expression patterns for public (Pfeiffer et al., 2008). This project released publicly available neuron-specific GAL4 driver lines that are now deposited in the Bloomington *Drosophila* Stock Center (BDSC). Individual GAL4 lines showed fairly specific labeling of neurons so that it became feasible to manipulate the activity of a subset of neurons **(Fig. 6).** Also good thing about the JF-GAL4 is that these lines are made of the defined fragment from a gene so that the expression pattern is more restricted compared to the conventional enhancer trap GAL4 lines the linkage between the neuron and the gene can be easily examined.

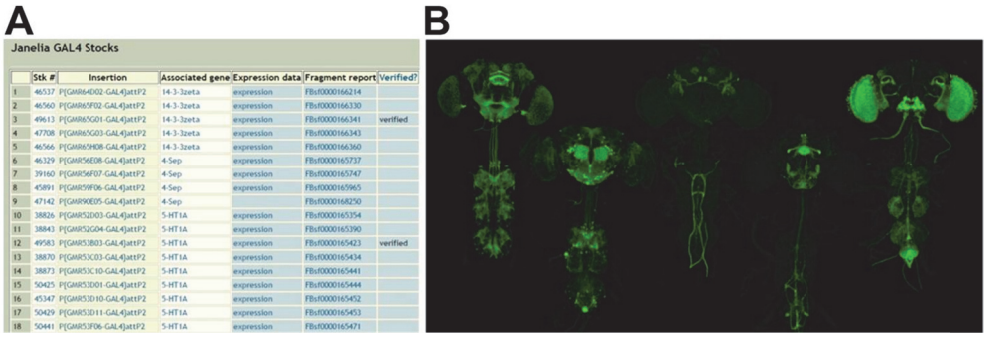

Figure 6. JF-GAL4 lines are available from BDSC to manipulate the activity of neurons (Images adopted from the BDSC website). (A) The glimpse image of the list of JF-GAL4 lines in the BDSC webpage. **(B)** Images of the CNS visualized by a set of JF-GAL4 lines. Note the characteristic expression patterns with specificity.

To identify a set of neurons and genes that regulate food intake, I sought to establish a screen pool comprised of ~200 JF-GAL4 **(Table 1)** and ~24 neuropeptide gene-fused GAL4 lines **(Table 2)** in addition to a library of 250 RNAi lines **(Table 3)** that had been obtained from bioinformatics searches by my coworkers on mitochondrial genes presumably expressed in the outer membrane. Since mitochondria function critically in cells by generating energy, I conceived that the mitochondrial outer membrane (MOM) genes act as an energy sensor in a specific locus *in vivo* monitoring internal energy level to direct food intake. In support with view, it has been reported that the mitochondrial fusion and fission process is sensitive to internal insulin and glucose levels and the mitochondrial dynamics in the hypothalamus involving Mitofusins (Mfn) functions critically in food intake in mice (Dietrich et al., 2013), suggesting the potential role of mitochondrial genes in feeding regulation.

In this chapter, I describe the establishment of a reliable high-throughput feeding assay, a collection of GAL4 and RNAi lines and the identification of two GAL4 lines and an RNAi lines that showed significant feeding alterations from a genetic screen on the collection using the feeding assay.

Table 1. The list of JF-GAL4 lines used in this study.

24903 [b]	46884	47613	47895	48868	48899 [a]	48945	48989
27894 [b]	46885	47621	47896	48869	48900	48946	48992
36359 [b]	46903	47623	47897	48870	48901	48947	48997
36360 [b]	46908	47626	47898	48871	48902	48948	48998
36361 [b]	46545	47634	47899	48873	48903	48950	48999
36362 [b]	46546	47638	47902	48874	48904	48951	49000
45110	46547	47640	47904	48875	48905	48952	49002
45112	46548	47641	47905	48876	48906	48953	49004
45113	46550 [a]	47645	48842	48878	48907	48955	49005
45114	46554	47652	48845	48879	48908	48956	49006
45117	46965	47657	48846	48880	48909	48961	49008
45836	46968	47659	48852	48882	48910	48962	49010
45901	46973	47670	48854	48883	48911	48963	49011
46080	47500	47673	48855	48884	48912	48964	49012
46161	47501	47687	48856	48885	48913	48967	49013
46162	47503	47697	48858	48886	48914	48968	49014
46163	47519	47699	48859	48887	48915	48970	49017
46167	47521	47700	48860	48888	48916	48971	49022
46556	47523	47701	48861	48889	48917	48973	49023
46677	47524	47703	48862	48890	48919	48976	49025
46859	47498	47704	48863	48892	48939	48978	49028
46860 [a]	47499	47707	48864	48894	48940	48979	49029
46864	47568	47712	48865	48895	48941	48980	49031
46882	47606	47713	48866	48896	48942	48985	49032
46883	47607	47894	48867	48898	48943	48986	49034

- Lines color-coded with magenta showed hyperphagia, whereas the lines marked with blue displayed hypophagia when crossed to *UAS-TNT*.

a. Lines that label the EB neurons.

b. Lines comprised of TRP channels.

Table 2. The neuropeptide GAL4 lines used in this study.

Peptide gene (CG number)	Forward primer*	Reverse primer*	Genomic fragments **
Myoinhibitory peptide, Mip (CG6456)	ctccagtttctccgcacaat	gcaccatcagaaagccgtaa	-7173 to +46
Allatostatin C, AstC (CG14919)	tata**gcggccgc**tttccacgaatgctatgcaa	gcgcgc**tctaga**tactcaccggtcctgtttcg	-5273 to +106
Akh-GAL4 (Lee and Park, 2004)	-	-	-
Npf-GAL4 (Wu et al., 2003)	-	-	-
Prothoracicotropic hormone, ptth(CG13687)	tata**gcggccgc**tgaaacggaaatgtcatcca	gcgcgc**tctaga**gaccagcgctgtactccttc	-510 to +46
Crz-GAL4 (Choi et al., 2006)	-	-	-
Insulin-like peptide 4, Ilp4 (CG6736)	tata**gcggccgc**tggtcgagcgacaaaaataa	gcgcgc**tctaga**agcgccagtcccagtctaat	-317 to +29
SIFa-GAL4 (Terhzaz et al., 2007)	-	-	-
FMRF-GAL4 (Suster et al., 2003)	-	-	-
Hugin-GAL4 (Melcher and Pankratz, 2005)	-	-	-
Drosokinin, (CG13480)	c**ggatcc**tgaggaaggaaacagcaagc	c**ggatcc**gctggctccatagacttgac	-3277 to +63
Pdf-GAL4(Renn et al., 1999b)	-	-	-
Allatostatin, AstA (CG13633)	tata**gcggccgc**tttcggtgggaagttagtgc	gcgcgc**tctaga**tgtacatataggcccgtcgtc	-5168 to +214
Insulin-like peptide 6, Ilp6 (CG14049)	tata**gcggccgc**cacttgctcgattttccaca	gcgcgc**tctaga**gtcggcactttgagaaccat	-1709 to +20
ion transport peptide, itp (CG13586)	tata**gcggccgc**gtccaaccaaaaacgacact	gcgcgc**tctaga**ggatgcttatcgctggttgt	-3112 to +44
Ilp2-GAL4(Rulifson et al., 2002)	-	-	-
Capability, capa (CG15520)	tata**gcggccgc**gcggaatccactttcatagc	gcgcgc**tctaga**actgaattcggcgattatga	-335 to +57
Dh44-GAL4 (Lee et al., 2015)	-	-	-
Neuropeptide-like precursor 1, Nplp1 (CG3441)	tata**gcggccgc**cccacagcgatttgctttac	gcgcgc**tctaga**ggagagcaacagcattagcc	-1431 to +57
Drosulfakinin, Dsk, (CG18090)	tata**gcggccgc**cgttcagaatgtaggcaacg	gcgcgc**tctaga**cagaaggctaatgcccagag	-1355 to +65

Proctolin, Proct (CG7105)	tata**gcggccgc**cccact aaaacccgcagtaa	tagcgc**ggtacc**accg tcatccaaaccaagag	-1385 to +77
Bursicon, burs (CG13419)	cc**tctaga**gattgccgtg gtcgtgc	gcgaattcgtcggcccg actgcgagt	-222 to -1
Orchokinin-GAL4 (Chen et al., 2015)	-	-	-
*Ecdysis Triggering Hormone, ETH (CG18105)****	tata**gcggccgc**gcattta catacgcaagtggt	gcgcgc**tctaga**cacc aagagcgaaacagaca	-263 to +39

* Primer sequences with underlines indicate the genomic region used for PCR amplification and bolded sequences denote the restriction enzyme sites.

** +1 indicates the translation start site of the first coding exon.

*** *ETH-GAL4* crossed with *UAS-TNT* yielded no progeny.

Table 3. The UAS-RNAi lines used in this study.

NIG	NIG	VDRC	TRiP (BDSC)
10007R-2	HMJ22586	1407	26005
10575R-2	HMJ22637	2507	26007
1134R-2	HMJ22736	5474	27083
12338R-1	HMJ23188	7018	27270
12397R-2	HMJ23203	7716	27307
13072R-1	HMJ23571	9049	27695
13570R-1	HMJ23820	13177	28306
1424R-1	HMJ23874	15886	28787
14690R-1	HMJ23990	16383	29573
14777R-3	HMJ24095	19125	**29601**
17870R-1	HMJ30028	19202	29608
17991R-1	HMJ30181	21054	31038
2022R-2	HMS00063	25640	31157
2163R-1	HMS00152	27680	31170
2621R-1	HMS00553	28533	31253
3016R-1	HMS00777	33207	31767
31722R-1	HMS00797	33309	33046
31873R-2	HMS00899	35337	33742
3210R-3	HMS01088	36006	33749
3434R-2	HMS01230	38460	34364
4006R-1	HMS01285	40148	35155
4209R-2	HMS01541	41269	35227
4623R-1	HMS01578	41644	35376
5047R-2	HMS02039	42113	35663
5662R-1	HMS02760	42439	35671
5685R-1	HMS03002	43115	35672
6235R-1	HMC02390	44400	35697
6756R-1	HMC03036	44969	35742
6870R-3	HMC03230	45130	35796
7436R-1	HMJ21250	46573	37499

7486R-1	HMJ21284	46870	38262
7654R-3	HMJ21422	47109	38325
8004R-3	HMJ21529	47154	38971
9819R-1	HMJ21554	47331	42639
9834R-3	HMJ21697	47988	43966
9842R-1	HMJ22270	52570	43973
GL00277		100931	50591
GL00366		101418	51690
		103445	53284
		106072	54835
		106356	55189
		106422	55679
		106470	57379
		107412	57404
		107429	57486
		110385	57535
		110422	57779
		110616	60090

* Bolded lines are against Misato.

Developing a high-throughput feeding assay

In need of a high-throughput feeding assay to screen all the collections within a time period, I developed a colored-feeding assay that facilitated the screen in short time with high accuracy and selectivity. The cuticle of abdomen of the fly is transparent so that I could easily see the ingested food through the cuticle. Based on this, I visually inspected the amount of ingested food and scored food intake as the following: 0=no eating, 1=0.1 μl eaten, 2=0.25 μl eaten, 3=0.5 μl eaten, 4=1 μl eaten. The correlation between the score and microliter was previously validated by feeding the flies with the actual microliters of food **(Fig. 7)**.

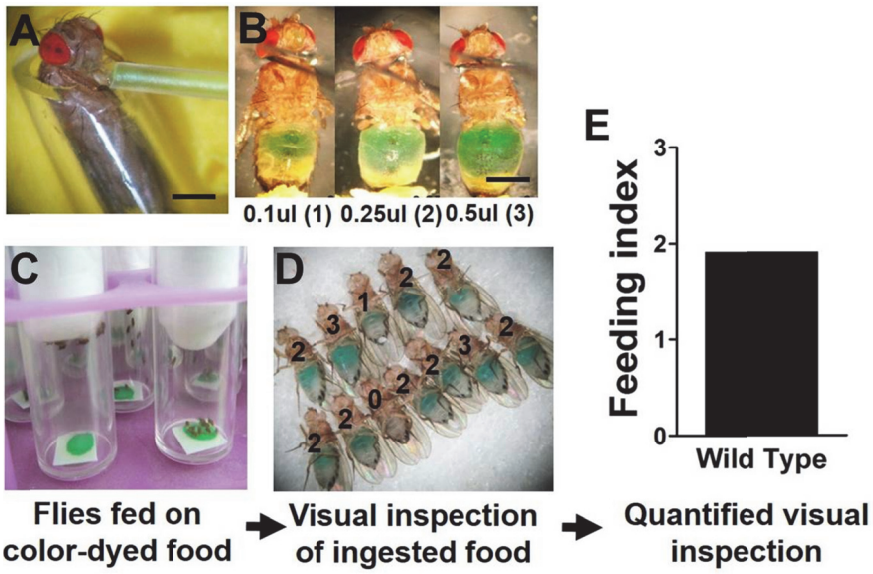

Figure 7. Visual inspection of food intake by flies. (A, B) Fixed amounts of food (0.1 µl, 0.25 µl, 0.5 µl) were provided and scored as 0=0 µl, 1=0.1 µl, 2=0.25 µl, 3= 0.5 µl, 4=1 µl, Scale bars: 0.5 mm. **(C, D)** Wild type flies were fed on green-dyed food and ingested food was quantified as the feeding scores. **(E)** Quantified feeding score as the "feeding index".

To examine whether the assay works using some of fly lines implicated in feeding. AstA and *Drosophila* insulin-like peptides (Dilps) pathway are reported to inhibit food intake (Hergarden et al., 2012; Liu et al., 2015; Ryuda et al., 2011; Zhao and Campos, 2012). Especially, activation of AstA suppresses the starvation-induced increase of food intake. Neural pathways involving Dilp2 and Dilp4 negatively regulate feeding by inhibition of the orexigenic NPF pathway or via a pathway independently of NPF. Consistent with these reports, flies with activated AstA or Dilp2 neurons using the warmth activated TRPA1 channel above 30°C showed reduced food intake compared to control flies. Conversely, the flies with activated NPF neurons exhibited moderate, but significant increase in food intake **(Fig. 8)**. Furthermore, the similar visual inspection method was reported in a study by others while I screened the collection.

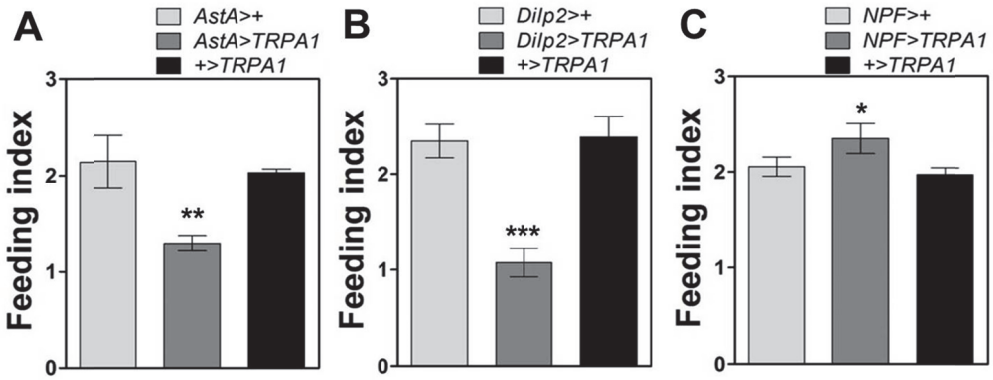

Figure 8. The feeding assay reproduces the feeding phenotype from the well-known feeding-related GAL4 lines. (A) Comparison of the feeding index shown by the flies with activated AstA neurons and control flies. **(B)** Comparison of the feeding index shown by the flies with activated Dilp2 neurons and control flies. **(C)** Comparison of the feeding index shown by the flies with activated NPF neurons and control flies. N=4-6. Error bars: S.E.M. *, $p<0.05$; **, $p<0.005$; ***, $p<0.0005$ by ANOVA Tukey's test.

Identification of candidate GAL4 and RNAi lines by a genetic screen using GAL4-UAS system

GAL4-UAS system is the most powerful genetic tool in *Drosophila* genetics. GAL4 is first found transcriptional activator binding the UAS sequence to express the gene of interest downstream of UAS. GAL4-UAS system allows tissue-specific and temporal expression of a gene. For example, fusion of the defined regulatory region from a pan-neuronal gene with GAL4 allows a pan-neuronal GAL4 line that can used to express a gene neuron-specifically. Crossing the GAL4 driver with UAS-temperature sensitive channel further makes the temporal manipulation of neurons feasible with the temperature stimuli. In this dissertation to take advantage of the GAL4-UAS system, I obtained ~200 JF-GAL4 driver lines and ~24 neuropeptide specific GAL4 drivers. To manipulate the neuronal activity of neurons, I crossed the individual lines to either *UAS-TNT* that inhibits neuronal activity by blocking the synaptic transmission through endocytosis of synaptic vesicles (Sweeney et al., 1995) or *UAS-TRPA1* that excites neurons upon temperature stimuli above 30°C (Rosenzweig et al., 2005). The progenies from the cross were assayed in the feeding assay to select a line that shows defects in food intake **(Fig. 9)**.

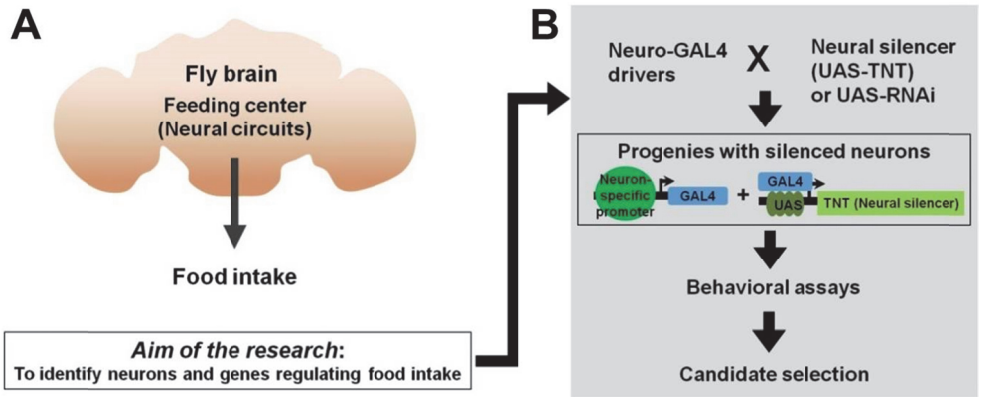

Figure 9. The screen aims to identify neurons and genes critical for feeding regulation by a genetic screen using neuron-specific GAL4 drivers and a library of RNAi lines. (A) The schematic drawing of the research idea and aim to identify neurons and genes involved in feeding regulation. **(B)** The flowchart for screening the neuron-specific GAL4 and RNAi lines using the feeding assay.

Among the lines with feeding defects, I sought a line that showed the converse phenotype when activated or silenced. In this way, I could have more opportunity to find candidates with selectivity. Out of the neuronal GAL4 driver lines, I identified two lines that showed significant increase in food intake when silenced and *vice versa* when activated **(Fig. 10)**. Additionally, I found an RNAi line that displayed hypophagic phenotype from the RNAi library.

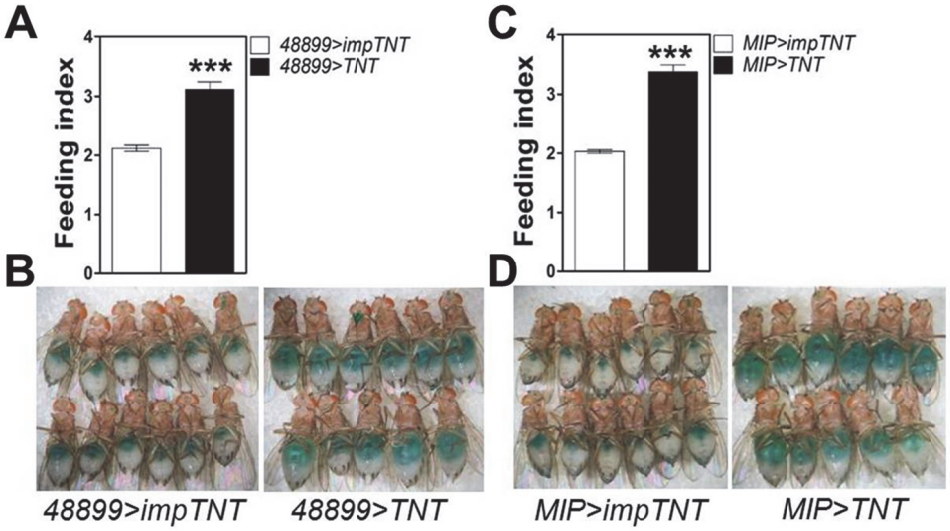

Figure 10. Identification of two GAL4 drivers showing feeding defects. **(A, B)** Comparison of feeding index and accumulated colored-food in the stomach shown by the flies with silenced 48899 neurons (*48899>TNT*) and the control flies (*48899>impTNT*). **(C, D)** Comparison of feeding index and accumulated colored-food in the stomach shown by the flies with silenced MIP neurons (*MIP>TNT*) and the control flies (*MIP>impTNT*). N=8. Error bars: S.E.M. ***, $p<0.0005$ by unpaired *t*-test.

PART 2

MIP pathway regulates body weight via controlling satiety

Introduction

Body weight (BW) is tightly linked to the appetite control in animals. For example, ablation of the anorexigenic POMC pathway or deletion of the satiety gene, leptin, increased BW along with augmented food intake. In *Drosophila*, allatonstatin A (AstA) and leukokinin (Lk) pathways have been reported to be anorexigenic regulators. Surprisingly, however, these pathways do not seem to affect BW. Although activation of AstA pathway inhibited a series of starvation-induced feeding responses including increased food intake and proboscis extension reflex (PER), it did not alter BW (Hergarden et al., 2012). Genetic disruption of the *Lk* gene and Lk-expressing neurons elicited larger meals by flies without affecting total food intake (Al-Anzi et al., 2010). Therefore, it is unclear how the changes by these pathways in appetite are conveyed to BW.

Myoinhibitory peptides (MIPs), also called AstB or prothorasicostatic peptides, belong to the allatostatin family that is well known for its inhibitory effect on food intake (Lorenz et al., 2000; Yamanaka et al., 2010). MIPs are neuropeptides found broadly in diverse invertebrates including insects (Davis et al., 2003; Simo et al., 2013). In *Drosophila*, MIP gene encodes five mature peptides (MIP1-5) highly related to one another (Poels et al., 2010;

Williamson et al., 2001). MIP activates strongly the sex peptide receptor (SPR) *ex vivo*, but does not affect a behavioral response known to be mediated by SPR *in vivo*, suggesting unknown receptor for MIP or other *in vivo* functions by MIP exist (Kim et al., 2010). Indeed, a recent report has revealed that MIP is involved in the sleep stabilizing pathway through SPR (Oh et al., 2014). Intriguingly, MIPs display a marked sequence similarity in the N-termini with vertebrate galanin (Blackburn et al., 1995; Gundlach, 2002), a neuropeptide previously implicated in feeding regulation. Moreover, a recent study using the marine annelid Platynereis has showed that MIP is involved in regulation of feeding (Williams et al., 2015). However, it is not known whether MIP regulates feeding in *Drosophila*.

In this chapter, I describe the role of MIP and MIP-expressing neurons in regulation of BW through controlling satiety independently of SPR.

Silencing MIP neurons increased food intake and BW

In addition to the dramatic increase in food intake by silencing MIP neurons as shown above "PART1", *MIP>TNT* flies also showed enlarged abdomen with 20-30% BW increase compared other control flies **(Fig. 11 and 12)**, and similarly the dry BW of *MIP>TNT* flies was heavier than controls **(Fig. 13)**. *MIP-GAL4* fly line carries a GAL4 transgene fused to 7.2 kb-long 5' upstream regulatory region of *mip* **(Fig. 14)**. To examine whether there exists another type of neuropeptide neurons affecting BW in *Drosophila*, I sought to establish a collection of neuropeptide GAL4 driver lines to test their role in BW. Among 24 neuropeptide GAL4 lines examined, most lines exhibited BW decrease and no significant changes in BW whereas *MIP-GAL4* specifically elicited striking BW increase when crossed with *UAS-TNT* **(Fig. 15)**. To monitor the time-course changes of BW by *MIP>TNT* flies, I measured BW of *MIP>TNT* flies for 20 days. As a result, the BW increase in *MIP>TNT* flies became evident as early as one day after eclosion, peaked within 5-10 days, and became stable thereafter **(Fig. 16)**.

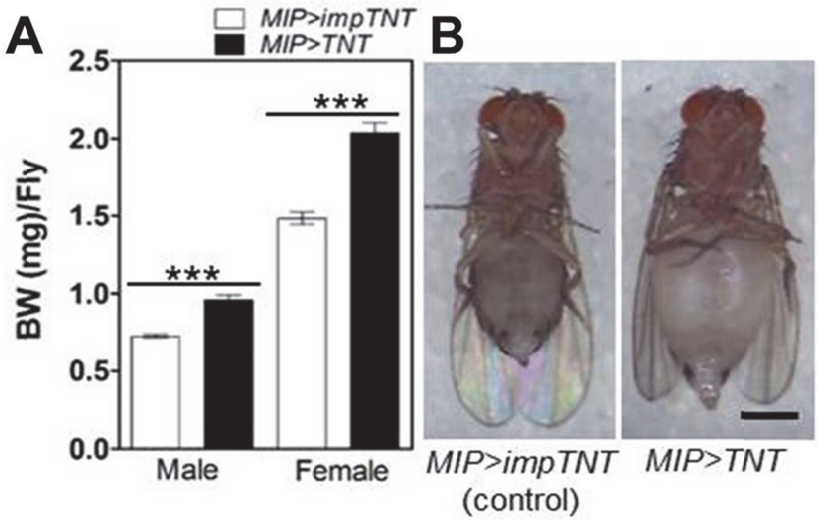

Figure 11. Silencing MIP neurons increased BW along with enlarged abdomen. (A) BW of *MIP>TNT* flies and control flies, *MIP>impTNT*, with inactivated tetanus toxin. N=4. Error bars: S.E.M. ***, $p < 0.0005$ by unpaired *t*-test. **(B)** Images of a *MIP>TNT* fly and a control are shown. The scale bar: 0.5 mm.

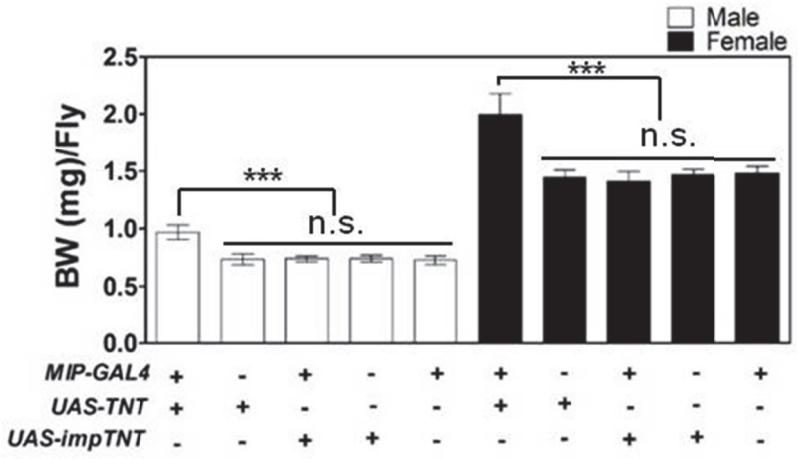

Figure 12. *MIP>TNT* flies are heavier than control flies. BW of the adult flies of indicated sex and genotype. '+' and '-' indicate presence and absence of indicated transgene, respectively. N=10-12. Error bars: S.E.M. ***, $p<0.0001$; n.s.: not significant by ANOVA Tukey's test.

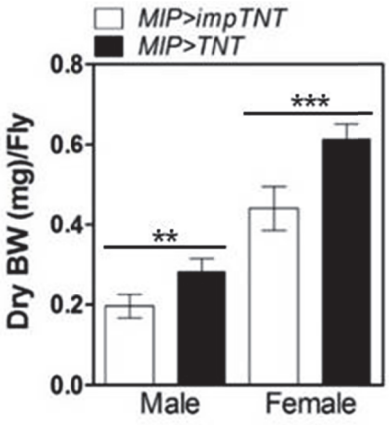

Figure 13. Comparison of dry weight of *MIP>TNT* and control flies. Dry BW of *MIP>TNT* and control *MIP>impTNT* desiccated at 75°C for 2 days. N=5. Error bars: S.E.M. **, $p<0.005$; ***, $p<0.0005$ by unpaired *t*-test.

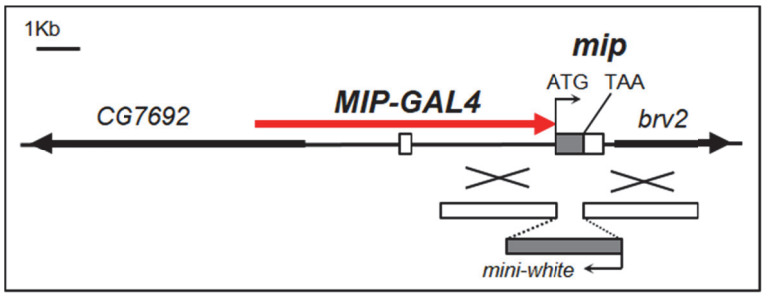

Figure 14. The schematic of generation of *MIP-GAL4*. A schematic diagram showing a deletion allele of *mip*^{1} and the genomic region used to generate *MIP-GAL4* (red arrow, 7.2 kb).

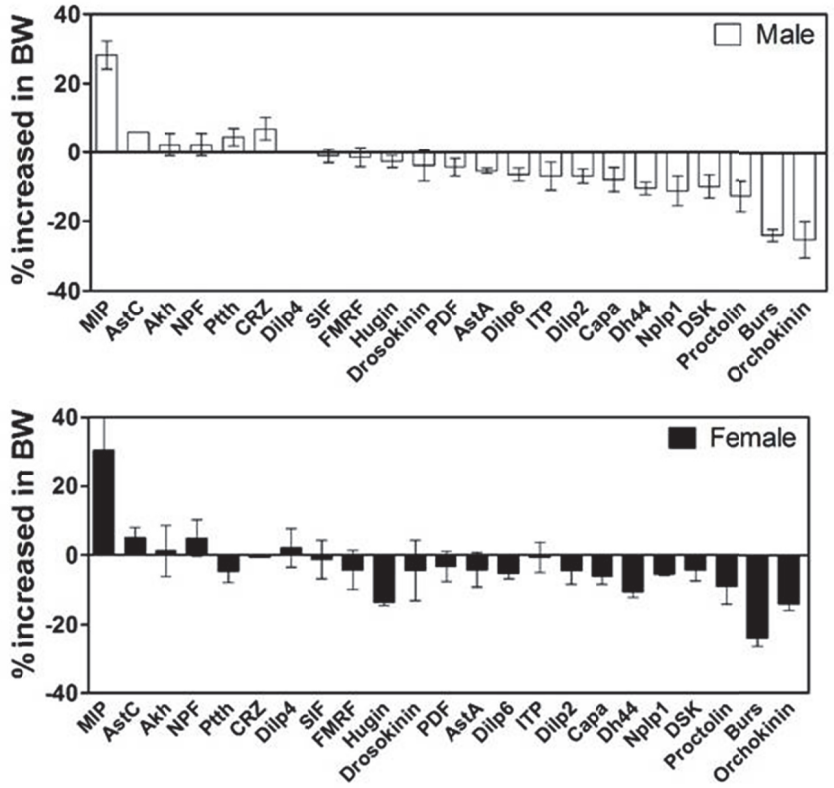

Figure 15. ***MIP-GAL4*** **specifically produces increased BW phenotype among 23 neuropeptide-GAL4 drivers crossed to** ***UAS-TNT.*** Percent increase in BW of flies with silenced neuropeptide-expressing neurons was compared. N=3-6. Error bars: S.E.M.

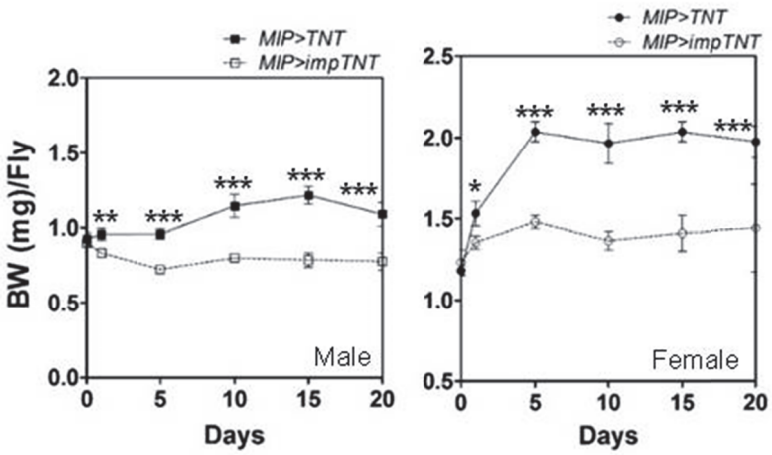

Figure 16. BW of *MIP>TNT* flies is gradually increased and reaches a steady state. Time-course BW measurement of *MIP>TNT* flies and controls. N=3-8. Error bars: S.E.M.

TNT expression in MIP neurons blocks MIP secretion

TNT interrupts the exocytic process of synaptic vesicles and blocks functions of various types of neurons including those expressing neuropeptides. In some peptidergic neurons, TNT-mediated blockade of the exocytosis resulted in accumulation of the neuropeptides in axons and termini (McNabb and Truman, 2008). Likewise, I also noted that anti-MIP immunoactivity in neural processes was elevated in the brains of *MIP>TNT* flies compared to *MIP>impTNT* controls **(Fig. 17)**. Kir2.1, another neuronal silencer that suppresses electric depolarization of neurons, also resulted in comparable BW increases when expressed in MIP neurons **(Fig. 18)**.

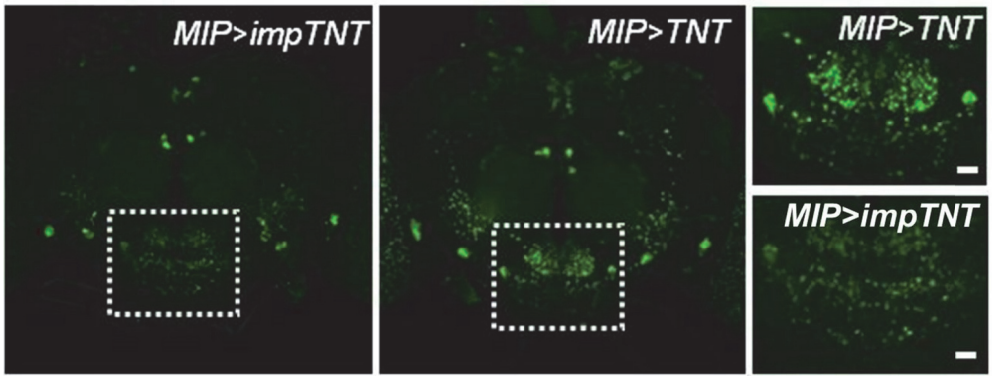

Figure 17. TNT expression in MIP neurons elicits the accumulation of MIP peptide in the axonal termini. Comparisons of confocal images of the brains expressing TNT or impTNT driven by *MIP-GAL4*, stained with anti-MIP antibody. Scale bars: 20 μm.

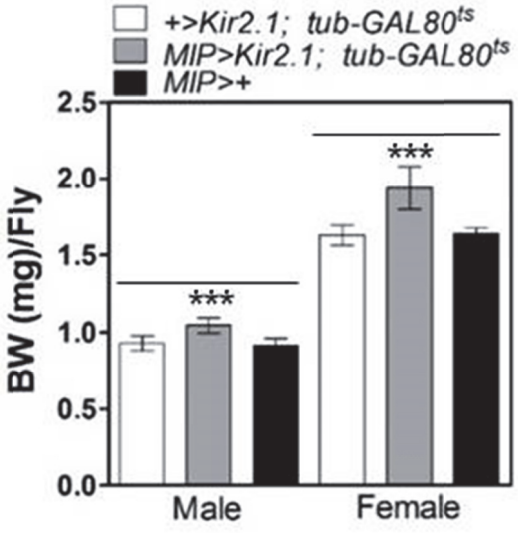

Figure 18. Expression of Kir2.1 in MIP neurons of the adult flies elicits BW increase. Comparisons of BW of the flies expressing Kir2.1 under the control of *MIP-GAL4* at 30°C. N=7-10. Error bars: S.E.M. ***, $p<0.0001$ by ANOVA Tukey's test.

Adult-specific silencing MIP neurons still increased BW

I concerned that *UAS-TNT* expression was driven by *MIP-GAL4* thtoughout the development and caused the defects. However, it was unlikely that silencing MIP neurons increases BW simply by promoting growth during development, since the BW of *MIP>TNT* flies measured immediately after eclosion was not different from that of the control flies. Consistent with this idea, there was no difference between *MIP>TNT* and *MIP>impTNT* flies in the body length and wing length measured shortly after eclosion **(Fig. 19)**.

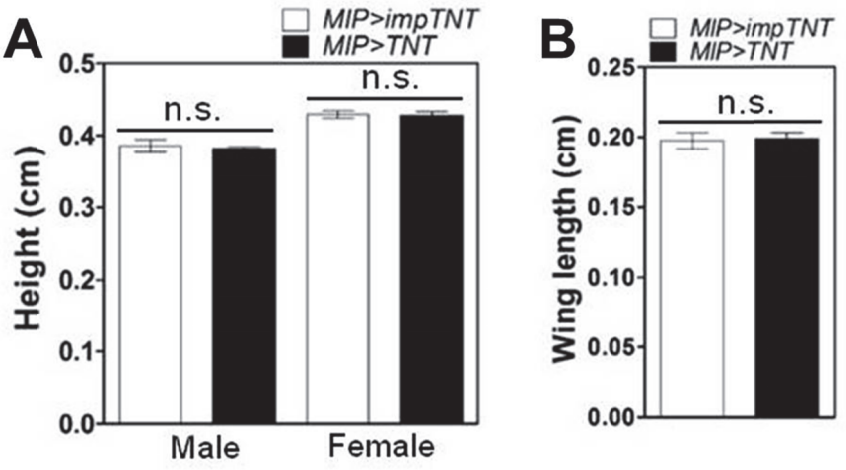

Figure 19. Comparisons of the height and wing length of *MIP>TNT* and control flies. (A) Heights of newly-eclosed *MIP>TNT* flies and control flies were compared. N=3. Error bars: S.E.M. n.s.: not significant by unpaired *t*-test. **(B)** Wing length of *MIP>TNT* flies and control flies. N=7. Error bars: S.E.M. n.s.: not significant by unpaired *t*-test.

Furthermore, I chose *tub-GAL80^{ts}* that encodes a ubiquitously expressing temperature-sensitive form of GAL80, and combined it with either *MIP>TNT* or *MIP>impTNT* to allow the expression of *UAS-TNT* only after eclosion. At 18°C, GAL80^{ts} suppresses GAL4 activity. However, it ceases to suppress GAL4 activity at 30°C and TNT is expressed in MIP neurons. After eclosion at 18°C, flies carrying three transgenes (*MIP-GAL4*, *tub-GAL80^{ts}*, and *UAS-TNT* or *UAS-impTNT*) were either subjected to a temperature shift to 30°C or were kept at 18°C for 3 days, and then their BW was measured. When incubated at 30°C, *MIP>TNT* flies carrying *tub-GAL80^{ts}* were significantly heavier than controls in both males and females, whereas those kept at 18°C were not **(Fig. 20)**.

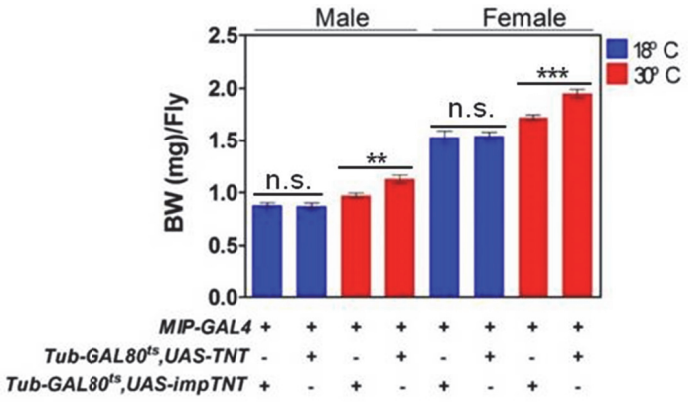

Figure 20. The adult-specific expression of TNT in MIP neurons elicits BW increase. BW of the adult flies of indicated sex and genotype. N=7-9. Error bars: S.E.M. **, $p<0.005$; ***, $p<0.0001$. n.s.: not significant by unpaired *t*-test.

Silencing MIP neurons also increased abdominal fat storage

BW increase of *MIP>TNT* flies accompanied larger abdomens compared to controls. Thus, I weighed the abdomen separately from the remaining body parts, head and thorax. As expected, the abdomen, but not the head and thorax, was significantly heavier in *MIP>TNT* flies compared to controls, attributing the increased BW to the heavier abdomen **(Fig. 21)**.

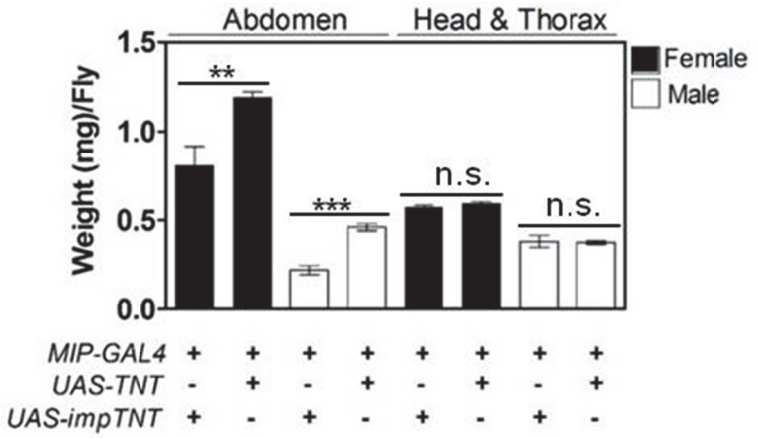

Figure 21. Comparisons of the weight of head & thorax, and abdomen of *MIP>TNT* flies and control flies. Weight of abdomen and head/thorax of the flies of indicated genotype. N=3. Error bars: S.E.M. **, $p<0.005$. ***, $p<0.0005$. n.s.: not significant by unpaired *t*-test.

Because the abdominal fat body is a major tissue for fat accumulation in flies, I examined it under bright-field microscopy and also stained it with Nile red, a lipophilic stain. As expected, I noted much denser layers of fat-body cells in the abdomens of *MIP>TNT* flies compared to *MIP>impTNT* controls. This result was further confirmed by a biochemical measurement on fat storage showing that *MIP>TNT* flies indeed possessed more triglyceride than *MIP>impTNT* flies **(Fig. 22)**.

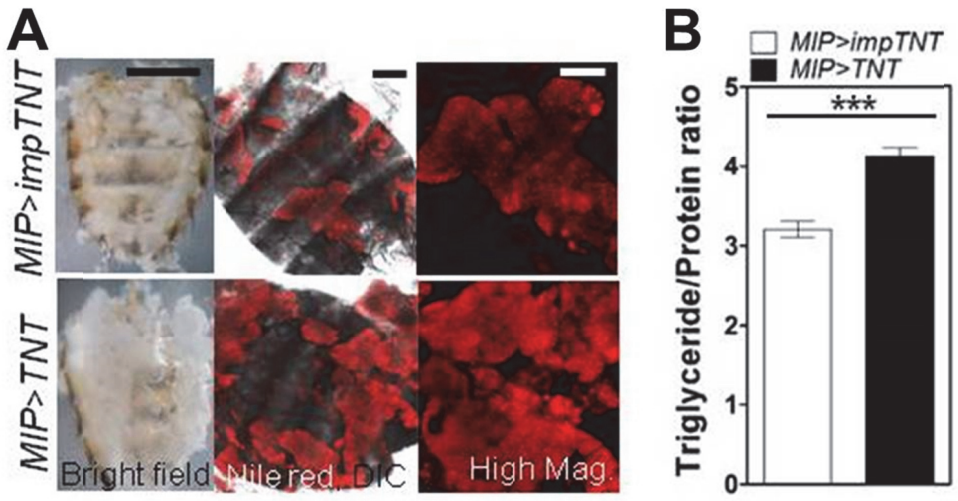

Figure 22. *MIP>TNT* flies show increased fat storage. (A) Left: Bright-field images of the dissected abdomens of *MIP>TNT* and a control fly. Scale bar: 0.5 mm. Middle: Confocal images of the fat tissues in abdomens stained with Nile Red. The abdomens of *MIP>TNT* and control fly were compared. Scale bar: 200 μm. Right: Zoomed-in images of the fat tissues stained with Nile red. Scale bar: 100 μm. **(B)** Normalized triglyceride level in the adult abdomens of *MIP>TNT* and controls. N=18. Error bars: S.E.M. ***, $p < 0.0005$ by unpaired *t*- test.

To address whether the accumulated fat serves as energy reserves, I examined how long these flies survive in the absence of food, and found that the survivorship of the obese *MIP>TNT* flies was twice as long as that of *MIP>impTNT* controls without food supply **(Fig. 23)**.

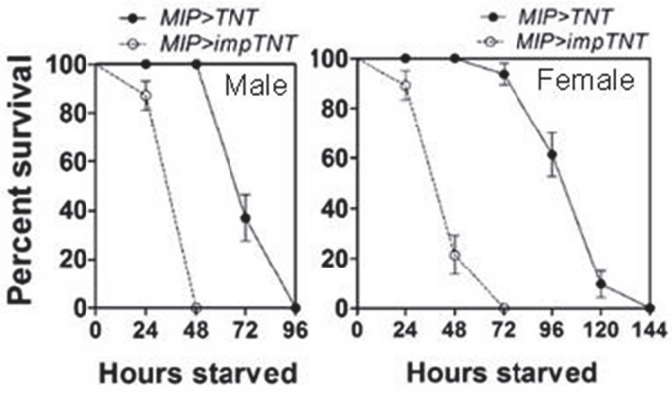

Figure 23. *MIP>TNT* flies exhibit increased starvation resistance. Percent survival of *MIP>TNT* flies and controls during starvation. N=3-5. Error bars: S.E.M.

BW increase of *MIP>TNT* flies was mediated by elevated food intake

To quantify food intake, I used the CAFE assay and a dyed-food assay. Using these independent assays I discovered that *MIP>TNT* flies ate twice as much as controls **(Fig. 24)**. This suggests that flies with silenced MIP neurons eat more and consequently become obese. To further test this, I compared BW in flies cultured under restricted and non-limiting (*ad libitum*) feeding conditions. As the restricted feeding condition, I provided ~0.2 mg of color-dyed standard cornmeal agar food to 50 flies for 2 days to ensure that all the flies consumed minimum food to survive. Remarkably, *MIP>TNT* flies showed the increased BW phenotype only when they were allowed access to unlimited food, further attributing the BW phenotype to the elevated feeding activity **(Fig. 25)**.

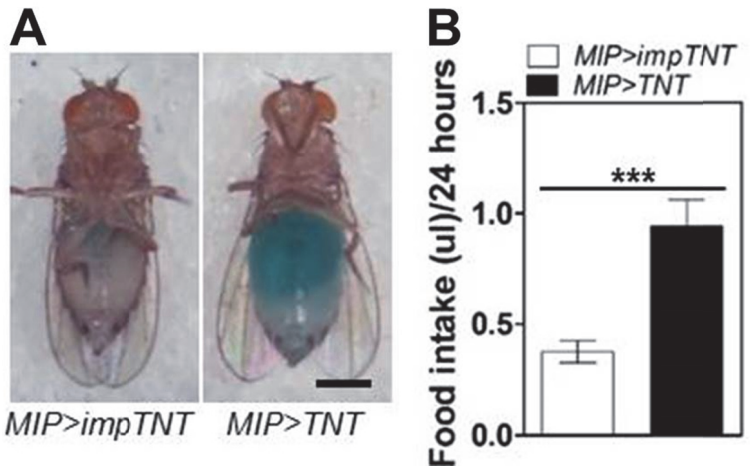

Figure 24. *MIP>TNT* show increased food intake. (A) Visualized food intake of a fly by accumulation of green-dyed food in the stomach. A *MIP>TNT* fly and a control fly were fed for 30 min. Scale bar: 0.5 mm. **(B)** 24-hr food intake by newly eclosed *MIP>TNT* and controls. N=5. Error bars: S.E.M. ***, $p < 0.0005$ by unpaired *t*- test.

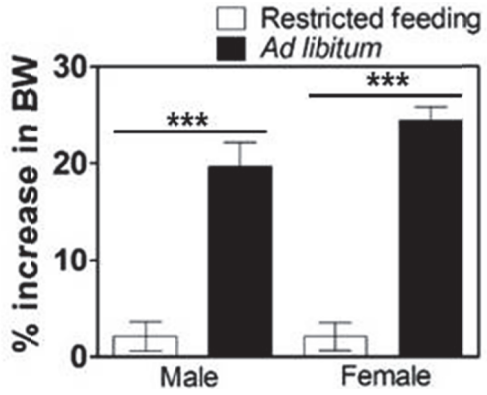

Figure 25. Restricted feeding completely rescued the BW increase of *MIP>TNT* flies. BW of *MIP>TNT* flies in a restricted feeding or ad libitum condition. N=13. Error bars: S.E.M. ***, $p < 0.0005$ by unpaired *t*- test.

Activation of MIP neurons decreased food intake and BW

To examine whether activating MIP neurons could make flies lose BW, I expressed TRPA1 channel in MIP neurons (*MIP>TRPA1*). By transferring flies from 18°C to 30°C, I could activate MIP neurons expressing TRPA1. When kept at 18°C, *MIP>TRPA1* flies showed no obvious BW change compared to controls. In contrast, 3 days after incubation at 30°C, *MIP>TRPA1* flies exhibited marked loss of BW (~ 30%) in both sexes compared to controls. Remarkably, the loss of BW induced by MIP neuron activation was completely reversed when MIP neuron activation was ceased by transferring *MIP>TRPA1* flies back to 18°C for 3 days **(Fig. 26)**. Subsequently, I monitored feeding activities using the CAFE assay before, during and after MIP neuron activation. Before activation, *MIP>TRPA1* flies and control flies showed no difference in food intake. When incubated at 30°C, the flies with activated MIP neurons ingested ~ 70% less food than controls. However, when they were transferred back to 18°C and the activation of MIP neurons ceased, *MIP>TRPA1* flies displayed a pronounced rebound in feeding activity and ate ~70% more food than controls for 24 hours after the temperature shift **(Fig. 27)**.

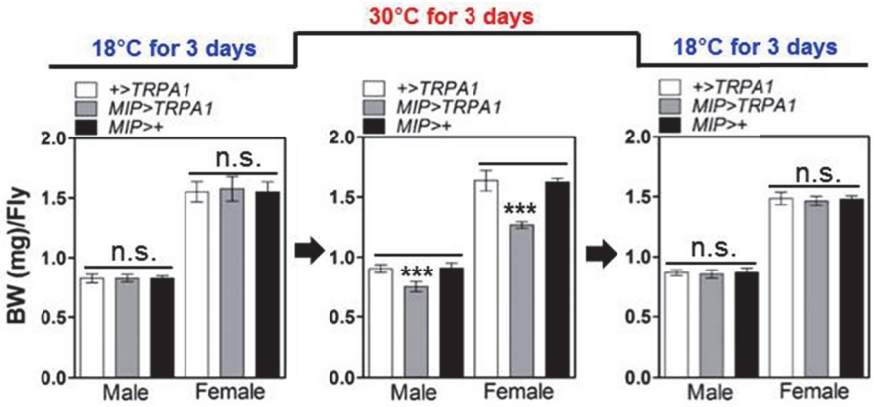

Figure 26. Activation of MIP neurons reduces BW. BW of *MIP>TRPA1* and control flies at 18°C or 30°C. N=8-14. Error bars: S.E.M. ***, $p < 0.0005$; n.s., not significant by ANOVA Tukey's test.

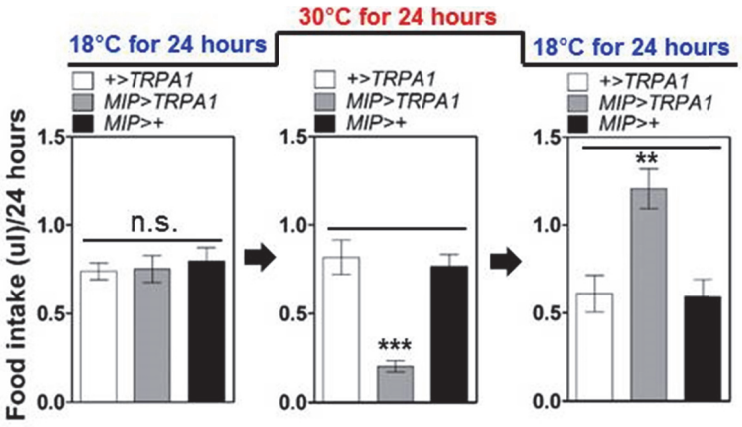

Figure 27. Activation of MIP neurons decreases food intake. Level of food intake of *MIP>TRPA1* and control flies at 18°C or 30°C. N=5-15. Error bars: S.E.M. **, $p < 0.01$;***, $p < 0.0005$; n.s., not significant by ANOVA Tukey's test.

Activation of MIP neurons made flies leaner

Based on the observation that food intake and BW were reduced by activation of MIP neurons, I wondered whether the flies with activated MIP neurons show lean phenotypes. Thus, I incubated *MIP>TRPA1* flies at 30°C and these flies indeed exhibited leaner abdomens with much less fat tissue and triglyceride level than controls **(Fig. 28)**.

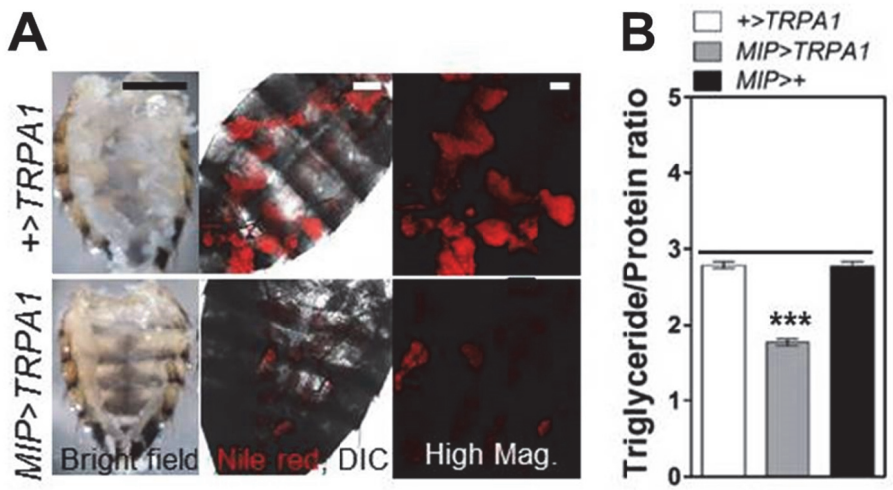

Figure 28. Activation of MIP neurons decreases fat storage. **(A)** Left: Bright-field images of the abdomen of indicated genotypes. The scale bar: 0.5 mm. Middle: Confocal images of the abdomens stained with Nile red are shown. The scale bar: 200 mm. Right: High-magnification images of Nile-red-stained fat tissues are shown. The scale bar: 100 mm. **(B)** Normalized triglyceride level of the adult abdomens of indicated genotypes. N=12. Error bars: S.E.M. ***, $p < 0.0005$ by ANOVA Tukey's test.

***MIP-GAL4* was expressed in the central nerve system (CNS) and gastrointestinal tract**

To visualize the expression pattern of *MIP-GAL4* used in the study, I generated flies bearing *MIP-GAL4* and *UAS-mCD8GFP* (*MIP>mCD8GFP*) and imaged the CNS and gastrointestinal tract from the GFP reporter fly. The GFP labeling was observed in various neural structures in the CNS including the antennal lobe (AL) and subesophageal zone (SEZ) important for searching and ingesting food and also in some cells in the midgut **(Fig. 29)**. The midgut cells were the enteroendocrine cells positive for anti-prospero antibody **(Fig. 30)**.

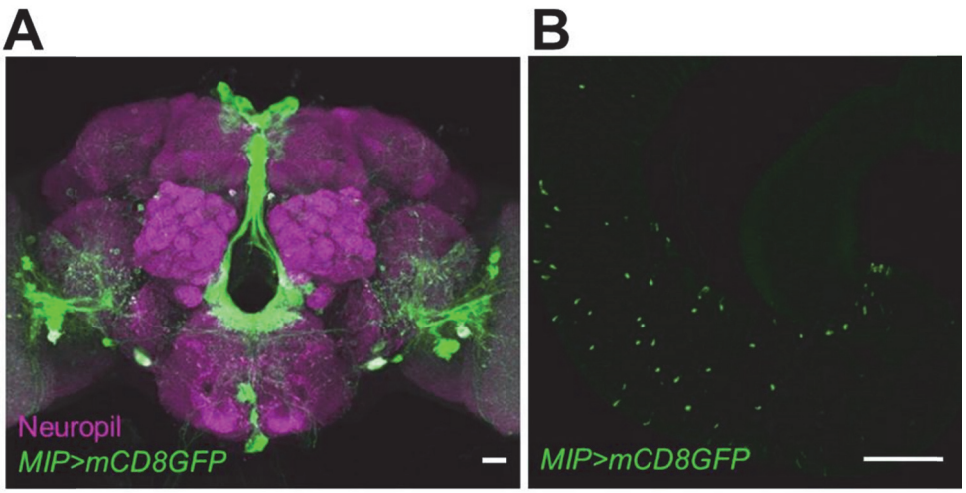

Figure 29. *MIP-GAL4* is expressed in the CNS neurons and intestine. (A) Confocal images of the brain and **(B)** the intestine expressing *MIP>mCD8GFP*. Scale bars: 20 and 100 μm, respectively.

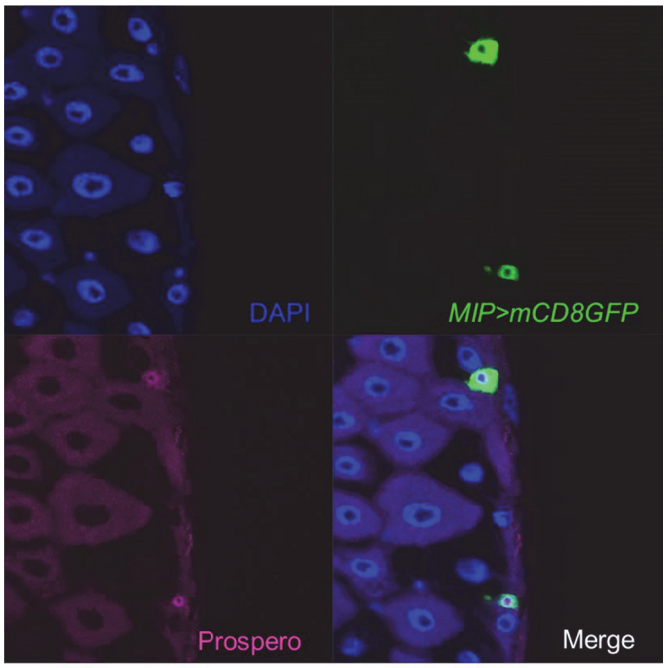

Figure 30. The *MIP-GAL4* cells in the intestine are the enteroendocrine cells. Confocal images of the intestine expressing *MIP>mCD8GFP* stained with anti-prospero antibody.

MIP was expressed in the central nerve system (CNS)

Next, I used anti-MIP antibody and mRNA *in situ* labeling to visualize the MIP expression. First, using the antibody MIP was detected in about 70 neurons that involved the AL and SEZ. By double labeling experiments using anti-MIP and MIP mRNA, I confirmed that 52 anti-MIP neurons were indeed positive for MIP mRNA. Using anti-MIP antibody on the *MIP>mCD8GFP* flies, I observed that the antibody was overlap with almost all GFP signals driven by *MIP-GAL4* except for 14 pairs of *MIP-GAL4* neurons **(Fig. 31 and 32)**.

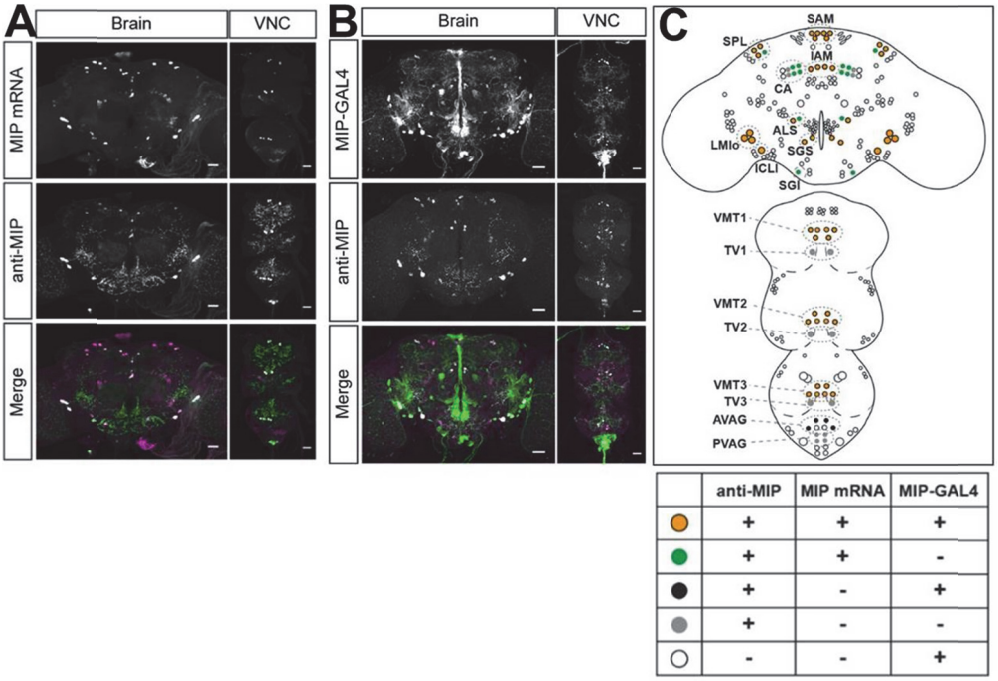

Figure 31. MIP-expressing and *MIP-GAL4* cells are mapped in the CNS. **(A)** Confocal images of the WT brain and VNC co-stained with anti-MIP antibody (green) and MIP RNA antisense probe (magenta). **(B)** Confocal images of the brain and VNC of *MIP>mCD8GFP* co-stained with anti-MIP (magenta) and anti-GFP (green). Scale bars: 30 μm. **(C)** The schematic map for location of MIP cells.

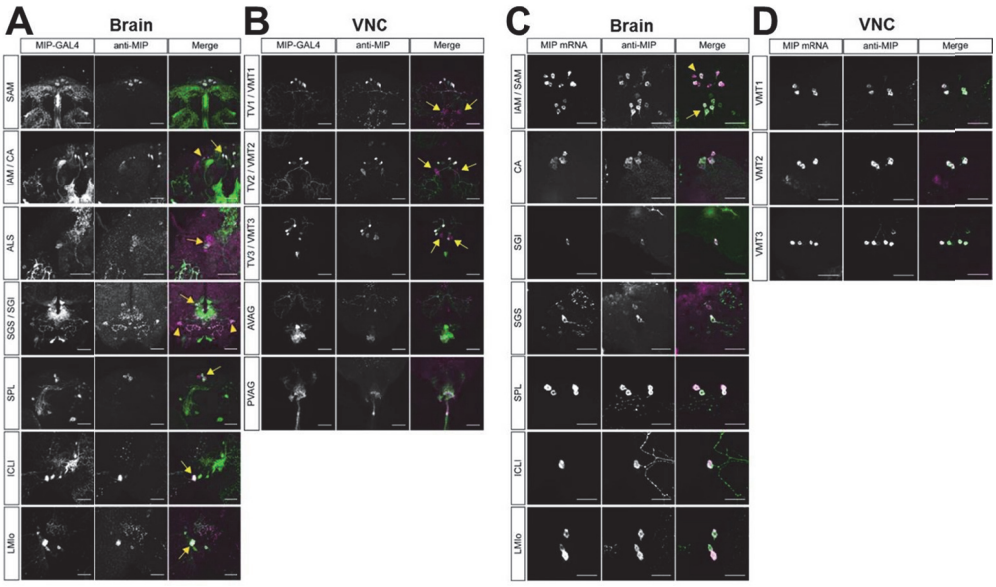

Figure 32. Every subset of MIP-expressing and *MIP-GAL4* neurons is visualized in the brain and VNC. (A) Confocal images of the subsets of MIP neurons in the brain expressing MIP>mCD8GFP co-stained with anti-MIP antibody (magenta) and anti-GFP antibody (green). The arrows indicate the IAM, SGS, SPL, ICLI, LMIo, and ALS cells, respectively. The arrowheads denote the CA and SGI cells, respectively. The scale bars: 30 μm. **(B)** Confocal images of the subsets of MIP neurons in the VNC expressing MIP>mCD8GFP co-stained with anti-MIP antibody (magenta) and anti-GFP antibody (green). The arrows indicate the TV1-3 cells, respectively. The scale bars: 30 μm. **(C)** Confocal images of the subsets of MIP neurons in WT brain co-stained with anti-MIP antibody (green) and MIP mRNA antisense probe (magenta). The arrow and arrowhead depict the IAM and SAM cells,

respectively. Note comprehensive co-localization of MIP mRNA and anti-MIP labeling. The scale bars: 30 μm. **(D)** Confocal images of the subsets of MIP neurons in WT VNC co-stained with anti-MIP antibody (green) and MIP mRNA antisense probe (magenta). The scale bars: 30 μm.

MIP expression responded to activation of MIP neurons and starvation

If MIP is physiologically involved in MIP neuron-mediated action in food intake and BW regulation, I would see the dynamic changes in MIP expression upon external stimuli that affect food intake or BW. To examine whether MIP is transported to axonal termini of the neurons to be secreted upon the neuronal activation, I activated MIP neurons and stained the expression pattern of MIP in the brain. Remarkably, MIP expression was mostly observed in axons and termini after the activation protocol rather than cell bodies like seen in control brain **(Fig. 33)**. Next, I asked whether MIP expression responded to hunger or satiety by staining MIP in the brains in 24 hours of starvation or *ad libitum* conditions. Remarkably, I observed less anti-MIP signals from the starved brains, indicating that MIP responds to the internal state to regulate food intake and BW **(Fig. 34)**.

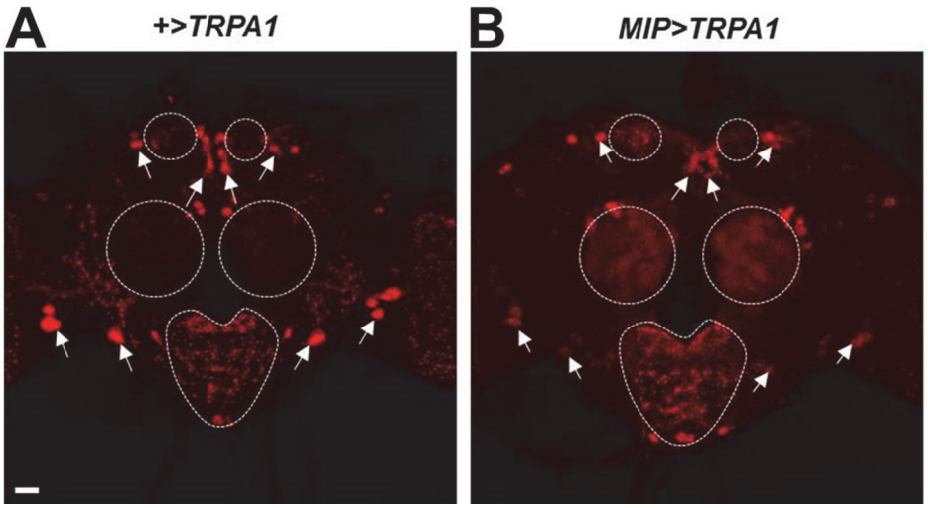

Figure 33. MIP peptide is transported to axonal termini upon the activation of MIP neurons. Confocal images of the brain of *MIP>TRPA1* **(A)** and the control flies **(B)** incubated at 30°C stained with anti-MIP antibody. Scale bar: 20 μm.

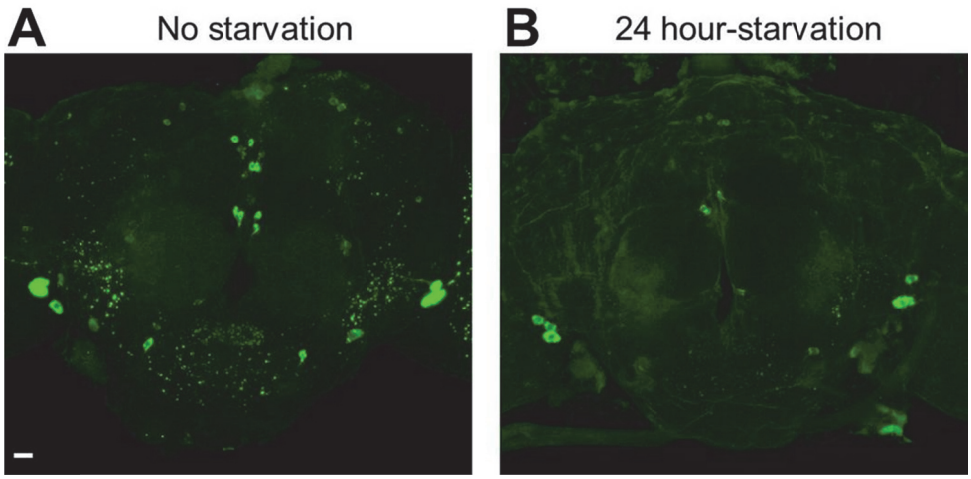

Figure 34. Expression of MIP peptide diminishes upon starvation. Confocal images of the WT brain subjected to no starvation **(A)** or 24 hours of starvation **(B)** stained with anti-MIP antibody. Scale bar: 20 μm.

Functional examination of the AL and SEZ expression by MIP

The notable expression of MIP in the AL and SEZ led me to hypothesize that *MIP>TNT* flies would show altered olfactory and gustatory sensitivity to food. First, I wondered whether the MIP expression in the AL and SEZ overlap with any known neural circuits. For the AL expression I examined *Orco-GAL4* (80% olfactory receptor neurons) that is supposedly expressed in the AL and I tested *Gr5a-GAL4* (sweet-sensing neurons) for the SEZ. Remarkably, MIP was overlap with *Orco-* and *Gr5a-GAL4* **(Fig. 35)**. Next, I functionally examined *MIP>TNT* flies in the electrophysiological recordings for their olfactory sensitivity to a food odor and observed that these flies indeed showed increased olfactory sensitivity compared to controls **(Fig. 36)**. For gustatory sensitivity, I fed the *MIP>TNT* flies on several compounds that taste sweet, bitter, or nothing (but nutritional) to check on which the flies preferentially overeat. As a result, I found that *MIP>TNT* flies selectively overfed on sweet compounds such as sucrose and arabinose, regardless of the nutritional value, indicating MIP neurons are specifically involved in sensing taste **(Fig. 37)**.

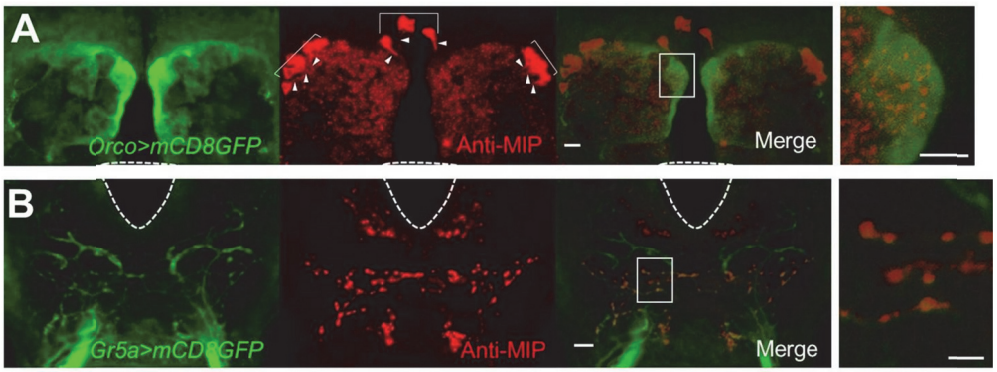

Figure 35. MIP peptide is co-localized with *Orco* and *Gr5a* neurons in the AL and SEZ, respectively. (A) Confocal images of the AL of the fly expressing mCD8GFP reporter driven by *Orco-GAL4* stained with anti-MIP antibody. Arrowheads denote the axons originated from the cell bodies (see the square brackets). Scale bar: 10 μm. Note the overlapping of the axonal termini of MIP-expressing neurons with the termini of *Orco*-expressing sensory neurons in the white-squared area. Scale bar: 20 μm. **(B)** Confocal images of the subesophageal zone (SEZ) of the fly expressing mCD8GFP reporter driven by *Gr5a-GAL4* stained with anti-MIP antibody. Scale bar: 10 μm. The region through which the esophagus passes is depicted by the dotted white line. Note co-localizations of the axonal termini of MIP-expressing neurons with the termini of *Gr5a*-expressing sensory neurons in the white-squared area. Scale bars: 10 μm.

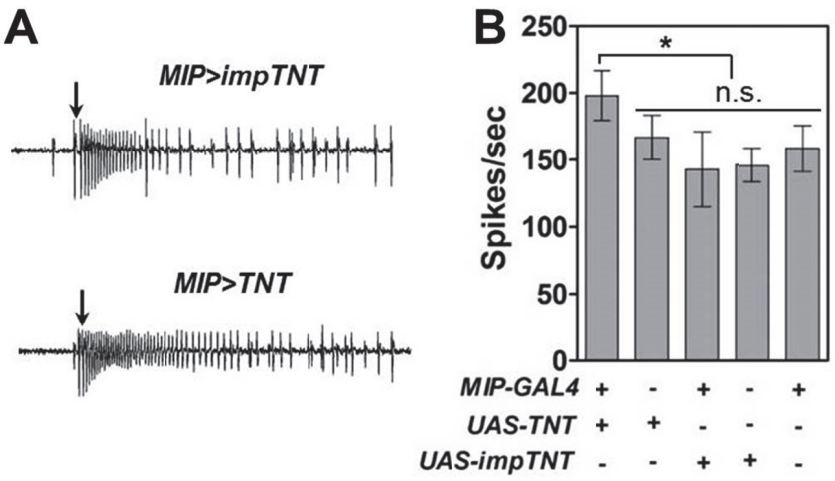

Figure 36. *MIP>TNT* flies show the enhanced activity of an olfactory receptor neuron to food odor. (A) A representative pattern of neuronal spikes and comparisons of the quantified spikes of the olfactory sensillum in the antenna of *MIP>TNT* and control flies in response to a food odor. **(B)** Spikes evoked immediately after odor puffing until 0.2 seconds were quantified. N=6-9. Error bars: S.E.M. *, $p<0.05$; n.s.: not significant by ANOVA Tukey's test.

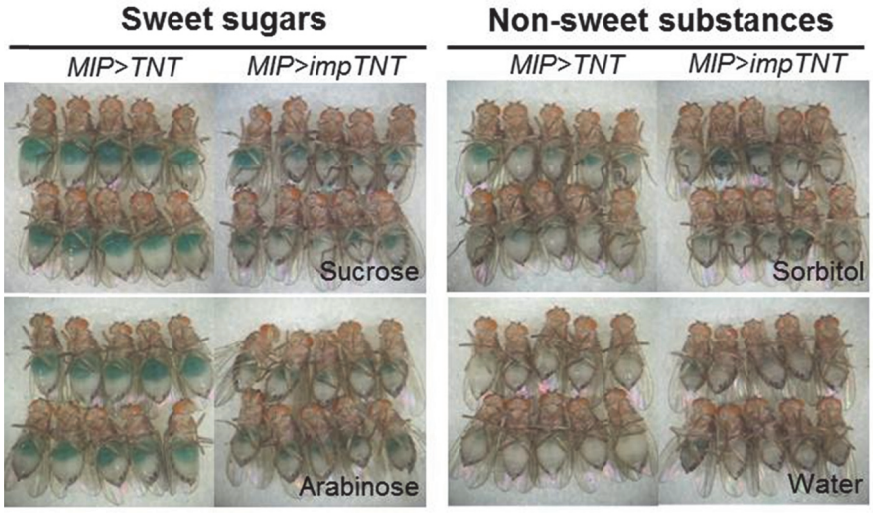

Figure 37. *MIP>TNT* flies preferentially overfeed on sweet compounds regardless of the nutritional value. Level of ingestion by the *MIP>TNT* and *MIP>impTNT* control flies on green color-dyed 10% sugar solutions. Each experiment was performed at least 3 times and the representative images were shown. Note the hyperphagic phenotype by *MIP>TNT* flies fed on the sweet sugars (sucrose and arabinose), but not on the non-sweet sugar (sorbitol).

MIP expression in *MIP-GAL4* neurons was required for BW regulation

To examine whether MIP expression in *MIP-GAL4* neurons is required for BW control, I drove the expression of *MIP RNAi* under the control of *MIP-GAL4*. The flies carrying *MIP>MIP RNAi* showed a significant BW increase with mostly eliminated anti-MIP labeling in the brain **(Fig. 38)**. However, I noted that the amplitude of BW increase by the RNAi knockdown is apparently smaller than that of silencing MIP neurons. With consistency, I observed significant numbers of ectopic *MIP-GAL4* cells in the CNS and the midgut that lack either anti-MIP or MIP mRNA labeling **(Fig. 39)**.

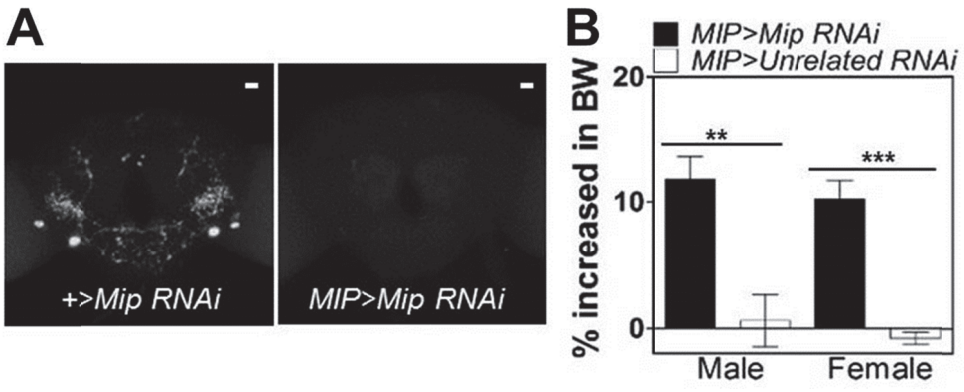

Figure 38. RNAi knockdown of MIP in MIP neurons increases BW. (A) Confocal images of the brain of indicated genotype stained with anti-MIP. Scale bars: 20 μm. **(B)** % increase in BW of the flies expressing *Mip RNAi* or an unrelated RNAi. N=5. Error bars: S.E.M. **, $p<0.005$; ***, $p=0.0001$ by unpaired *t*-test.

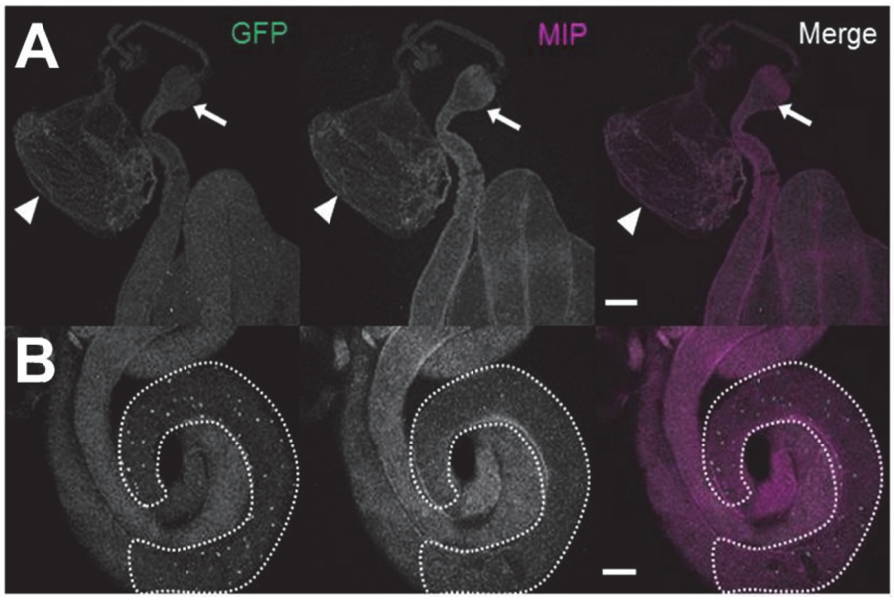

Figure 39. *MIP-GAL4* is expressed in the midgut. (A) Representative confocal images of the crop, the foregut and a part of the midgut of *MIP>mCD8GFP* stained with anti-MIP. Note absence of anti-MIP and anti-GFP activity in the proventriculus (arrow) and the crop (arrowhead). Scale bar: 100 µm. (B) Representative confocal images of the midgut and the hindgut of *MIP>mCD8GFP* stained with anti-MIP. Dotted lines depict the midgut region expressing *MIP>mCD8GFP*. Scale bar: 100 µm.

Cha-GAL80 fully rescued the defective BW increase of *MIP>TNT* flies

Thus, to define the subset of MIP neurons responsible for BW regulation, I combined cell-specific GAL80 transgenes with *MIP>TNT* to suppress TNT expression in genetically defined subsets of *MIP-GAL4* neurons. Remarkably, I found that the inclusion of *Cha-GAL80* fully suppressed the increased BW phenotype of *MIP>TNT* flies **(Fig. 40)**.

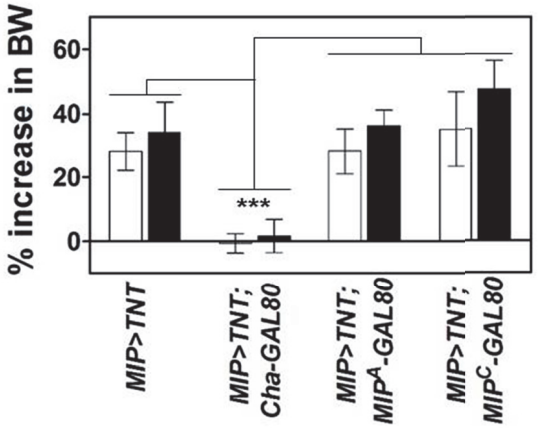

Figure 40. Inclusion of *Cha-GAL80* fully rescues the BW increase phenotype of *MIP>TNT* flies. Comparison of the BW phenotype of *MIP>TNT* flies bearing three different subset-specific GAL80 lines. N=6, Error bars: S.E.M. ***, $p<0.0005$ by two-way ANOVA Bonferroni posttest.

A subset of MIP neurons in the CNS was responsible for BW regulation

To further map *Cha-GAL80*-positive MIP neurons, I compared GFP labeling of *MIP>mCD8GFP* flies with and without *Cha-GAL80*. *Cha-GAL80* suppressed mCD8GFP expression in several groups of *MIP>mCD8GFP* neurons in the CNS with varying strengths, whereas it failed to do so in the midgut cells. Among ~ 42 central MIP neurons positive for *MIP-GAL4* and anti-MIP antibody labeling, I noted only one subset of *MIP-GAL4* neurons named as Inferior Anterior Medial (IAM) has a discernible suppression of anti-GFP labeling **(Fig. 41 and Table 4)**.

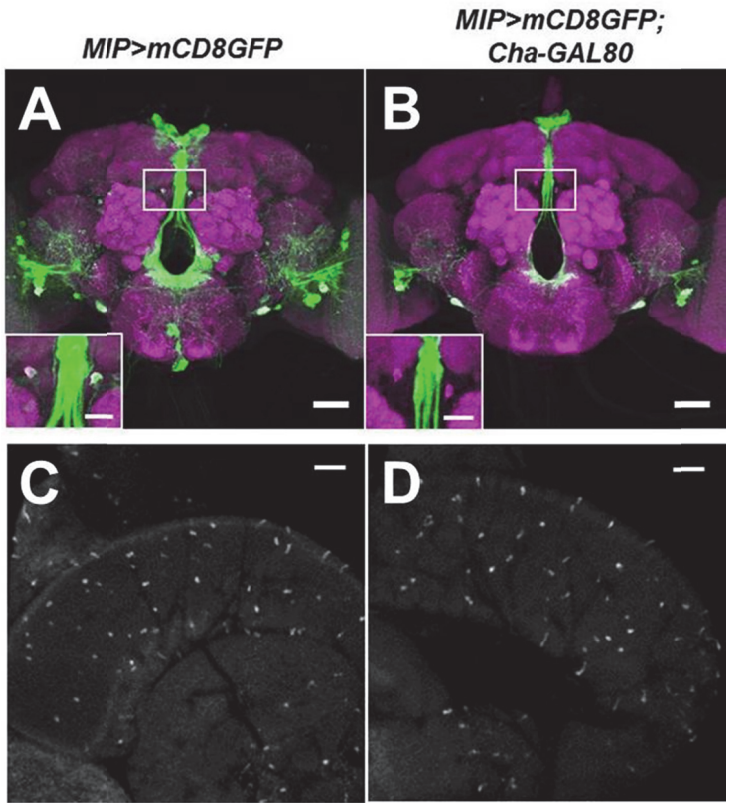

Figure 41. *Cha-GAL80* selectively suppresses *MIP-GAL4*-driven mCD8GFP signal in the IAM cells. (A, B) Confocal images of the brains expressing mCD8GFP reporter driven by *MIP-GAL4* (green), co-stained with nc82 (magenta). **(C, D)** Note that the inclusion of *Cha-GAL80* suppressed the *MIP-GAL4*-driven mCD8GFP signal in the IAM cells but not in the midgut. Scale bars: 30 μm and 10 μm for inset images.

Table 4. Anti-MIP, MIP mRNA and *MIP-GAL4* cells in the CNS.

Name of Cell Type[a]	anti-MIP		MIP mRNA		*MIP-GAL4*		*MIP-GAL4* w/ *Cha-GAL80*		P-value between *MIP-GAL4* and *MIP GAL 4* w/*Cha-GAL 80*[c]
	Number of Cells[b]	*n*	Number of Cells	*n*	Number of Cells	*n*	Number of Cells	*n*	
Superior Anterior Medial (SAM)	6.2 ± 1.6	13	5.6 ± 1.6	13	5.1 ± 1.4	9	5.7 ± 0.5	7	0.5686
Superior Posterior Lateral (SPL)	7.8 ± 0.4	13	0.8 ± 2.2	13	5.1 ± 0.8	9	5.1 ± 1.5	7	1.0000
Inferior Anterior Medial (IAM)	4.0 ± 0	13	3.7 ± 1.4	13	3.9 ± 0.6	9	0 ± 0	7	< 0.0001
Antennal Lobe Superior (ALS)	4.6 ± 2.8	13	4.9 ± 3.0	13	0.2 ± 0.4	9	0 ± 0	7	0.3559
Subesophageal Superior (SGS)	3.6 ± 2.1	13	2.5 ± 1.6	13	2.7 ± 1.2	9	3.1 ± 2.3	7	0.6493
Central Anterior (CA)	11.6 ± 1.9	13	8.5 ± 2.7	13	1.6 ± 1.7	9	0.1 ± 0.4	7	0.0815
Inferior Contralateral Interneurons (ICLI)	2.0 ± 0	13	2.0 ± 0	13	2.7 ± 1.1	9	3.1 ± 0.7	7	0.5222
Subesophageal Inferior (SGI)	1.8 ± 0.4	13	1.9 ± 0.3	13	0.2 ± 0.4	9	0.3 ± 0.8	7	1.0000
Lateral MIP-IR	7.5 ± 1.0	13	6.0 ± 0	13	8.8 ± 2.3	9	9.0 ± 1.6	7	0.8382

Optic Lobe (LMIo)									
Ventral Medial Thoracic 1 (VMT1)	5.9 ± 0.3	13	4.6 ± 1.3	10	5.3 ± 0.8	7	6.0 ± 0	3	0.1835
Thoracic Ventral 1 (TV1)	2.0 ± 0	13	0 ± 0	10	0 ± 0	7	0 ± 0	3	1.0000
Ventral Medial Thoracic 2 (VMT2)	2.5 ± 1.9	13	5 ± 1.5	10	5.7 ± 0.5	7	6.0 ± 0	3	1.0000
Thoracic Ventral 2 (TV2)	2.0 ± 0	13	0 ± 0	10	0 ± 0	7	0 ± 0	3	1.0000
Ventral Medial Thoracic 3 (VMT3)	2.0 ± 2.0	13	4.9 ± 1.9	10	5.4 ± 0.8	7	6.0 ± 0	3	0.4226
Thoracic Ventral 3 (TV3)	2.0 ± 0	13	0 ± 0	10	0 ± 0	7	0 ± 0	3	1.0000
Anterior Ventral Abdominal Ganglion (AVAG)	2.3 ± 1.9	13	0 ± 0	13	5.7 ± 0.8	7	6.0 ± 0	3	0.1835
Posterior Ventral Abdominal Ganglion (PVAG)	2.9 ± 1.8	13	0 ± 0	13	0 ± 0	7	0 ± 0	3	1.0000

a. Note ICLI expressing Natalisin and LMIo were previously described.

b. Average ± S.D.

c. *P* value in comparison of GAL4 activity between *MIP-GAL4* alone and *MIP-GAL4* combined with *Cha-GAL80* (unpaired *t*-test). Inclusion of *Cha-GAL80* suppresses *MIP-GAL4* activity significantly only in IAM.

Generation of a null mutation for *mip*

To examine the requirement of MIP gene in food intake and BW regulation, I sought to generate a null allele of *mip* (*mip*^{1}) by replacing the entire coding sequence of MIP with the mini-w^{+} cassette using homologous recombination. Using Anti-MIP antibody, I confirmed that the MIP mutant flies (*mip*$^{1/1}$) were null because the MIP expression in WT brain was wipe out in the mutant brain, except for a pair of cells at the tip of the brain. Unlike other MIP cells in the brain, these two cells lacked *MIP-GAL4* expression and did not observe in other staining experiments using the antibody **(Fig. 42)**.

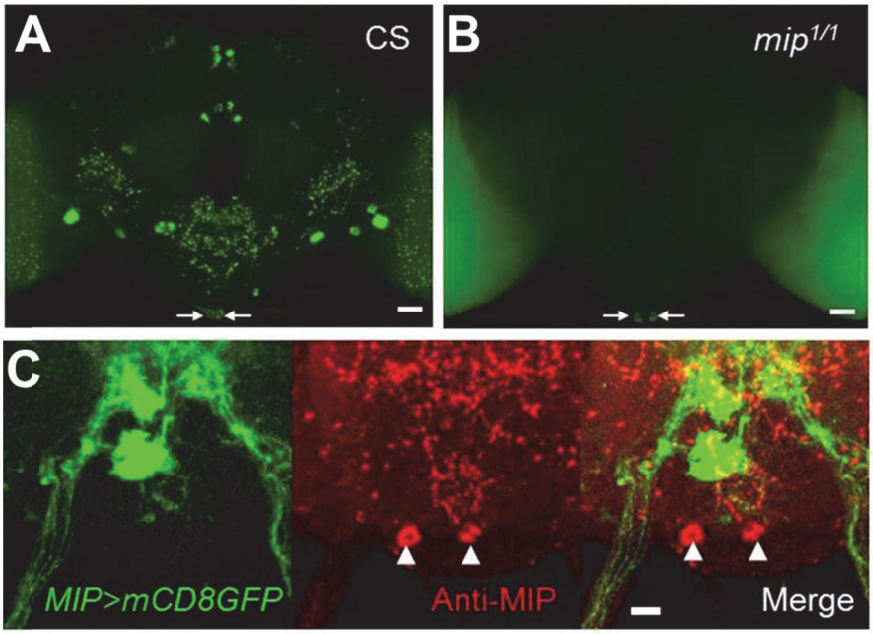

Figure 42. MIP expression is eliminated in the fly mutants for MIP. (A, B) Confocal images of WT (CS) and *mip*$^{1/1}$ knockout fly, stained with anti-MIP antibody. Non-specific signals are depicted by arrows. The scale bar represents 20 μm. **(C)** Confocal images of the brain expressing *MIP>mCD8GFP*, stained with anti-MIP antibody. Note that the non-specific signals are not labeled by *MIP-GAL4*. Scale bar: 10 μm.

Mip was necessary for food intake and BW control

Using the MIP mutants, I examined the requirement of *mip* in BW regulation, fat storage, and feeding activity. Indeed, I found that *mip* null mutant flies carrying either two copies of mip^{1} or a copy of mip^{1} over *mip* deficiency ($mip^{1/Df}$) were 13% heavier and consumed 25% more food compared to controls **(Fig. 43 and 44)**. The abdominal fat accumulation and fat storage were also more pronounced in *mip* null mutants than in controls. These obese phenotypes of the *mip* null mutant were rescued by restoring *mip* expression with *MIP-GAL4* (*MIP>mip;* $mip^{1/1}$) **(Fig. 45)**. Nevertheless, I noted that the magnitude of BW increase observed in *mip* mutants was approximately 50% of what I observed in MIP neuron silencing. Again like the *MIP RNAi* results, this raises a possibility that the ectopic *MIP-GAL4* neurons independent of MIP attribute to the residual BW increase.

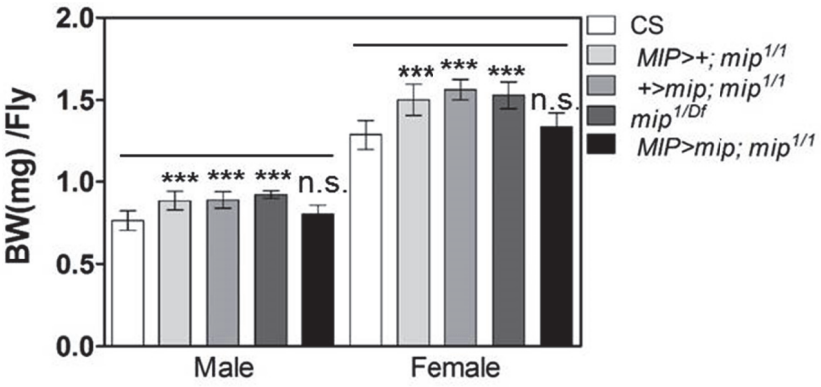

Figure 43. The fly mutants for MIP show BW increase phenotype which could be fully rescued by the exogenous expression of MIP in MIP neurons. Comparison of BW of the adult flies with indicated genotypes. N=16-23. Error bars: S.E.M. ***, $p < 0.0005$; n.s.: not significant by ANOVA Tukey's test.

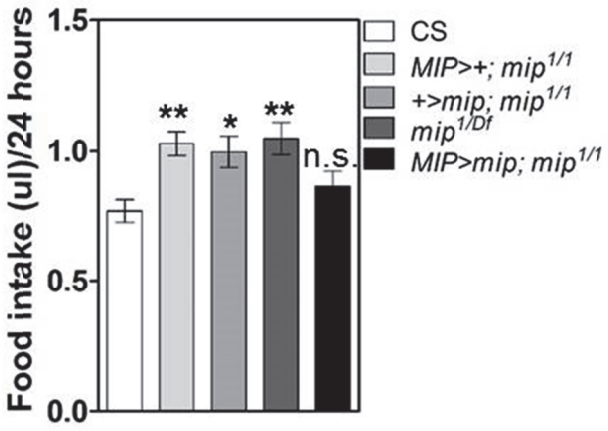

Figure 44. The fly mutants for MIP show increased food intake which could be fully rescued by the exogenous expression of MIP in MIP neurons. Twenty-four-hour food intake by the adult flies with indicated genotypes. N=13-18. Error bars: S.E.M. *, $p < 0.05$; **, $p < 0.005$; n.s.: not significant by by ANOVA Tukey's test.

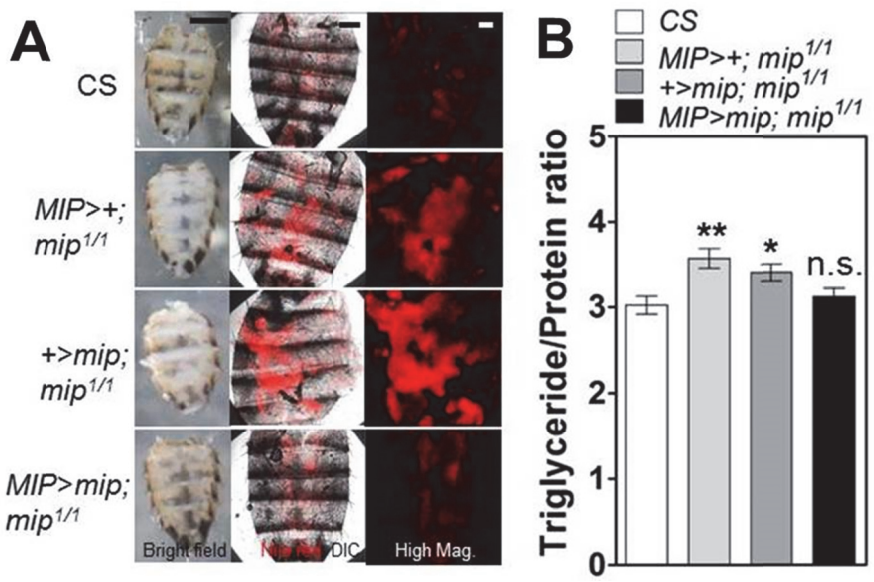

Figure 45. The fly mutants for MIP show increased fat storage which could be fully rescued by the exogenous expression of MIP in MIP neurons. (A) Left: Bright-field images of the adult abdomen of indicated genotypes. The scale bar represents 0.5 mm. Middle: Confocal images of the abdomens stained with Nile red are shown. The scale bar represents 200 μm. Right: High-magnification images of Nile-red-stained fat tissues are shown. The scale bar represents 100 μm. **(B)** Normalized triglyceride level of the adult abdomens of indicated genotypes. N=12. Error bars: S.E.M. *, $p < 0.05$; **, $p < 0.005$; n.s.: not significant by ANOVA Tukey's test.

MIP was required for MIP neuron-mediated BW regulation

To examine whether *mip* is required for the BW loss caused by MIP neuron activation. Remarkably, activating MIP neurons in the flies lacking *mip* gene ($mip^{1/1}$) could not reduce BW, whereas the same manipulation reduced BW by 20% in the flies with intact *mip* **(Fig. 46)**. These results confirm that MIP regulates BW negatively: elevating MIP signaling decreases BW, whereas suppressing MIP signaling increases BW.

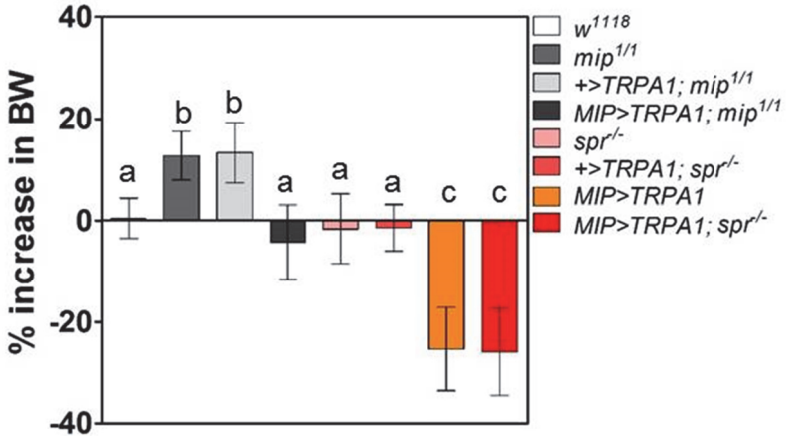

Figure 46. Activation of MIP neurons in WT and SPR mutant background decreases BW, but not in the MIP mutant flies. Comparison of BW of the adult flies with indicated genotypes. N=16-27. Error bars: S.E.M. Different alphabetic letters indicate the statistical significance ($p < 0.0005$ by one-way ANOVA Tukey's test).

MIP regulates BW independently of the sex peptide receptor (SPR)

To further understand through what mechanism MIP regulates feeding activity and BW, I examined the role of the SPR, the only known receptor for MIP. Previous studies showed that *mip* encodes agonists that are highly potent and selective for SPR and that MIP signals through SPR to promote the sleep-like state in *Drosophila* (Oh et al., 2014). Thus, I asked whether SPR also mediates MIP functions in BW regulation. To our surprise, unlike *mip* mutants, the SPR-deficient mutant ($spr^{-/-}$) showed no sign of BW increase compared to controls. Furthermore, activation of MIP neurons could still reduce BW in the SPR-deficient mutant, to the same degree as in the control background **(Fig. 46)**. These observations indicate that SPR does not likely to mediate MIP actions relevant to the BW control, suggesting the presence of at least one additional receptor for MIP.

MIP neurons mediate olfactory anorexigenic responses

Based on the observations that disruption of MIP pathway induced obesity by making flies overeat and silencing MIP neurons did not cause obesity in the restricted food condition, I thus wondered whether MIP activity is associated directly with feeding motivation. To examine this, I performed a T-maze assay in which flies were given a choice between food odor and no odor. When flies become hungry and motivated to eat, they are readily attracted to food odor (Miyamoto et al., 2012) **(Fig. 47)**. I observed that *MIP>TNT* flies became highly attracted to various food odors more strongly than *MIP>impTNT* control flies did **(Fig. 48)**. Similar results were obtained from *mip* mutant flies. Furthermore, restoring *mip* expression in the mutant suppressed the elevated attraction to the food odor to the WT level **(Fig. 49)**. Conversely, activation of MIP neurons made flies exhibit moderate, but significant avoidance to the food odors, producing a characteristic anorexic symptom.

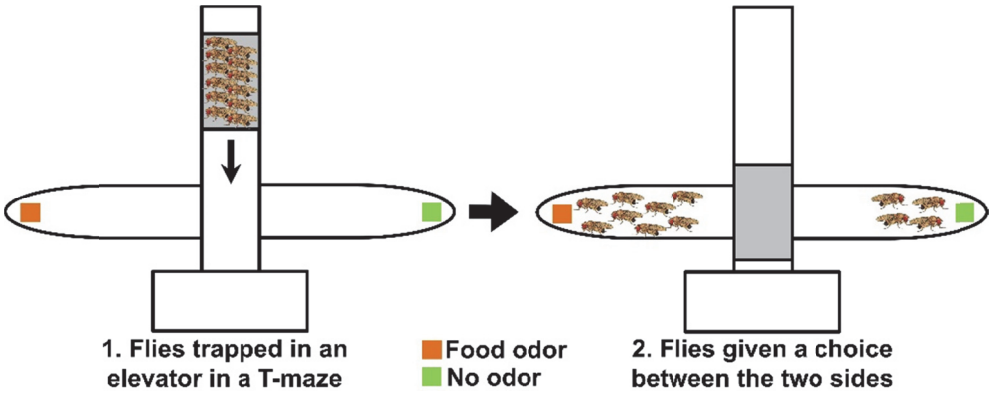

Figure 47. Attraction response of starved flies can be measured in a T-maze. Schematic diagram describing T-maze olfactory choice assay. The orange and green squares indicate source of food odor and water (no odor).

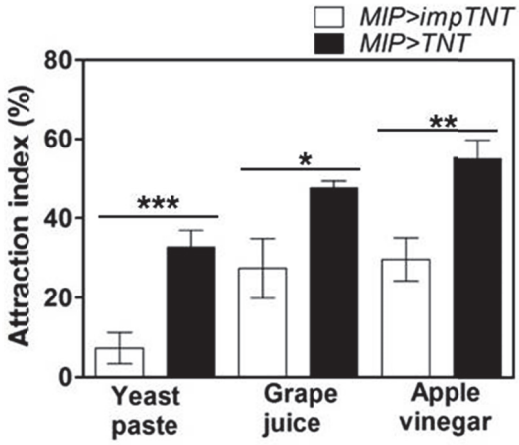

Figure 48. *MIP>TNT* flies are readily attracted to various food odors. Level of attraction to three different food odors by the flies with indicated genotypes. N=6-13. Error bars: S.E.M. *, $p < 0.05$; **, $p < 0.005$; ***, $p < 0.0005$ by unpaired *t-test*.

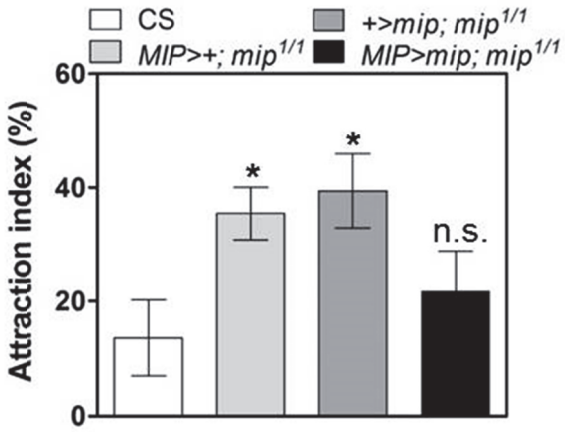

Figure 49. The fly mutants for MIP show BW increase phenotype which can be rescued by the exogenous expression of MIP in MIP neurons. Level of attraction to yeast paste by the flies with indicated genotypes. N=23. Error bars: S.E.M. *, $p < 0.05$; n.s.: not significant by ANOVA Tukey's test.

Behavioral paradigm to measure satiety using PER

Satiety is a motivational state of feeding, and the hallmark of satiation is blunted sensitivity to food tastes, particularly to sugars (Edgecomb et al., 1994; Kawai et al., 2000; Shiraiwa and Carlson, 2007). In flies, the gustatory sensitivity to food can be measured by monitoring the PER (Shiraiwa and Carlson, 2007), of which frequency decreases proportionally as degrees of satiety increase. Indeed, I observed that WT flies raised under *ad libitum* conditions exhibited weak PER to 10% (292 mM) sucrose solution, and the PER gradually increased as the starvation period increased and the degree of satiety decreased. In our setup, the increase in PER peaked at approximately 18 hours of starvation **(Fig. 50)**.

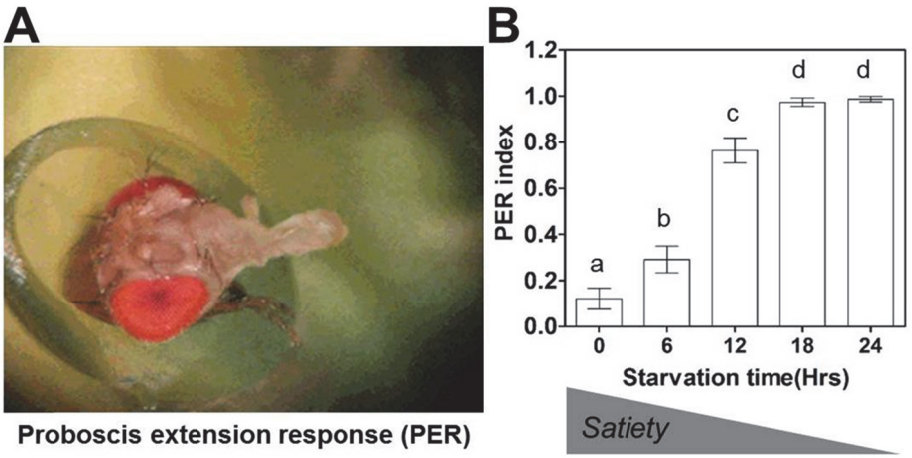

Figure 50. Satiety negatively correlates with the PER responses induced by increasing starvation times. (A) A fly extending its proboscis to food source as a PER response. **(B)** PER profile by WT (CS) flies to 292 mM (10%) sucrose after various starvation periods. N=12. Error bars: S.E.M. Different alphabetic letters indicate the statistical significance ($p<0.05$ by ANOVA Tukey's test).

Suppressing MIP pathway made flies lack satiety

Using the PER response, I asked whether the activity of MIP neurons is linked to the state of satiety. I compared PER of the flies having silenced MIP neurons in high (0 hours of starvation) and low satiety (18 hours of starvation) conditions. Remarkably, satiated *MIP>TNT* flies exhibited significantly increased PER, as if they were starved, compared to controls (*MIP>impTNT*). However, this effect was not present when these flies were starved for 18 hours, likely due to a ceiling effect. Notably, 18 hr-starved *MIP>TNT* flies still exhibited elevated level of food intake regardless of starvation compared to *MIP>impTNT* control flies, indicating that MIP neuron silencing-induced increased feeding is starvation-independent **(Fig. 51)**. The elevated PER in satiated *MIP>TNT* flies was tightly associated with increase of food intake **(Fig. 52)**. Likewise, *mip* mutants also exhibited elevated PER regardless of previous feeding experience, and restoring *mip* expression in the mutants rescued the PER phenotype **(Fig. 53)**.

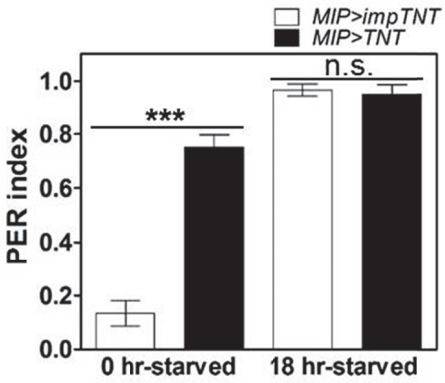

Figure 51. Satiated *MIP>TNT* flies still show increased PER response to food. PER of the flies with indicated genotypes in satiated condition (0 hr starved) and starved condition (18 hr starved). N=10. Error bars: S.E.M. ***, $p < 0.0005$; n.s.: not significant by unpaired *t*-test.

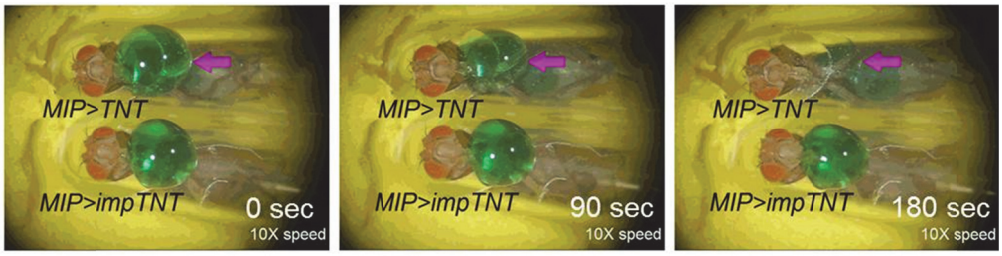

Figure 52. A satiated *MIP>TNT* fly eats as if starved. Captured images from video recording of a satiated *MIP>TNT* fly responding to green food solution.

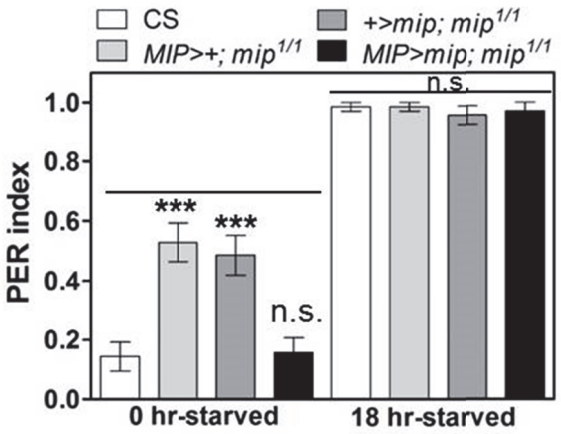

Figure 53. Satiated fly mutants for MIP show increased PER. PER of the flies with indicated genotypes in satiated condition (0 hr starved) and starved condition (18 hr starved). N=22. Error bars: S.E.M. ***, $p < 0.0005$; n.s.: not significant by ANOVA Tukey's test.

Activating MIP pathway induced satiety

Conversely, I examined whether activation of MIP neurons makes flies induce satiety by incubating *MIP>TRPA1* flies at 30°C and testing their PER. Remarkably, the starved flies with activated MIP neurons showed markedly reduced PER compared to control flies **(Fig. 54)**. Thus, enhancing MIP activity made 18 hour-starved flies behave like those that never experienced starvation. Taken together, I concluded that MIP neurons function as an anorexigenic center whose activity encodes the state of satiety in the *Drosophila* brain.

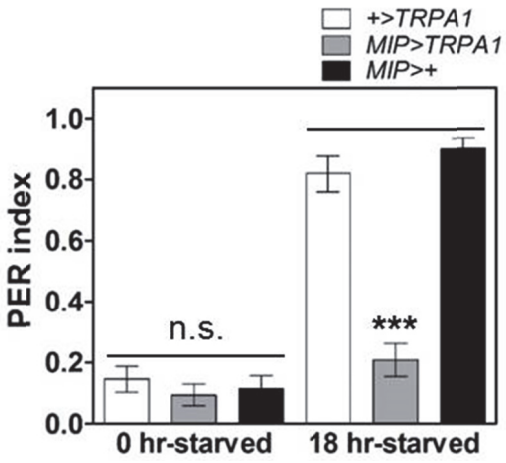

Figure 54. Starved flies with activated MIP neurons show blunted PER responses to food at 30°C. PER of the flies with indicated genotypes in satiated and starved condition. N=12. Error bars: S.E.M. ***, $p < 0.0005$; n.s.: not significant by ANOVA Tukey's test.

PART 3

A subset of the ellipsoid body neurons labeled by 48899-GAL4 negatively regulates food intake

Introduction

The ellipsoid body (EB) is a characteristic ring-shaped neural structure that comprises the central complex in *Drosophila* brain. The EB neurons are subdivided by R1-4 subgroups of neurons and each subgroup is known to be specifically involved in visual perception, locomotive activity and olfactory memory (Ilius et al., 1994; Neuser et al., 2008; Ofstad et al., 2011; Wu et al., 2007; Zhang et al., 2013). Recently, a subgroup of the EB neurons has been reported to mediate hunger responses via a brain-specific sodium/solute co-transporter, indicating its role in feeding regulation (Dus et al., 2013; Park et al., 2016).

48899-GAL4 is made of ~3 kb intronic fragment of the gene encoding a nicotinic acetylcholine receptor alpha 5 (*nAChRalpha5*; CG32975) fused with GAL4. I observed that *48899-GAL4* labels a subgroup of the EB neurons with the characteristic expression pattern.

In this chapter, I show that the EB subset is required for 48899 neuron-mediated feeding regulations possibly involving a type of serotonin receptor.

Satiated flies with silenced 48899 neurons still overfed

Initially from the screen, I revealed that the flies with silenced 48899 neurons showed hyperphagic phenotype. In the assay, I used starved flies. Thus, I wondered whether *48899>TNT* flies still overeat in *ad libitum* condition (satiated). Remarkably, I observed that *48899>TNT* flies reared on a fly instant food containing blue dye were still hyperphagic compared to control flies (*48899>impTNT*) **(Fig. 55)**.

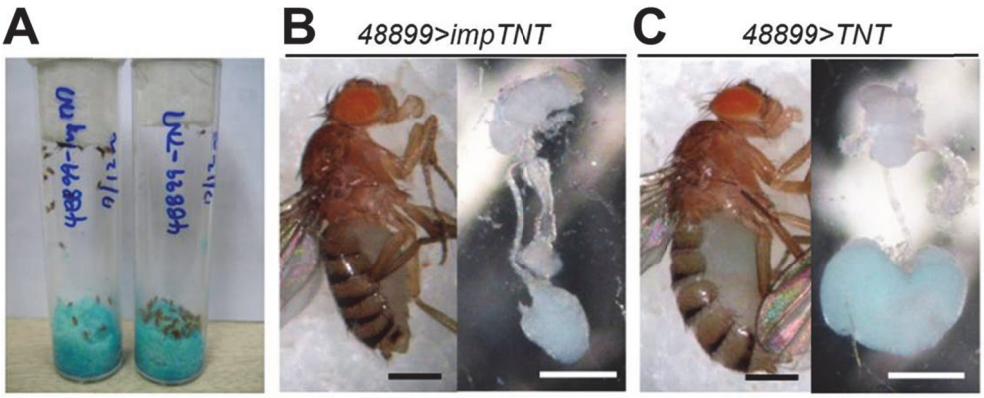

Figure 55. Satiated *48899>TNT* flies show hyperphagic symptom. (A) Two fly vials containing *48899>TNT* and *48899>impTNT* control flies reared on a colored fly instant food (blue material on the bottom). **(B)** Image of a satiated control fly and the dissected stomach (blue). Scale bars: 0.5 mm. **(C)** Image of a satiated *48899>TNT* fly and the dissected stomach (blue). Scale bars: 0.5 mm.

Activation of 48899 neurons induces hypophagia

To examine alteration of food intake by activation 48899 neurons, I made flies carrying UAS-TRPA1 and *48899-GAL4* (*48899>TRPA1*), incubated *48899>TRPA1* flies at 30°C and tested their food intake. As a result, I observed that the flies with activated 48899 neurons showed significant reduction of food intake **(Fig. 56)**.

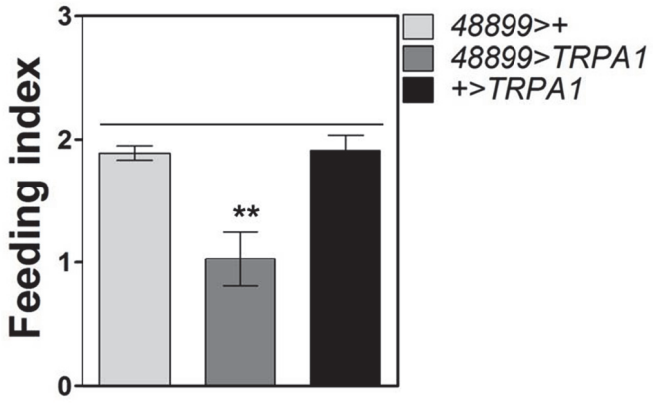

Figure 56. Activation of 48899 neurons elicits decreased food intake. Comparison of feeding score by *48899>TRPA1* and the control flies at 30°C. N=8. Error bars: S.E.M. **, $p<0.001$ by ANOVA Tukey's test.

Mimicry of hunger states induced by silencing 48899 neurons

To analyze the feeding response of satiated *48899>TNT* flies, I video recorded PER of the flies upon providing food. As a result, I observed that satiated *48899>TNT* flies manifested the earlier initiation of food intake compared to controls **(Fig. 57)**. This indicates that 48899 neurons normally suppress food intake likely via inducing satiety. In other words, silencing 48899 neurons induces flies hungry state to initiate food intake. Another trait of hunger response is the enhanced attractive responses to food odor upon prolonged starvation of flies. Thus, I asked whether *48899>TNT* flies become attracted to a food odor and indeed these flies showed enhanced olfactory preference to food odor **(Fig. 58)**.

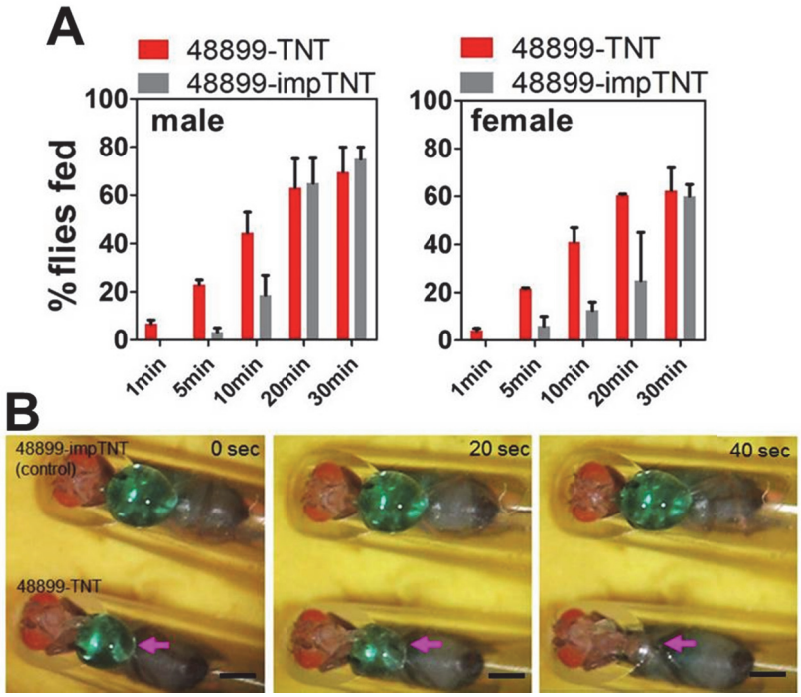

Figure 57. Satiated *48899>TNT* flies showed traits of hunger. (A) Comparisons of % of fed *48899>TNT* and control flies for the given periods of feeding. N=5. Error bars: S.E.M. Statistical significance was observed at 5 and 10 minute of two groups by two-way ANOVA Bonferroni post-test. **(B)** Captured images from a video recording from feeding responses of *48899>TNT* and control flies.

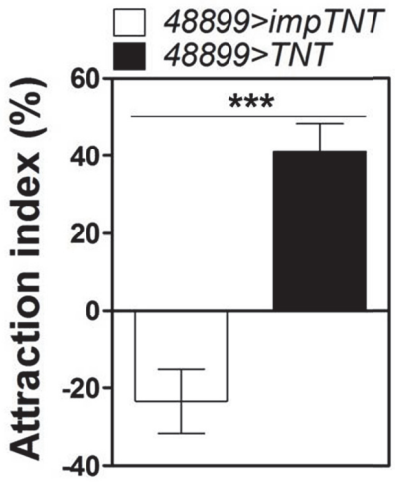

Figure 58. Satiated *48899>TNT* flies show attraction responses to food. Comparison of olfactory preference to food odor by satiated *48899>TNT* flies and the control flies. N=6. Error bars: S.E.M. ***, $p<0.0005$ by unpaired *t*-test.

Visualization of 48899 neurons

Next, I visualized 48899 neurons by driving the expression of mCD8GFP reporter using *48899-GAL4*. I found that *48899-GAL4* labeled a few neural structures in the brain including the optic lobes, *pars intercerebralis* (PI) and the ellipsoid body (EB) **(Fig. 59)**.

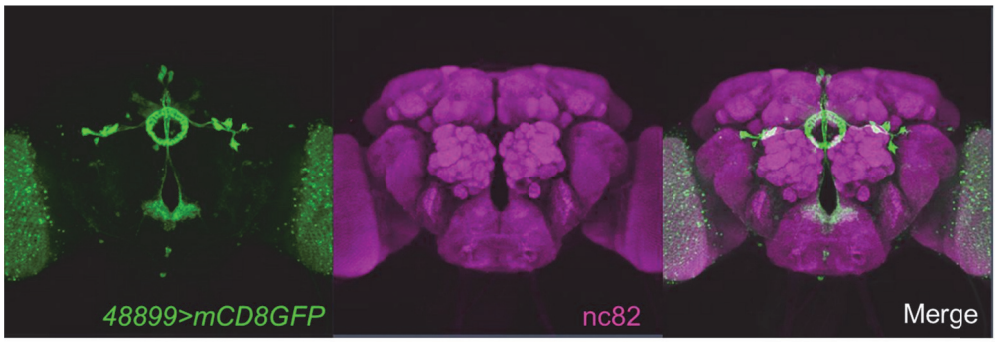

Figure 59. *48899-GAL4* is expressed in a few characteristic regions of the brain. Confocal images of the brain expressing *48899>mCD8GFP* stained with the neuropil marker, nc82.

The PI cells of 48899 neurons were DH44-expressing neurons

Among the neural structures, I paid first attention to the PI neurons, since PI neurons produce variety of neuropeptides such as Dilps that are implicated in feeding regulation (Dus et al., 2015; Soderberg et al., 2012). Indeed, I observed that the diuretic hormone 44 (DH44) among neuropeptides tested was colocalized with the PI cells of 48899 neurons **(Fig. 60)**.

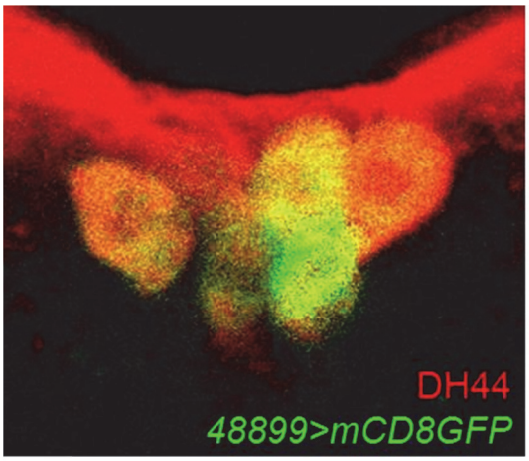

Figure 60. DH44 is expressed in *pars intercerebralis* (PI) of 48899 neurons. Confocal image of the cell bodies of PI, the counterpart of mammalian hypothalamus, expressing mCD8GFP reporter driven under *48899-GAL4* driver, co-stained anti-GFP and anti-DH44 antibody.

The DH44 neurons were dispensable for 48899 neuron-mediated feeding control

To examine whether the DH44 neurons are required for 48899-mediated feeding phenotype, I obtained a *DH44-GAL4* driver and *DH44-GAL80* lines. Using *DH44-GAL4* driving expression of mCD8GFP, I confirmed that the cell bodies of DH44 neurons were located in the PI and send axons to the SEZ like the 48899-DH44 neurons **(Fig. 61)**. I then either silenced the DH44 neurons by expressing *UAS-TNT* driven by *DH44-GAL4* driver or relived the TNT expression in DH44 cells in 48899>TNT flies using *DH44-GAL80* to check the requirement of DH44 cells in feeding regulation. I observed that *DH44>TNT* flies did not show any sign of feeding defects **(Fig. 61)** and also *48899>TNT* flies carrying *DH44-GAL80* still showed the overeating phenotype **(Fig. 62)**, indicating DH44 neurons were dispensable for food intake control.

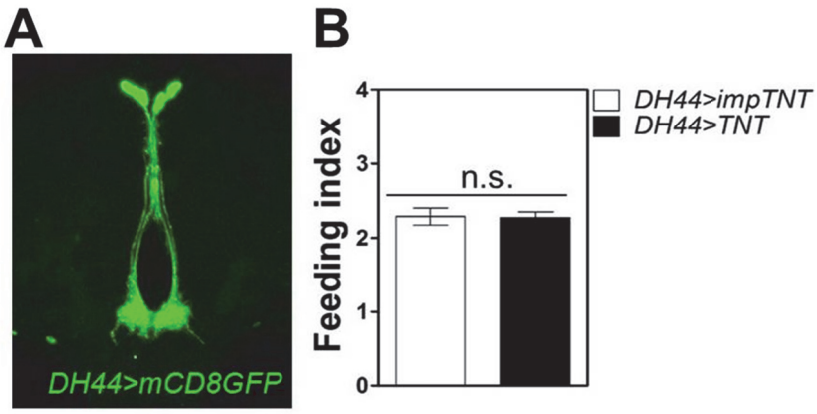

Figure 61. *DH44-GAL4* labels the PI of 48899 neurons and silencing DH44 neurons did not alter food intake. (A) Confocal image of the brain expressing *DH44>mCD8GFP.* **(B)** Comparison of feeding score by the flies with silenced DH44 neurons (*DH44>TNT*) and control flies (*DH44>impTNT*). N=5. Error bars: S.E.M. n.s. not significant by unpaired *t*-test.

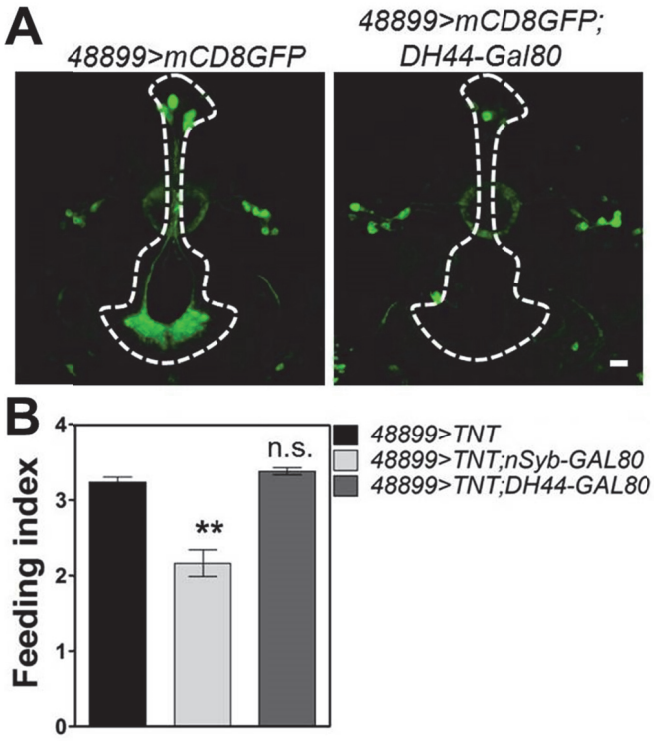

Figure 62. *DH44-GAL80* selectively suppresses *48899-GAL4*-driven GFP signal in the PI and the selective blocking of TNT expression in the PI of *48899>TNT* flies has no effect in food intake. (A) Confocal images of the brain expressing *48899>mCD8GFP* (left) and *48899>mCD8GFP; DH44-GAL80* (right). Scale bar: 10 μm. **(B)** Comparison of food intake by *48899>TNT* flies and *48899>TNT* flies carrying either *nSyb-GAL80* or *DH44-GAL80*. N=8. Error bars: S.E.M. **, $p<0.005$; n.s.: not significant by ANOVA Tukey's test.

EB R4 neurons were responsible for the feeding phenotype

Another prominent structure in 48899 neurons was the EB that was labeled by anti-NMDAR2 antibody indicating that the subgroup of the EB is R4 (Wu et al., 2007) **(Fig. 63)**. Interestingly, I observed that *Cha-GAL80* selectively suppressed GFP signals in the EB R4 neurons. Therefore, I wondered whether inclusion of *Cha-GAL80* rescues the feeding phenotype by *48899>TNT* flies. Remarkably, the flies with silenced 48899 neurons except for the EB neurons indeed showed restored feeding phenotype, suggesting the critical role of EB R4 neurons in food intake **(Fig. 64)**.

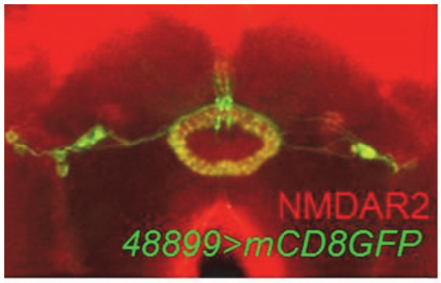

Figure 63. The EB R4 specific NMDAR2 is expressed in the EB subset of 48899 neurons. Confocal image of the brain expressing *48899>mCD8GFP* stained with anti-NMDAR2 antibody.

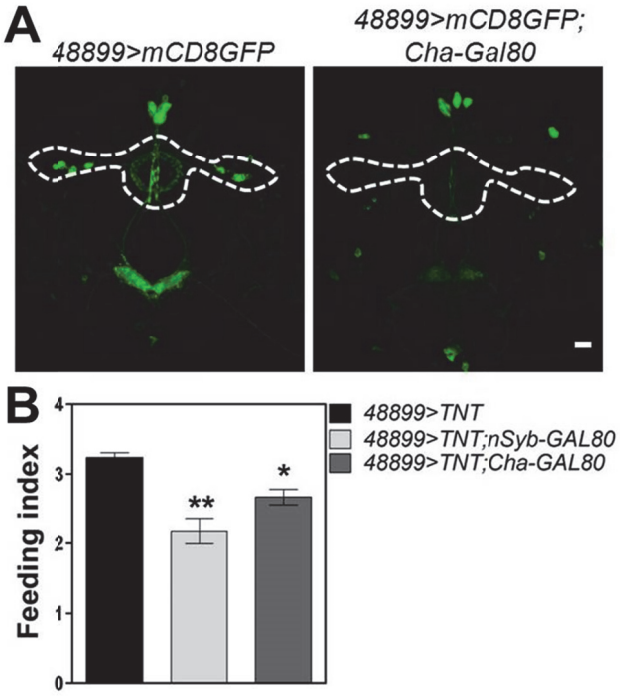

Figure 64. *Cha-GAL80* selectively suppresses *48899-GAL4*-driven GFP signal in the EB subset and the selective blocking of TNT expression in the EB rescue the overeating phenotype of *48899>TNT* flies. (A) Confocal images of the brain expressing *48899>mCD8GFP* (left) and *48899>mCD8GFP; Cha-GAL80* (right). Scale bar: 10 μm. **(B)** Comparison of food intake by *48899>TNT* flies and *48899>TNT* flies carrying either *nSyb-GAL80* or *Cha-GAL80*. N = 8. Error bars: S.E.M. *, $p < 0.05$; **, $p < 0.005$ by ANOVA Tukey's test.

Additional GAL4 lines that label EB R4 neurons elicited hyperphagic phenotype when silenced

Consistent with the results, I found that additional GAL4 drivers that labeled EB R4 neurons also showed similar feeding phenotype when crossed to TNT like *48899-GAL4* driver during the course of the screen. *46550-GAL4* also marked EB R4 neurons and exhibited a dramatic hyperphagic symptom upon the neuronal silencing **(Fig. 65)**. Additionally, I obtained defined EB-specific GAL4 lines and examined the role of EB R1, 2 and 3 neurons in comparison to EB R4 neurons (Renn et al., 1999a). Flies in which each group of R1, 2 or 3 neurons was silenced showed no considerable changes in food intake, except for the EB R4 neurons showing significant feeding increase when silenced (data not shown), further substantiating our conclusion that EB R4 neurons are critical for feeding phenotype.

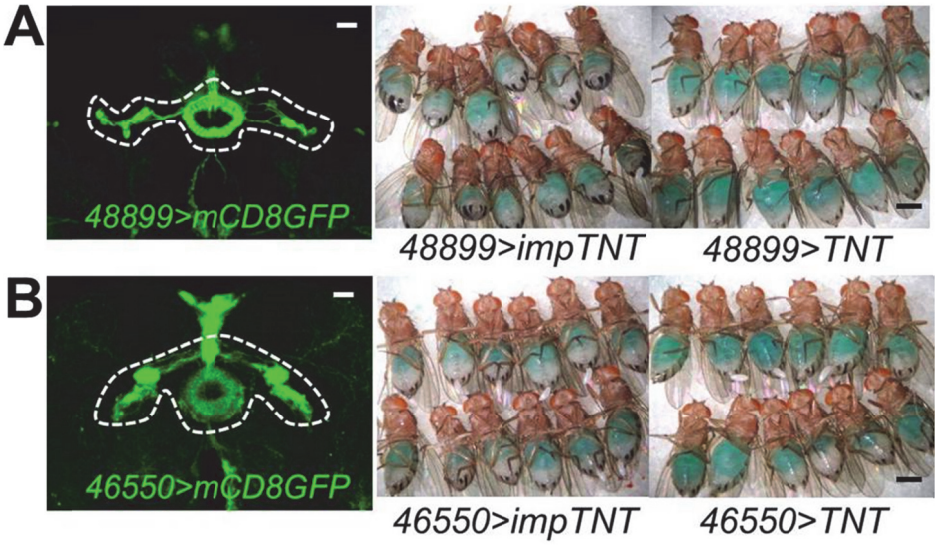

Figure 65. ***46550-GAL4*** **driver that labels the EB R4 neurons showed hyperphagic phenotype similar to 48899 when silenced. (A)** Left: Confocal image of the brain expressing *48899>mCD8GFP* stained with anti-GFP antibody. Scale bar: 20 μm. Middle and right: visualized accumulation of green-dyed food in the stomach of 48899>TNT flies and the control flies. Scale bar: 0.5 mm. **(B)** Left: Confocal image of the brain expressing *46550>mCD8GFP* stained with anti-GFP antibody. Scale bar: 20 μm. Middle and right: visualized accumulation of green-dyed food in the stomach of *46550>TNT* flies and the control flies. Scale bar: 0.5 mm.

Serotonin receptors might function in 48899 neurons to mediate feeding

Drosophila possesses five different serotonin (5-HT) receptors: 5-HT1A, 5-HT1B, 5-HT2A, 5-HT2B, and 5-HT7). 5-HT receptors are expressed in various regions in the CNS including the EB structures and 5-HT signaling mediates various behavioral responses such as feeding behaviors (Becnel et al., 2011; Mabuchi and Tanaka, 2016). Therefore, I sought to examine whether 5-HT receptors are required for the 48899-mediated feeding responses. To do so, I used UAS-RNAi lines against each 5-HT receptor driven by *48899-GAL4* driver and compared the flies' food intake. Interestingly, the knockdown of 5-HT1A using two different RNAi lines in 48899 neurons strongly inhibited food intake compared to controls and *48899>TNT* flies that showed increased food intake. This indicates that 5-HT1A likely suppresses the activity of 48899 neurons in mediating food intake. Notably, 5-HT2A also showed moderate hypophagic phenotype **(Fig. 66 and Table 5)**.

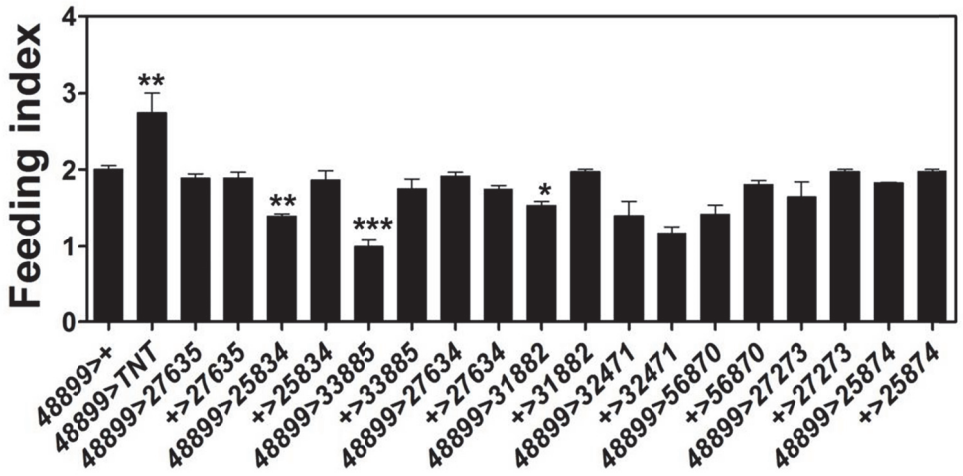

Figure 66. RNAi knockdown of 5-HT1A in 48899 neurons elicits hypophagic phenotype. Comparisons of food intake of the flies expressing 5-HT receptor RNAi driven by *48899-GAL4* and the GAL4 alone or UAS transgene alone control flies. N=5-6. Error bars: S.E.M. *, $p < 0.05$; **, $p < 0.005$; ***, $p<0.0005$ by ANOVA Dunnett's test.

Table 5. The BDSC stock numbers of 5-HT receptor RNAi lines.

5-HT1A RNAi	25834, 33885
5-HT1B RNAi	27635, 27634
5-HT2A RNAi	31882, 56870
5-HT2B RNAi	25874
5-HT7 RNAi	32471, 27273

48899 neurons responding to internal energy level

Having shown that 48899 neurons regulate the level of food intake, I wondered whether these neurons function in selection of nutritive food. To test this, I fed *48899>TNT* flies on D-glucose, a metabolizable sugar or L-glucose a non-metabolizable sugar that produces no energy. Remarkably, *48899>TNT* flies became preferentially hyperphagic on D-glucose **(Fig. 67)**. To check whether 48899 neurons respond to internal energy status, I monitored the strength of GFP expression driven by *48899-GAL4* under starvation. After 24 hours of starvation, *48899>mCD8GFP* flies showed markedly reduced level of GFP expression in 48899 neurons **(Fig. 67)**. Together, I concluded that 48899 neurons comprise a part of neural machinery responding to internal nutritive status.

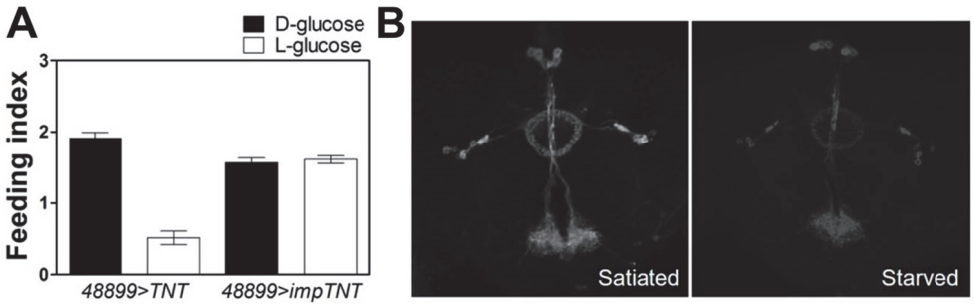

Figure 67. 48899 neurons respond to the internal energy level. (A) Comparison of food intake by *48899>TNT* and control flies on D- versus L-glucose. N=9-13. Error bars: S.E.M. **(B)** Confocal images of the brain expressing *48899>mCD8GFP* in a satiated or starved condition.

PART 4

Misato is required for the visceral muscle maintenance for intestinal homeostasis in *Drosophila*

Introduction

Misato (mst) encodes a protein that is highly conserved among animal species and that retains a mixture of peptide motifs found in tubulins and myosins (Gurvitz et al., 2002). In human, *misato* is named as *misato homolog 1 (msto1)* shown to localize to mitochondria to regulate subcellular distribution of mitochondria and their morphology (Kimura and Okano, 2007). Intriguingly, the investigation of the population with inflammatory bowel disease (IBD) has revealed an SNP on the locus 1q22 containing *msto1* (Jostins et al., 2012). In *Drosophila* null mutations on *mst* elicited larval lethal phenotype associated with abnormal chromosomal segregation during cell division (Mottier-Pavie et al., 2011). A recent study has revealed that *mst* regulates the formation of mitotic spindles during mitosis by interacting with the TCP-1 tubulin chaperone complex (Palumbo et al., 2015).

The *Drosophila* intestine is comprised of the intestinal epithelial cells that include enterocytes (ECs), enteroblasts (EBs), enteroendocrine cells (EEs) and intestinal stem cells (ISCs), and the surrounding visceral muscles (Guo et al., 2016). Upon damage on the intestine, division of the ISCs is initiated by signaling pathways involving Notch, UPD/JAK/STAT and Hippo signaling pathways to give rise to the intestinal cells for compensation of the

cell loss (Huang et al., 2014; Jiang et al., 2009; Ren et al., 2010). The visceral muscle is known to provide the niche for the dividing ISCs via *wingless* and *egfr* pathways (Lin et al., 2008; Takashima et al., 2008). From the screen, I found that RNAi knockdown of *mst* in the visceral muscles significantly reduced food intake accompanying abnormally enlarged intestine phenotype associated with increased number of ISCs that could be fully rescued by the exogenous expression of *mst*.

In this chapter, I describe a role of *mst* in the visceral muscle survival to maintain the intestinal homeostasis.

RNAi knockdown of *mst* in the muscle tissue elicits decreased food intake.

To investigate the tissue specific role of *mst* in food intake, I expressed *mst RNAi* in the neural tissue, fat body and muscle tissues using *nSyb-GAL4* (Chin et al., 1993)*, cg-GAL4* (Yasothornsrikul et al., 1997) and *mef2-GAL4* drivers (Bour et al., 1995). Remarkably, muscle specific expression of *mst RNAi* (MOM#211) (henceforth, *mef2>mst RNAi*) only elicited significant decrease in food intake compared to other GAL4 lines driving the expression of *mst RNAi* **(Fig. 68)**.

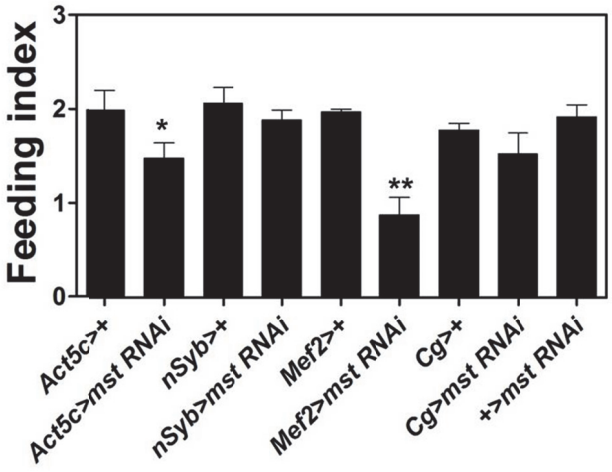

Figure 68. The flies expressing *mst RNAi* driven by *mef2-GAL4* show a severe hypophagic phenotype. Comparisons of food intake of the flies expressing *mst RNAi* in various tissues by tissue-specific GAL4 drivers. N=6. Error bars: S.E.M. *, $p<0.05$; **, $p<0.005$ by ANOVA Tukey's test.

Aged *mef2>mst RNAi* flies exhibit enlarged intestine

After 5days of rearing the *mef2>mst RNAi* flies on a normal fly food, I observed that the flies' abdomen became abnormally swelled compared to control flies **(Fig. 69)**. Based on the observation that these flies were hypophagic, I reasoned why the flies displayed enlarged abdomen by dissecting their belly. Remarkably, the *mef2>mst RNAi* flies had abnormally enlarged intestine compared to controls'. This phenotype was also reproduced with another *mst RNAi* **(Fig. 70)**. To examine whether enlarged intestine was due to the defects in excretion, I fed the flies on the food containing green dye so that I could see their feces. *Mef2>mst RNAi* flies produced much less feces compared to controls, indicating the enlarged intestine is partially owing to the excretion defect **(Fig. 71)**. It is also possible that the enlarged intestine of *mef2>mst RNAi* flies contained increased number of intestinal cells. To test this, I stained the intestine with Hoechst, the marker for nucleus to check the number of cells and observed that the aged *mef2>mst RNAi* flies had more intestinal cells compared to controls **(Fig. 72)**.

Figure 69. *Mef2>mst RNAi* flies display enlarged abdomen. Whole body images of the flies with indicated genotypes.

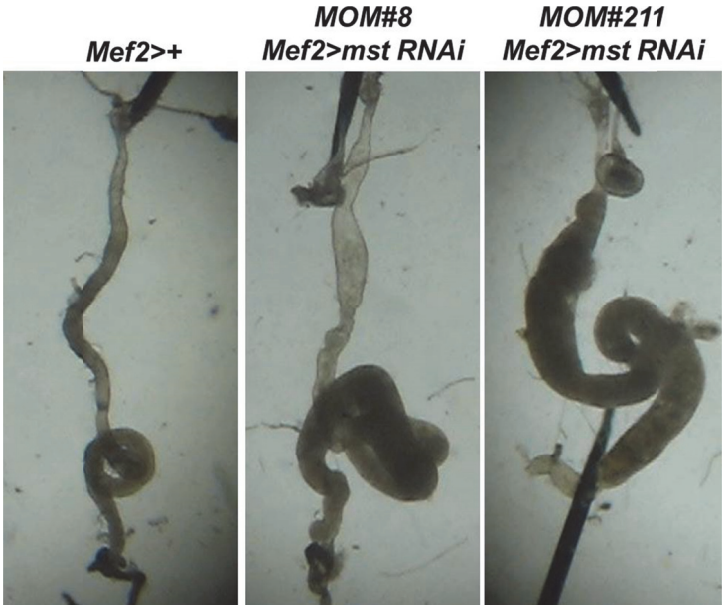

Figure 70. Knockdown of *mst* using two different RNAi lines driven by *Mef2-GAL4* elicited the similar intestinal phenotype. Images of intestines with indicated genotypes.

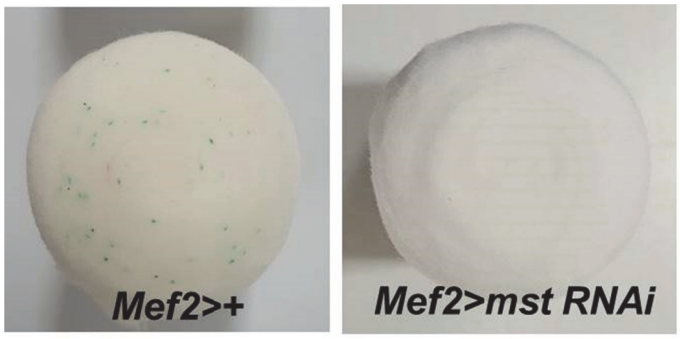

Figure 71. ***Mef2>mst RNAi*** **flies show defects in excretion.** Images of the fly vial cap housed the flies with indicated genotypes fed on green-dyed food.

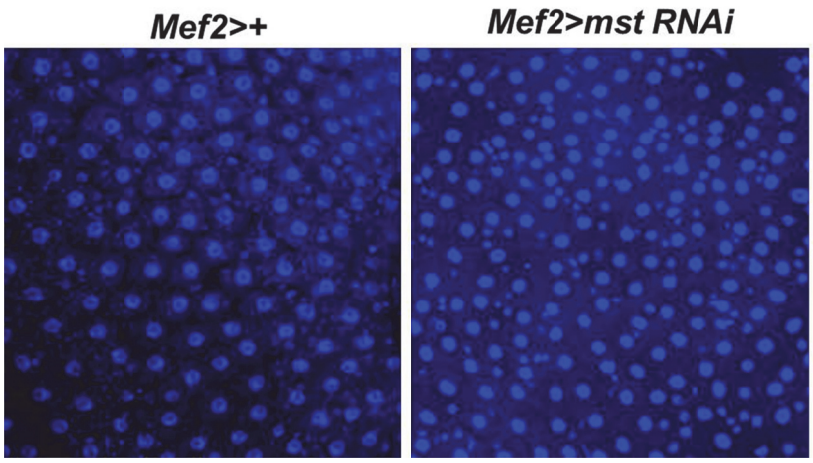

Figure 72. *Mef2>mst RNAi* flies show increased number of intestinal cells.

Images of the intestinal cells with indicated genotypes stained with Hoechst.

Newly-born *mef2>mst RNAi* flies do not show the intestinal phenotypes

To examine whether the intestinal phenotype of *mef2>mst RNAi* flies was due to the developmental defect, I dissected the intestine of newly-born flies and checked the size and intestinal cell number, showing that no significant defect in size and the number was observed compared controls. Also the young *mef2>mst RNAi* flies excrete well comparable to control flies **(Fig. 73)**.

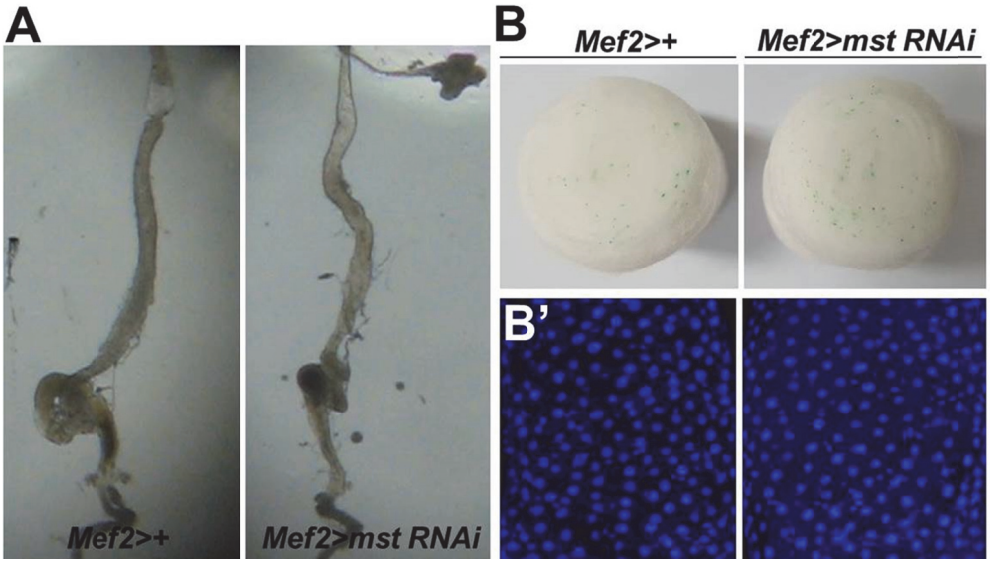

Figure 73. Newly-born *mef2>mst RNAi* flies show normality in the morphology of intestine, excretion and the number of intestinal cells. (A) Images of the dissected intestine from the newly-born flies with indicated genotypes. **(B)** Images of the vial caps that housed the flies with indicated genotypes. **(B')** Confocal images of intestinal cells stained with Hoechst from the young flies with indicated genotypes.

Phenotypical analysis on aged *mef2>mst RNAi* flies

To analyze more phenotypes of aged *mef2>mst RNAi* flie besides the intestinal symptoms, I examined them for locomotive activity **(Fig. 74)**, life span **(Fig. 75)**, starvation sensitivity **(Fig. 76)**, melanization in the intestine **(Fig. 77)**, intestinal permeability **(Fig. 78)**. I observed that the aged flies showed shortened life span, less resistance to starvation, increased level of melanization and permeabilization in the intestine compared to control flies. Intriguingly, however, aged *mef2>mst RNAi* flies showed fairly normal locomotive activity comparable to control flies.

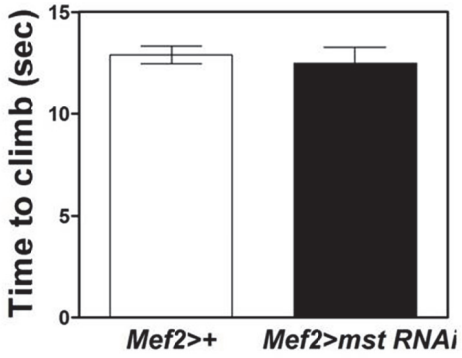

Figure 74. *mef2>mst RNAi* flies show normal locomotive ability. Comparison of the locomotive ability of *mef2>mst RNAi* and control flies. N=6. Error bars: S.E.M. No significant statistical difference was observed by unpaired *t*-test.

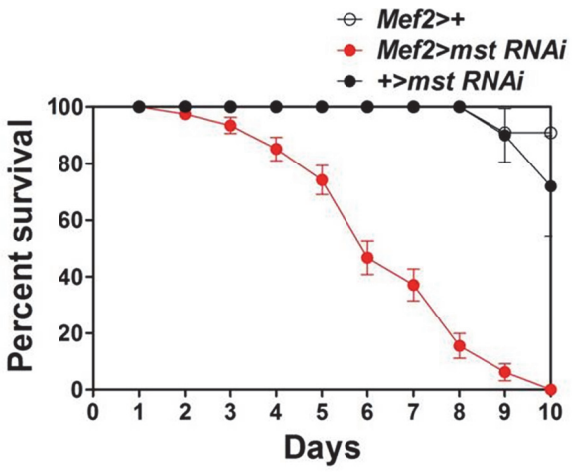

Figure 75. *mef2>mst RNAi* flies show shortened life span. Comparison of life span of *mef2>mst RNAi* and control flies. N=5. Error bars: S.E.M.

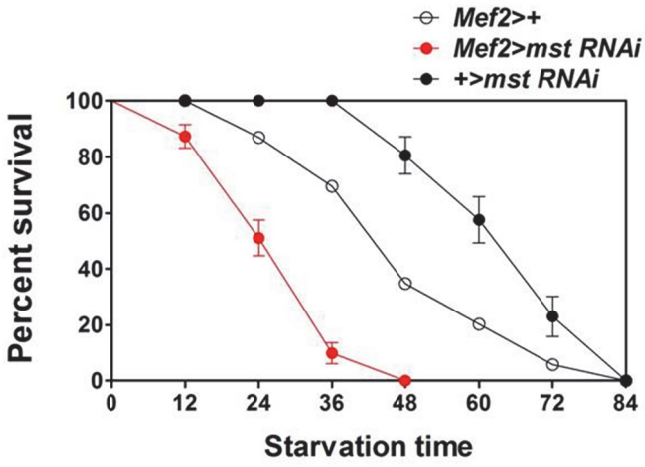

Figure 76. *mef2>mst RNAi* flies show reduced starvation resistance. Comparison of percent survival by *mef2>mst RNAi* and control flies at different starvation periods. N=3-4. Error bars: S.E.M.

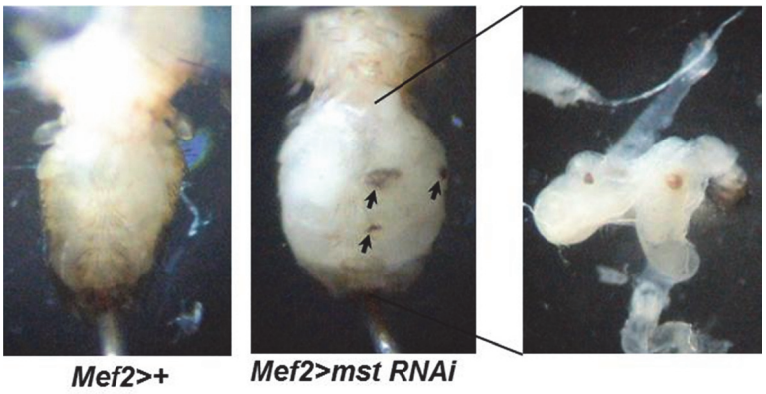

Figure 77. *Mef2>mst RNAi* flies show increased melanization in the intestine. Images of the abdomen and intestine of *mef2>mst RNAi* and control flies.

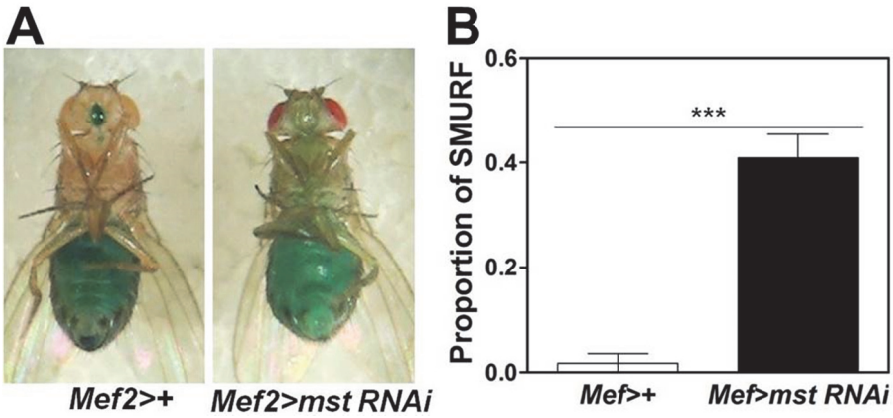

Figure 78. ***Mef2>mst RNAi*** **flies show increased intestinal permeability.** **(A)** Images of the flies with indicated genotypes having the green dye in the body. **(B)** Comparison of proportion of the flies having the dye outside the intestine. N=5. Error bars: S.E.M. ***, $p<0.0005$ by unpaired *t*-test.

Mef2-GAL4 is expressed in the outer layer of the visceral muscle

Mef2-GAL4 is presumed to drive expression of *mst RNAi* specifically in the muscle tissues in *mef2>mst RNAi* flies. To further pinpoint the tissue responsible for the intestinal phenotype, expression pattern of *mef2-GAL4* was visualized by crossing the GAL4 driver to *UAS-mCD8GFP* reporter line. Indeed, *mef2-GAL4* was specifically expressed in the outer layer of the visceral muscle **(Fig. 79)**.

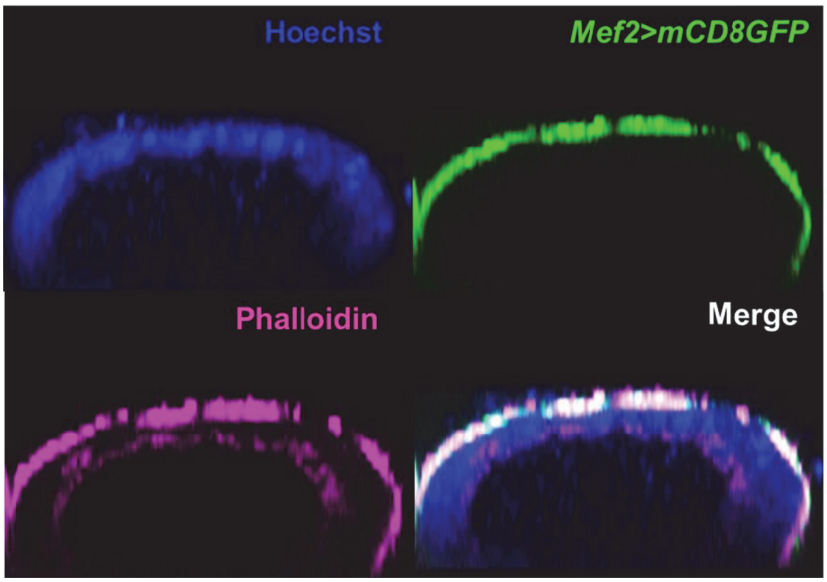

Figure 79. *Mef2-GAL4* is expressed in the outer layer of the visceral muscle. Confocal images of the intestine expressing *mef2>mCD8GFP* stained with Hoechst and Phalloidin-TRITC.

The visceral muscle is responsible for the intestinal phenotype

Surprisingly, *mef2-GAL4* was expressed not only in the visceral muscle, but also the skeletal muscle and neuronal tissues **(Fig. 80)**. To test if any neuronal contribution to the intestinal phenotype exists, I combined the *nSyb-GAL80* (GAL80 inhibits GAL4) transgene with *mef2>mst RNAi* flies. Theoretically, *nSyb-GAL80* inhibits the expression of *mst RNAi* driven by *mef2-GAL4* specifically in neuronal tissues. To support this, *nSyb-GAL80* suppressed the expression of mCD8GFP reporter in the neuronal tissues driven by *mef2-GAL4* **(Fig. 81)**. Based on this, I predicted that *mef2>mst RNAi* flies bearing *nSyb-GAL80* would still show the enlarged intestine if the neuronal tissues are not required for the phenotype. As expected, the flies still exhibited enlarged intestine phenotype, indicating the neuronal tissues are dispensable for the intestinal phenotype by *mst RNAi* **(Fig. 82)**. Also the skeletal muscle-specific GAL4 driver, *mhc-GAL4* (Hunt and Demontis, 2013) driving *mst RNAi* did not elicit any sign of the intestinal phenotype **(Fig. 83)**.

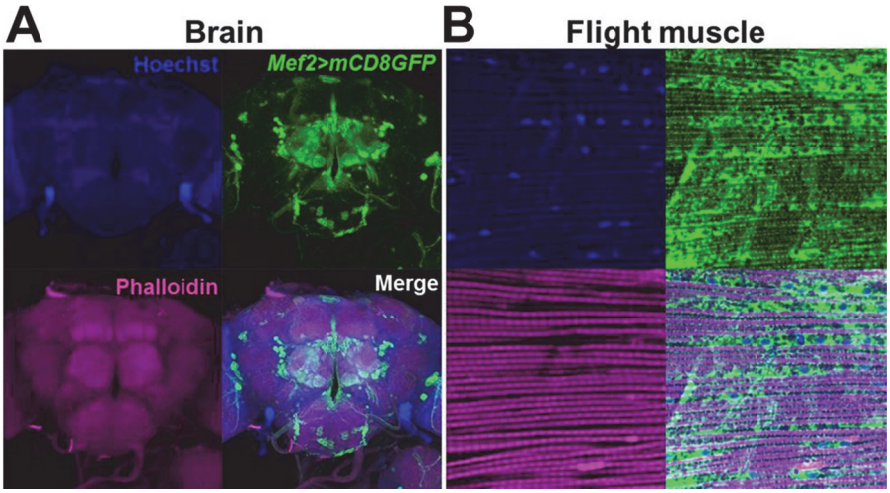

Figure 80. ***Mef2-GAL4*** **is expressed not only in the visceral muscle but also in the neurons and skeletal muscles.** Confocal images of the brain **(A)** and indirect flight muscle **(B)** expressing *mef2>mCD8GFP* stained with Hoechst and Phalloidin-TRITC.

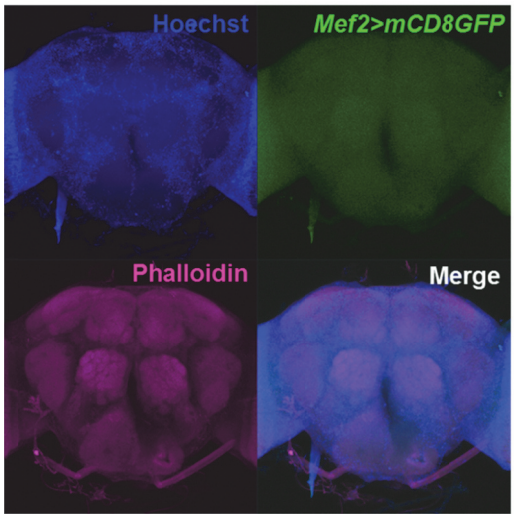

Figure 81. *nSyb-GAL80* suppresses the expression of *mef2-GAL4*-driven GFP expression in the brain. Confocal images of the brain *mef2>mCD8GFP* flies carrying *nSyb-GAL80* stained with Hoechst and Phalloidin-TRITC.

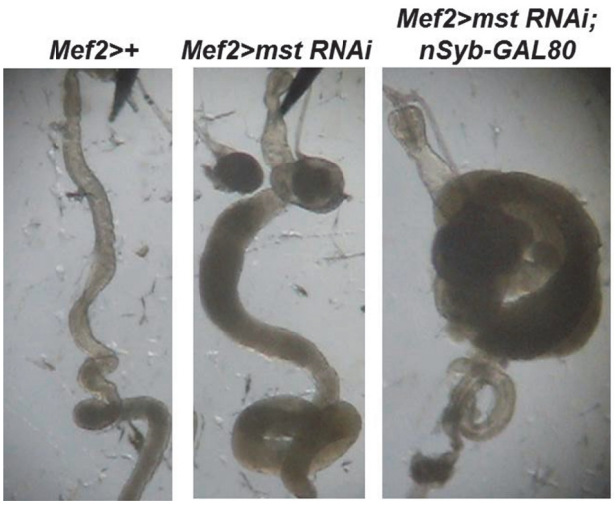

Figure 82. *nSyb-GAL80* does not have an effect on the enlarged intestine phenotype of *mef2>mst RNAi* flies. Bright field images of the intestines with indicated genotypes.

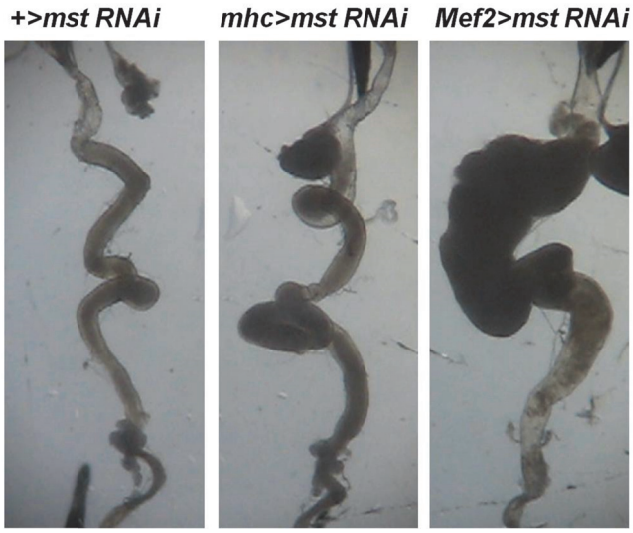

Figure 83. The skeletal muscle GAL4 driver, *mhc-GAL4* does not induce the enlarged intestine phenotype. Bright field **i**mages of the intestines with indicated genotypes.

The visceral muscle is damaged in the aged *mef2>mst RNAi* flies

To examine whether there are any morphological alterations of visceral muscle by RNAi knockdown of *mst*, I stained the visceral muscle tissue of aged *mef2>mst RNAi* flies using phalloidin, a marker for muscle fibers. Remarkably, the aged *mef2>mst RNAi* flies had severely damaged visceral muscle tissues compared to control flies, indicating *mst* functions in the visceral muscle maintenance **(Fig. 84)**.

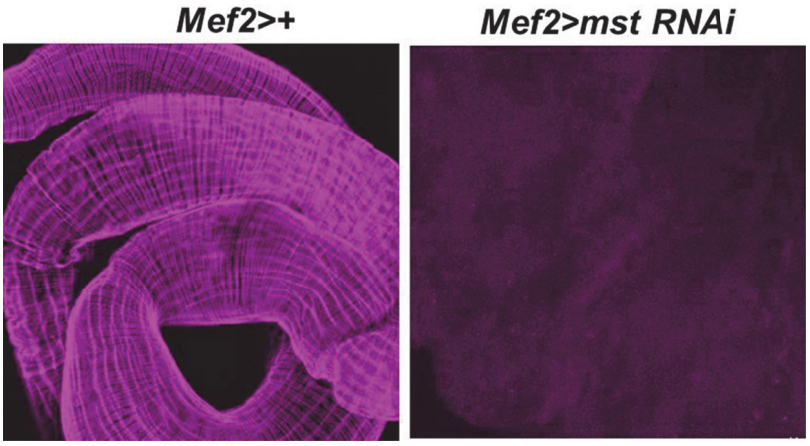

Figure 84. RNAi knockdown of *mst* using *mef2-GAL4* damages the visceral muscle. Images of the intestines with indicated genotypes, stained with Phalloidin-TRITC.

Aged *mef2>mst RNAi* flies showed increased apoptosis in the intestine

Hinted from damaged muscle, I predicted that the intestine became susceptible to the surrounding apoptotic stimuli. To examine this, I performed TUNEL assay on the intestine and showed that TUNEL signal was dramatically elevated in the intestine of the aged *mef2>mst RNAi* flies compared to control and young *mef2>mst RNAi* flies **(Fig. 85)**.

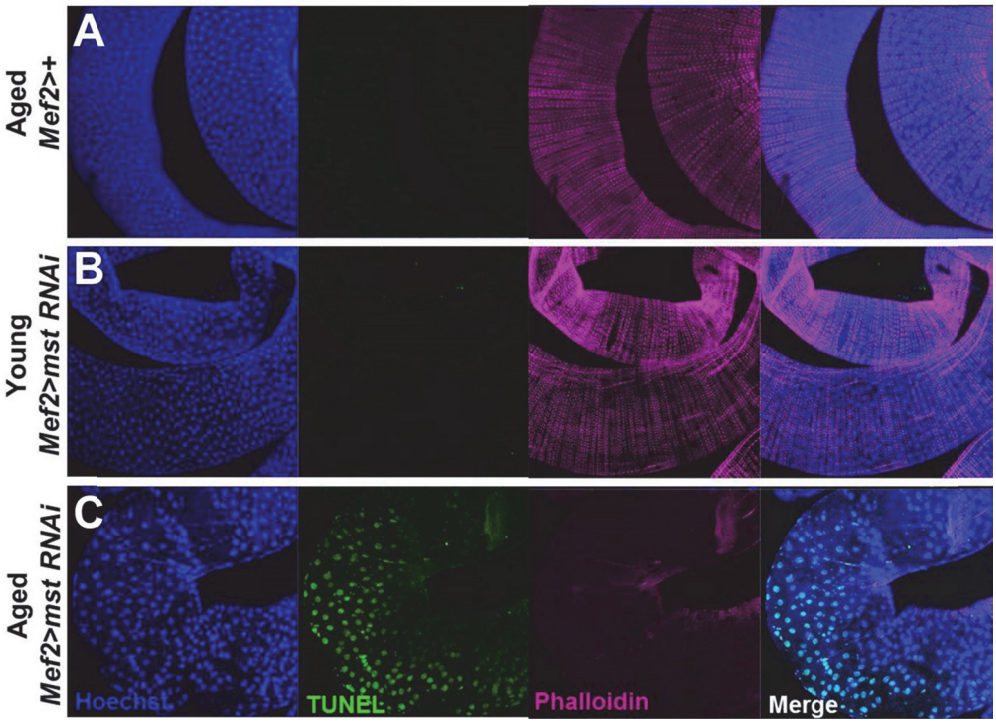

Figure 85. Aged *mef2>mst RNAi* flies exhibit increased apoptosis in the intestine. (A) Confocal images of the intestine of aged control flies, **(B)** young *mef2>mst RNAi* flies, and **(C)** aged *mef2>mst RNAi* flies, treated with the TUNEL reagent.

Intestine of aged *mef2>mst RNAi* flies showed increased level of ISCs

Because the aged *mef2>mst RNAi* flies have more cells to die, there would be a need for ISCs to divide more rapidly. Consistence with this, aged *mef2>mst RNAi* flies showed increased number of BrdU+ cells in the intestine **(Fig. 86)**. To test whether BrdU+ cells are indeed ISCs, I stained the intestine with the antibody against delta, a marker for ISCs and almost BrdU+ cells were delta positive **(Fig. 87)**.

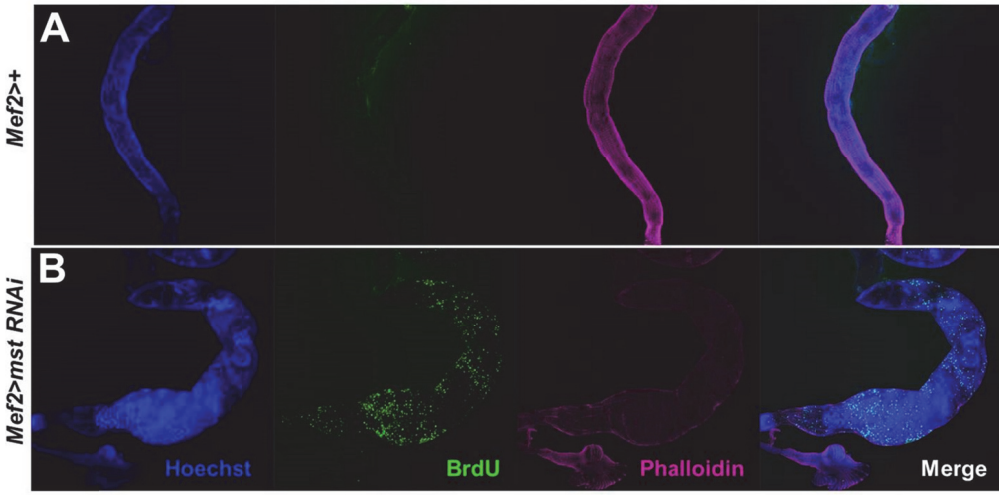

Figure 86. Aged *mef2>mst RNAi* flies exhibit increased number of ISCs in the intestine. (A) Confocal images of the control intestine. **(B)** Confocal images of aged *mef2>mst RNAi* flies treated with BrdU incorporation and stained with Hoechst and Phalloidin-TRITC.

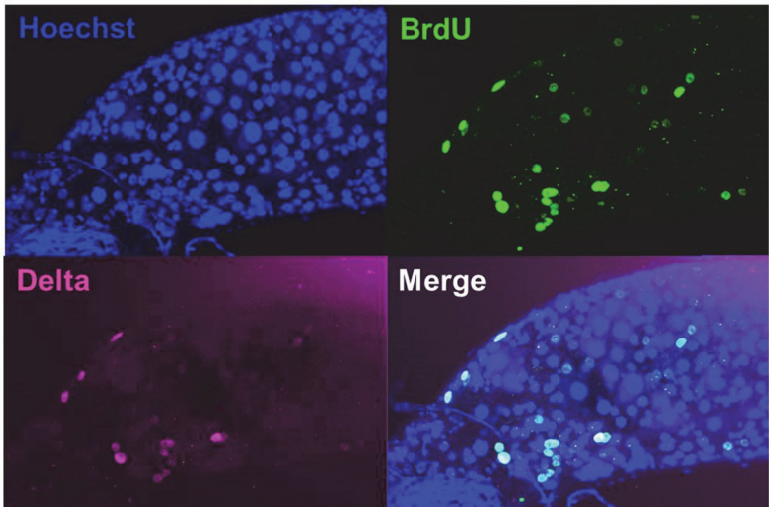

Figure 87. The BrdU-positive cells are indeed ISCs. Confocal images of ISCs in the WT intestine stained with Hoechst, BrdU and anti-Delta antibody (ISC marker).

Exogenous expression of *mst* in the muscle fully rescued the intestinal defects of *mef2>mst RNAi* flies

Having shown that RNAi knockdown of *mst* in the visceral muscles produced morphological defects in the intestine, I sought to examine whether genetic restoration of *mst* expression could rescue the defects. To do so, I combined *UAS-mst* transgene with *mef2>mst RNAi* to express *mst* in the muscle and checked the morphology of the intestine. As a result, the exogenous expression of *mst* in the *mst RNAi* background completely rescued the intestinal defects **(Fig. 88)**.

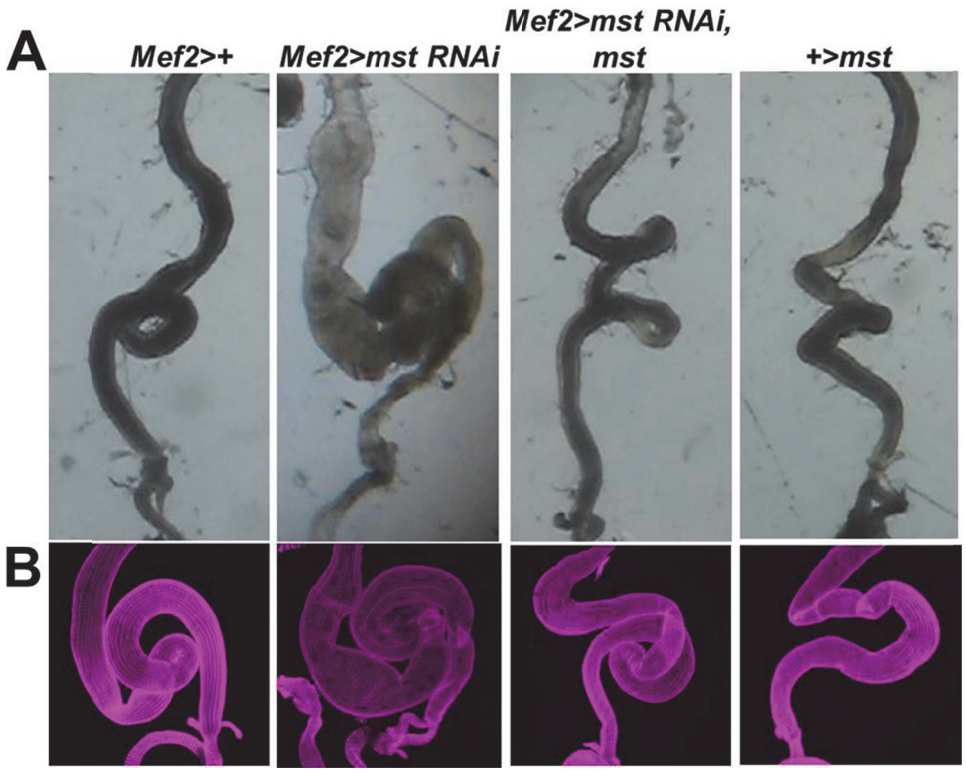

Figure 88. The exogenous expression of *mst* driven by *mef2-GAL4* fully rescue the intestinal defects in *mef2>mst RNAi* flies. (A) Bright field images of the intestine with indicated genotypes. **(B)** Confocal images of the intestine with indicated genotypes stained with Phalloidin-TRITC.

Mst functions in the visceral muscle independently of the TCP-1 tubulin chaperone complex

RNAi knockdown of TCP-1 subunits phenocopies the mst-deficient mitotic phenotype and mst interacts with TCP-1 tubulin chaperone complex to function in the tubulin formation during cell division (Palumbo et al., 2015). To examine whether this is also true for *mst*-mediated defects of the visceral muscle, I RNAi knocked down TCP-1α. Intriguingly, I did not observe any sign of intestinal defects caused by the RNAi knockdown **(Fig. 89)**.

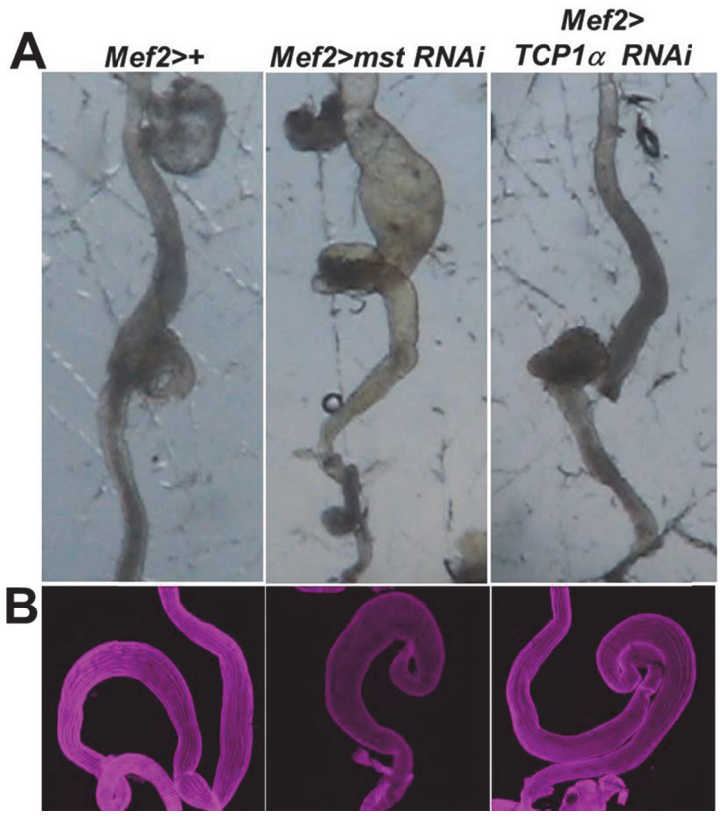

Figure 89. *Mst* function in the visceral muscle independently of TCP-1 tubulin chaperone complex. (A) Bright field images of the intestine with indicated genotypes. **(B)** Confocal images of the intestine with indicated genotypes stained with Phalloidin-TRITC.

Discussion

Discussion

To summarize my Ph.D. study, I have shown here that feeding is influenced by MIP, 48899 and Misato pathways respectively. The initial research plan aimed to identify genes and neurons important for food intake control through signaling satiety. As a result, I discovered MIP and 48899 as the key players in signaling satiety. Unexpectedly, I also found Misato that produced severe defects in food intake when knocked down using RNAi lines. Later it appeared that the RNAi knockdown phenotypes were actually resulted from the role of Misato in the maintenance of visceral muscle rather than its direct role in feeding regulation. Nevertheless, I included the results in the Ph.D. dissertation to broaden the scope of my research. In this study, I attempted to address the most significant questions raised from each project and the results were shown; several open questions and future directions remain. Therefore, I list some of the important points to discuss in this section.

The identity of the neural pathway post-synaptic to MIP neurons

Hinted from the observation that MIP pathway regulates BW independently of SPR, I predicted the presence of the unknown MIP receptor

in BW regulation. To identify such receptor, I screened a list of RNAi lines against GPCRs including orphan receptors to obtain candidates with BW changes, since the most peptides bind to GPCR for activation. Unfortunately, however, I was not able to find considerable candidates from the screen. First of all, it was uncertain where the post-synaptic neurons reside, even though I used different tissue-specific GAL4 drivers such as a whole body, pan-neuronal and fat body-specific GAL4 lines to drive the expression of the RNAi lines. It might be the case that these knockdown experiments were not simply strong enough to elicit the BW phenotype. On the other hand, an early study suggested that MIP is related to galanin, another neuropeptide that regulates feeding in mammals, based on the sequence similarity occurring in the N-termini of the two peptides (Blackburn et al., 1995; Gundlach, 2002). Thus, I raised a possibility that MIP may act through receptors closely related to mammalian galanin receptors. According to phylogenetic analysis, allatostatin A receptors (AstA-R1 and AstA-R2) are the most closely related to galanin receptors. However, MIP could not activate AstA-R1 or AstA-R2 in a biochemical GPCR assay (personal communication). Nevertheless, it remains plausible that the GPCR assay system may not be able to provide a cellular environment which AstA receptors require to mediate MIP actions.

Is MIP pathway the sole mediator for signaling satiety?

Previously, AstA and Lk pathways were shown to be also involved in signaling satiety. For example, allatostatin A neurons suppress starvation-induced increase of food intake and reduce PER responses to sucrose, but have no effect on energy storage levels measured by BW, starvation resistance and total triglyceride levels. Flies with impaired drosokinin signaling usually have bigger meals, but eat less frequently than controls, resulting in no net changes in total food intake and presumably in BW as well. Thus, they are likely dispensable for BW control. In mammals, the anorexigenic POMC system regulates both the food intake and BW. An earlier study indicated the presence of POMC-like system in *Drosophila,* of which activity affects both the feeding activity and BW; blockade of of c673a-GAL4 neural population caused of feeding activity and fat storage (Al-Anzi et al., 2010). Thus, it would be interesting to test whether our MIP system and the c673a-GAL4 pathway interact to regulate BW. Also it is now important to understand how the MIP pathway interacts with other feeding and metabolic regulators to set and maintain the target BW.

The mechanism underlying the MIP pathway-mediated satiety

Studies on other insect models suggest that satiety is induced by mechanosensory signals originating from the foregut and crop, where the extra food is stored. Thus, I examined whether MIP is expressed in peripheral neurons that innervate those intestinal organs by performing anti-MIP immunostaining, but I found no evidence that MIP neurons innervate those organs. Instead, MIP was expressed mostly in the interneurons of the CNS and some enteroendocrine cells that were shown to be dispensable for BW phenotype, raising the possibility that MIP functions centrally. Indeed, MIP was expressed in the brain structures conveying olfactory and gustatory sensory inputs from food and also functionally involved in sensing food odor and taste, suggesting that MIP pathway signals satiety through controlling the peripheral sensitivity to food. Future work should address whether and how central MIP neurons communicate with the peripheral mechanosensory neurons that sense satiety.

The relationship of MIP and 48899 pathways in signaling satiety

Although many aspects of feeding phenotype induced by *48899-GAL4* are similar with those by *MIP-GAL4*, the anatomical locus critical for feeding regulation by them differed. These data suggest the presence of

multiple loci in the brain to regulate satiety. To further uncouple these two pathways in regulation of food intake, I tried to manipulate the activity of 48899 neurons in MIP mutant background and observed that the experiment showed 48899 neuron-mediated feeding phenotypes. This result indicates that MIP and 48899 pathways are parallel at least in this context.

The role of 48899 neurons in feeding choices

Notably, silencing 48899 neurons made flies preferentially consume D-glucose over L-glucose. This indicates the neuron normally inhibits the neural machinery that senses nutritional value of food and promotes food intake. Intriguingly, a subset of the R4 neurons expressing a member of sodium/salute cotransporters was reported to mediate the selection of nutritive sugars including D-glucose over sugars lacking nutritional value such as L-glucose (Park et al., 2016). Since 48899 neurons also harbor a subset of the EB R4 neurons, how these two pathways mediate the opposite feeding behaviors would be an interesting question.

Conclusions

1. A genetic screen identified candidate neurons and genes critical for feeding control using a high-throughput feeding assay

Out of 224 neuron-specific GAL4 driver lines together with 250 RNAi lines, I selected two GAL4 drivers showing overeating phenotypes when silenced and an RNAi line with hypophagic symptom. The chance to get a hit was less than 1%, representing high selectivity of my screen. Nevertheless, there were also some hits that showed feeding defects. However, the feeding phenotypes from these lines were appeared to be by the sickness such as motor deficits by the neuronal manipulation or were through indirect mechanisms including metabolism. To overcome these issues, I sought to select candidates that elicited the opposite phenotypes when silenced and activated. This way guaranteed the specificity of my candidates in feeding regulation. While I was screening with the high-throughput feeding assay, there came out a paper that used similar visual inspection method to reveal a subset of serotonergic neurons eliciting hunger responses in *Drosophila* (Albin et al., 2015). This further confirms that the feeding assay is reliable for other researchers. Compared to other feeding assays, this is more straightforward in that one can see the ingested food in

the stomach directly. This prevents from the possible artifacts from the analyzing processes for feeding amount.

2. MIP pathway maintains a constant BW through signaling satiety

The initial feeding screen identified *MIP-GAL4* as a strong candidate for feeding regulation. Later, I figured that MIP neurons indeed regulate BW through feeding control; silencing MIP neurons increased BW and activation reduced BW associated with the control of fat storage. MIP was discovered to be expressed throughout the CNS and some parts of gastrointestinal tract. Among the neural population, a subset of MIP-expressing neurons in the CNS was found to be responsible for BW regulation. MIP gene expression in MIP neurons was required for BW control independently of SPR, only known receptor for MIP so far. Using two behavioral approaches, I found that MIP pathway induces satiety to control BW. Disruption of MIP pathway in a fly increased olfactory and gustatory sensitivity to food quality as if the fly had been starved. Conversely, activation of MIP neurons in a fly decreased the peripheral sensitivity even though the fly had been starved. Based on these results, I propose a model in which MIP neurons induce satiety through MIP peptide independently of SPR and subsequently food intake and BW are decreased upon the induction of satiety **(Fig. 90)**.

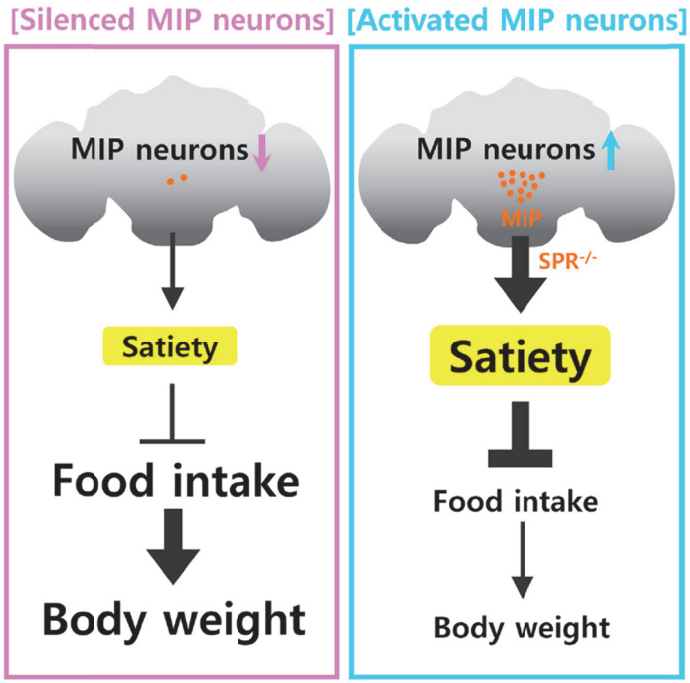

Figure 90. The proposed model for *Drosophila* BW control via MIP pathway inducing satiety (Adopted from Min et al., *Current Biology*, 2016). MIP neurons induce satiety. In a condition where MIP neurons are silenced satiety cannot be properly evoked and thus food intake continues. Therefore, BW increases. By contrast, when MIP neurons are activated, MIP neurons strongly induce satiety through MIP signaling independently of SPR. Thus food intake and BW become reduced.

3. A subset of the EB neurons labeled by 48899-GAL4 suppresses food intake.

The flies with silenced 48899 neurons exhibited a series of hunger responses including increased food intake, quicker feeding initiation and enhanced olfactory responses to food. By contrast, activation of 48899 neurons decreased food intake. *48899-GAL4* was expressed in the brain with characteristic pattern involving the PI and EB structures. The PI cells were DH44 positive neurons that were dispensable for 48899-mediated feeding phenotype. The EB neurons were labeled by *Cha-GAL80* that rescued the overeating phenotype by *48899>TNT* indicating that the EB neurons are important. Interestingly, RNAi knockdown of serotonin receptor 1A (5-HT1A) among the other receptors in 48899 neurons specifically reduced food intake. Considering the inhibitory effect on food intake by 48899 neurons, I speculated that 5-HT1A plays an inhibitory role in 48899 neurons to regulate food intake **(Fig. 91)**.

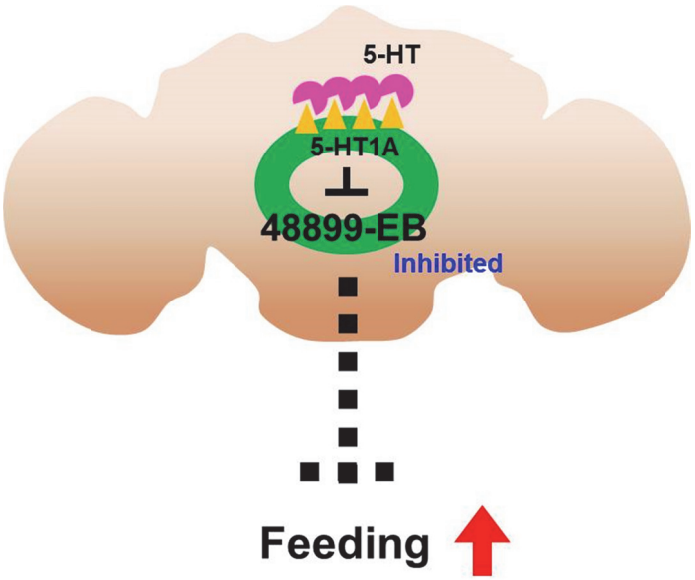

Figure 91. The proposed model for 48899 neurons in mediating food intake. The EB subset of 48899 neurons involving the inhibitory serotonin receptor 1A normally suppresses feeding. Therefore, feeding is upregulated upon the serotonin signaling inhibiting the 48899-EB neurons.

4. Misato is required for the visceral muscle maintenance for intestinal homeostasis in *Drosophila*

RNAi knockdown of *mst* in visceral muscle elicited muscle loss and morphological changes, mainly the enlargement of intestine. However, this effect was appeared only after some aging periods, indicating an aging-related prerequisite for inducing phenotype - possibly degeneration of the muscles via the yet-to-be known mechanism. Another most striking phenotype from *mst* knockdown in the visceral muscle is the dramatic over-populating ISCs in the intestine. To proliferate, ISCs receive inputs from a variety of signaling system including Wingless, EGFR, Notch, Hippo and UPD/JAK/STAT pathways. However, the question is how Mst in the visceral muscle interact with the signaling pathways to regulate ISCs in the remote tissue. Intriguingly, it has been shown that *wingless* is expressed in the muscle to regulate the ISC population by providing the niche to the cells. Likewise, Mst might regulate ISCs through the similar mechanism or simply Mst is required for the muscle maintenance and thus other critical signaling factors for ISCs become eliminated ultimately inducing ISC proliferation.

References

Al-Anzi, B., Armand, E., Nagamei, P., Olszewski, M., Sapin, V., Waters, C., Zinn, K., Wyman, R.J., and Benzer, S. (2010). The leucokinin pathway and its neurons regulate meal size in Drosophila. Curr Biol *20*, 969-978.

Albin, S.D., Kaun, K.R., Knapp, J.M., Chung, P., Heberlein, U., and Simpson, J.H. (2015). A Subset of Serotonergic Neurons Evokes Hunger in Adult Drosophila. Curr Biol *25*, 2435-2440.

Anand, B.K., and Pillai, R.V. (1967). Activity of single neurones in the hypothalamic feeding centres: effect of gastric distension. J Physiol *192*, 63-77.

Baver, S.B., Hope, K., Guyot, S., Bjorbaek, C., Kaczorowski, C., and O'Connell, K.M. (2014). Leptin modulates the intrinsic excitability of AgRP/NPY neurons in the arcuate nucleus of the hypothalamus. J Neurosci *34*, 5486-5496.

Becnel, J., Johnson, O., Luo, J., Nassel, D.R., and Nichols, C.D. (2011). The serotonin 5-HT7Dro receptor is expressed in the brain of Drosophila, and is essential for normal courtship and mating. PLoS One *6*, e20800.

Blackburn, M.B., Wagner, R.M., Kochansky, J.P., Harrison, D.J., Thomas-Laemont, P., and Raina, A.K. (1995). The identification of two myoinhibitory peptides, with sequence similarities to the galanins, isolated from the ventral nerve cord of Manduca sexta. Regul Pept *57*, 213-219.

Bour, B.A., Obrien, M.A., Lockwood, W.L., Goldstein, E.S., Bodmer, R., Taghert, P.H., Abmayr, S.M., and Nguyen, H.T. (1995). Drosophila Mef2, a Transcription Factor That Is Essential for Myogenesis. Gene Dev *9*, 730-741.

Chen, J., Choi, M.S., Mizoguchi, A., Veenstra, J.A., Kang, K., Kim, Y.J., and Kwon, J.Y. (2015). Isoform-specific expression of the neuropeptide orcokinin in Drosophila melanogaster. Peptides *68*, 50-57.

Chin, A.C., Burgess, R.W., Wong, B.R., Schwarz, T.L., and Scheller, R.H. (1993). Differential expression of transcripts from syb, a Drosophila melanogaster gene encoding VAMP (synaptobrevin) that is abundant in non-neuronal cells. Gene *131*, 175-181.

Choi, Y.J., Lee, G., and Park, J.H. (2006). Programmed cell death mechanisms of identifiable peptidergic neurons in Drosophila melanogaster. Development *133*, 2223-2232.

Cowley, M.A., Smart, J.L., Rubinstein, M., Cerdan, M.G., Diano, S., Horvath, T.L., Cone, R.D., and Low, M.J. (2001). Leptin activates anorexigenic POMC neurons through a neural network in the arcuate nucleus. Nature *411*, 480-484.

Davis, N.T., Blackburn, M.B., Golubeva, E.G., and Hildebrand, J.G. (2003). Localization of myoinhibitory peptide immunoreactivity in Manduca sexta and Bombyx mori, with indications that the peptide has a role in molting and ecdysis. J Exp Biol *206*, 1449-1460.

Dethier, V. (1967). Hungry Fly. Psychol Today *1*, 64-72.

Dietrich, M.O., Liu, Z.W., and Horvath, T.L. (2013). Mitochondrial dynamics controlled by mitofusins regulate Agrp neuronal activity and diet-induced obesity. Cell *155*, 188-199.

Dus, M., Ai, M., and Suh, G.S. (2013). Taste-independent nutrient selection is mediated by a brain-specific Na+ /solute co-transporter in Drosophila. Nat Neurosci *16*, 526-528.

Dus, M., Lai, J.S., Gunapala, K.M., Min, S., Tayler, T.D., Hergarden, A.C., Geraud, E., Joseph, C.M., and Suh, G.S. (2015). Nutrient Sensor in the Brain Directs the Action of the Brain-Gut Axis in Drosophila. Neuron *87*, 139-151.

Dus, M., Min, S., Keene, A.C., Lee, G.Y., and Suh, G.S. (2011). Taste-independent detection of the caloric content of sugar in Drosophila. Proc Natl Acad Sci U S A *108*, 11644-11649.

Edgecomb, R.S., Harth, C.E., and Schneiderman, A.M. (1994). Regulation of feeding behavior in adult Drosophila melanogaster varies with feeding regime and nutritional state. J Exp Biol *197*, 215-235.

Friedman, J. (2014). 20 years of leptin: leptin at 20: an overview. J Endocrinol *223*, T1-8.

Friedman, J. (2015). Leptin and the Regulation of Food Intake and Body Weight. J Nutr Sci Vitaminol (Tokyo) *61 Suppl*, S202.

Friedman, J.M., and Halaas, J.L. (1998). Leptin and the regulation of body weight in mammals. Nature *395*, 763-770.

Geffeney, S.L., and Goodman, M.B. (2012). How We Feel: Ion Channel Partnerships that Detect Mechanical Inputs and Give Rise to Touch and Pain Perception. Neuron *74*, 609-619.

Gillard, L., Billiauws, L., Stan-Iuga, B., Ribeiro-Parenti, L., Jarry, A.C., Cavin, J.B., Cluzeaud, F., Mayeur, C., Thomas, M., Freund, J.N.*, et al.* (2016). Enhanced Ghrelin Levels and Hypothalamic Orexigenic AgRP and NPY Neuropeptide Expression in Models of Jejuno-Colonic Short Bowel Syndrome. Sci Rep *6*, 28345.

Gong, W.J., and Golic, K.G. (2003). Ends-out, or replacement, gene targeting in Drosophila. Proceedings of the National Academy of Sciences of the United States of America *100*, 2556-2561.

Gundlach, A.L. (2002). Galanin/GALP and galanin receptors: role in central control of feeding, body weight/obesity and reproduction? Eur J Pharmacol *440*, 255-268.

Guo, Z., Lucchetta, E., Rafel, N., and Ohlstein, B. (2016). Maintenance of the adult Drosophila intestine: all roads lead to homeostasis. Curr Opin Genet Dev *40*, 81-86.

Gurvitz, A., Hartig, A., Ruis, H., Hamilton, B., and de Couet, H.G. (2002). Preliminary characterisation of DML1, an essential Saccharomyces cerevisiae gene related to misato of Drosophila melanogaster. FEMS Yeast Res *2*, 123-135.

Hergarden, A.C., Tayler, T.D., and Anderson, D.J. (2012). Allatostatin-A neurons inhibit feeding behavior in adult Drosophila. Proc Natl Acad Sci U S A *109*, 3967-3972.

Hong, S.H., Lee, K.S., Kwak, S.J., Kim, A.K., Bai, H., Jung, M.S., Kwon, O.Y., Song, W.J., Tatar, M., and Yu, K. (2012). Minibrain/Dyrk1a regulates food intake through the Sir2-FOXO-sNPF/NPY pathway in Drosophila and mammals. PLoS Genet *8*, e1002857.

Hu, J., Zhong, C., Ding, C., Chi, Q., Walz, A., Mombaerts, P., Matsunami, H., and Luo, M. (2007). Detection of near-atmospheric concentrations of CO2

by an olfactory subsystem in the mouse. Science *317*, 953-957.

Huang, H., Li, J., Hu, L., Ge, L., Ji, H., Zhao, Y., and Zhang, L. (2014). Bantam is essential for Drosophila intestinal stem cell proliferation in response to Hippo signaling. Dev Biol *385*, 211-219.

Hunt, L.C., and Demontis, F. (2013). Whole-mount immunostaining of Drosophila skeletal muscle. Nat Protoc *8*, 2496-2501.

Ilius, M., Wolf, R., and Heisenberg, M. (1994). The central complex of Drosophila melanogaster is involved in flight control: studies on mutants and mosaics of the gene ellipsoid body open. J Neurogenet *9*, 189-206.

Ja, W.W., Carvalho, G.B., Mak, E.M., de la Rosa, N.N., Fang, A.Y., Liong, J.C., Brummel, T., and Benzer, S. (2007). Prandiology of Drosophila and the CAFE assay. Proc Natl Acad Sci U S A *104*, 8253-8256.

Jiang, H., Patel, P.H., Kohlmaier, A., Grenley, M.O., McEwen, D.G., and Edgar, B.A. (2009). Cytokine/Jak/Stat signaling mediates regeneration and homeostasis in the Drosophila midgut. Cell *137*, 1343-1355.

Jostins, L., Ripke, S., Weersma, R.K., Duerr, R.H., McGovern, D.P., Hui, K.Y., Lee, J.C., Schumm, L.P., Sharma, Y., Anderson, C.A.*, et al.* (2012). Host-microbe interactions have shaped the genetic architecture of inflammatory bowel disease. Nature *491*, 119-124.

Kaushik, S., Rodriguez-Navarro, J.A., Arias, E., Kiffin, R., Sahu, S., Schwartz, G.J., Cuervo, A.M., and Singh, R. (2011). Autophagy in hypothalamic AgRP neurons regulates food intake and energy balance. Cell Metab *14*, 173-183.

Kawai, K., Sugimoto, K., Nakashima, K., Miura, H., and Ninomiya, Y. (2000). Leptin as a modulator of sweet taste sensitivities in mice. P Natl Acad Sci USA *97*, 11044-11049.

Kim, Y.J., Bartalska, K., Audsley, N., Yamanaka, N., Yapici, N., Lee, J.Y., Kim, Y.C., Markovic, M., Isaac, E., Tanaka, Y.*, et al.* (2010). MIPs are ancestral ligands for the sex peptide receptor. Proc Natl Acad Sci U S A *107*, 6520-6525.

Kimura, M., and Okano, Y. (2007). Human Misato regulates mitochondrial

distribution and morphology. Exp Cell Res *313*, 1393-1404.

Klueg, K.M., Alvarado, D., Muskavitch, M.A., and Duffy, J.B. (2002). Creation of a GAL4/UAS-coupled inducible gene expression system for use in Drosophila cultured cell lines. Genesis *34*, 119-122.

Lee, G., and Park, J.H. (2004). Hemolymph sugar homeostasis and starvation-induced hyperactivity affected by genetic manipulations of the adipokinetic hormone-encoding gene in Drosophila melanogaster. Genetics *167*, 311-323.

Lee, K.M., Daubnerova, I., Isaac, R.E., Zhang, C., Choi, S., Chung, J., and Kim, Y.J. (2015). A Neuronal Pathway that Controls Sperm Ejection and Storage in Female Drosophila. Current Biology *25*, 790-797.

Lee, K.S., You, K.H., Choo, J.K., Han, Y.M., and Yu, K. (2004). Drosophila short neuropeptide F regulates food intake and body size. J Biol Chem *279*, 50781-50789.

Lin, G., Xu, N., and Xi, R. (2008). Paracrine Wingless signalling controls self-renewal of Drosophila intestinal stem cells. Nature *455*, 1119-1123.

Liu, Y., Luo, J., Carlsson, M.A., and Nassel, D.R. (2015). Serotonin and insulin-like peptides modulate leucokinin-producing neurons that affect feeding and water homeostasis in Drosophila. J Comp Neurol *523*, 1840-1863.

Lorenz, M.W., Kellner, R., Hoffmann, K.H., and Gade, G. (2000). Identification of multiple peptides homologous to cockroach and cricket allatostatins in the stick insect Carausius morosus. Insect Biochem Mol Biol *30*, 711-718.

Mabuchi, Y., and Tanaka, N. (2016). Serotonin 5-HT2A receptor expressed in the insulin pathway regulating the feeding behavior in Drosophila. Chem Senses *41*, E222-E222.

McNabb, S.L., and Truman, J.W. (2008). Light and peptidergic eclosion hormone neurons stimulate a rapid eclosion response that masks circadian emergence in Drosophila. J Exp Biol *211*, 2263-2274.

Melcher, C., and Pankratz, M.J. (2005). Candidate gustatory interneurons

modulating feeding behavior in the Drosophila brain. PLoS Biol *3*, e305.

Mineur, Y.S., Abizaid, A., Rao, Y., Salas, R., DiLeone, R.J., Gundisch, D., Diano, S., De Biasi, M., Horvath, T.L., Gao, X.B.*, et al.* (2011). Nicotine decreases food intake through activation of POMC neurons. Science *332*, 1330-1332.

Miyamoto, T., Slone, J., Song, X., and Amrein, H. (2012). A fructose receptor functions as a nutrient sensor in the Drosophila brain. Cell *151*, 1113-1125.

Morrison, C.D., Morton, G.J., Niswender, K.D., Gelling, R.W., and Schwartz, M.W. (2005). Leptin inhibits hypothalamic Npy and Agrp gene expression via a mechanism that requires phosphatidylinositol 3-OH-kinase signaling. Am J Physiol Endocrinol Metab *289*, E1051-1057.

Mottier-Pavie, V., Cenci, G., Verni, F., Gatti, M., and Bonaccorsi, S. (2011). Phenotypic analysis of misato function reveals roles of noncentrosomal microtubules in Drosophila spindle formation. J Cell Sci *124*, 706-717.

Neuser, K., Triphan, T., Mronz, M., Poeck, B., and Strauss, R. (2008). Analysis of a spatial orientation memory in Drosophila. Nature *453*, 1244-1247.

Ofstad, T.A., Zuker, C.S., and Reiser, M.B. (2011). Visual place learning in Drosophila melanogaster. Nature *474*, 204-207.

Oh, Y., Yoon, S.E., Zhang, Q., Chae, H.S., Daubnerova, I., Shafer, O.T., Choe, J., and Kim, Y.J. (2014). A homeostatic sleep-stabilizing pathway in Drosophila composed of the sex peptide receptor and its ligand, the myoinhibitory peptide. PLoS Biol *12*, e1001974.

Olds, W.H., and Xu, T. (2014). Regulation of food intake by mechanosensory ion channels in enteric neurons. Elife *3*.

Paintal, A.S. (1954). A Study of Gastric Stretch Receptors - Their Role in the Peripheral Mechanism of Satiation of Hunger and Thirst. J Physiol-London *126*, 255-270.

Palumbo, V., Pellacani, C., Heesom, K.J., Rogala, K.B., Deane, C.M., Mottier-Pavie, V., Gatti, M., Bonaccorsi, S., and Wakefield, J.G. (2015).

Misato Controls Mitotic Microtubule Generation by Stabilizing the TCP-1 Tubulin Chaperone Complex [corrected]. Curr Biol *25*, 1777-1783.

Park, J.Y., Dus, M., Kim, S., Abu, F., Kanai, M.I., Rudy, B., and Suh, G.S. (2016). Drosophila SLC5A11 Mediates Hunger by Regulating K(+) Channel Activity. Curr Biol *26*, 1965-1974.

Pfeiffer, B.D., Jenett, A., Hammonds, A.S., Ngo, T.T., Misra, S., Murphy, C., Scully, A., Carlson, J.W., Wan, K.H., Laverty, T.R.*, et al.* (2008). Tools for neuroanatomy and neurogenetics in Drosophila. Proc Natl Acad Sci U S A *105*, 9715-9720.

Poels, J., Van Loy, T., Vandersmissen, H.P., Van Hiel, B., Van Soest, S., Nachman, R.J., and Vanden Broeck, J. (2010). Myoinhibiting peptides are the ancestral ligands of the promiscuous Drosophila sex peptide receptor. Cell Mol Life Sci *67*, 3511-3522.

Ren, F., Wang, B., Yue, T., Yun, E.Y., Ip, Y.T., and Jiang, J. (2010). Hippo signaling regulates Drosophila intestine stem cell proliferation through multiple pathways. Proc Natl Acad Sci U S A *107*, 21064-21069.

Ren, H., Cook, J.R., Kon, N., and Accili, D. (2015). Gpr17 in AgRP Neurons Regulates Feeding and Sensitivity to Insulin and Leptin. Diabetes *64*, 3670-3679.

Ren, H., Orozco, I.J., Su, Y., Suyama, S., Gutierrez-Juarez, R., Horvath, T.L., Wardlaw, S.L., Plum, L., Arancio, O., and Accili, D. (2012). FoxO1 target Gpr17 activates AgRP neurons to regulate food intake. Cell *149*, 1314-1326.

Renn, S.C., Armstrong, J.D., Yang, M., Wang, Z., An, X., Kaiser, K., and Taghert, P.H. (1999a). Genetic analysis of the Drosophila ellipsoid body neuropil: organization and development of the central complex. J Neurobiol *41*, 189-207.

Renn, S.C.P., Park, J.H., Rosbash, M., Hall, J.C., and Taghert, P.H. (1999b). A pdf neuropeptide gene mutation and ablation of PDF neurons each cause severe abnormalities of behavioral circadian rhythms in Drosophila. Cell *99*, 791-802.

Rezaie, P., Mazidi, M., and Nematy, M. (2015). Ghrelin, food intake, and botanical extracts: A Review. Avicenna J Phytomed *5*, 271-281.

Rosenzweig, M., Brennan, K.M., Tayler, T.D., Phelps, P.O., Patapoutian, A., and Garrity, P.A. (2005). The Drosophila ortholog of vertebrate TRPA1 regulates thermotaxis. Genes Dev *19*, 419-424.

Rulifson, E.J., Kim, S.K., and Nusse, R. (2002). Ablation of insulin-producing neurons in flies: growth and diabetic phenotypes. Science *296*, 1118-1120.

Ryuda, M., Tsuzuki, S., Matsumoto, H., Oda, Y., Tanimura, T., and Hayakawa, Y. (2011). Identification of a novel gene, anorexia, regulating feeding activity via insulin signaling in Drosophila melanogaster. J Biol Chem *286*, 38417-38426.

Shiraiwa, T., and Carlson, J.R. (2007). Proboscis extension response (PER) assay in Drosophila. J Vis Exp, 193.

Shrestha, Y.B., Wickwire, K., and Giraudo, S.Q. (2006). Role of AgRP on Ghrelin-induced feeding in the hypothalamic paraventricular nucleus. Regul Pept *133*, 68-73.

Simo, L., Koci, J., and Park, Y. (2013). Receptors for the neuropeptides, myoinhibitory peptide and SIFamide, in control of the salivary glands of the blacklegged tick Ixodes scapularis. Insect Biochem Mol Biol *43*, 376-387.

Soares-Cunha, C., Coimbra, B., David-Pereira, A., Borges, S., Pinto, L., Costa, P., Sousa, N., and Rodrigues, A.J. (2016). Activation of D2 dopamine receptor-expressing neurons in the nucleus accumbens increases motivation. Nat Commun *7*, 11829.

Soderberg, J.A., Carlsson, M.A., and Nassel, D.R. (2012). Insulin-Producing Cells in the Drosophila Brain also Express Satiety-Inducing Cholecystokinin-Like Peptide, Drosulfakinin. Front Endocrinol (Lausanne) *3*, 109.

Suh, G.S., Ben-Tabou de Leon, S., Tanimoto, H., Fiala, A., Benzer, S., and Anderson, D.J. (2007). Light activation of an innate olfactory avoidance response in Drosophila. Curr Biol *17*, 905-908.

Suh, G.S., Wong, A.M., Hergarden, A.C., Wang, J.W., Simon, A.F., Benzer, S., Axel, R., and Anderson, D.J. (2004). A single population of olfactory sensory neurons mediates an innate avoidance behaviour in Drosophila.

Nature *431*, 854-859.

Suster, M.L., Martin, J.R., Sung, C., and Robinow, S. (2003). Targeted expression of tetanus toxin reveals sets of neurons involved in larval locomotion in Drosophila. J Neurobiol *55*, 233-246.

Swart, I., Jahng, J.W., Overton, J.M., and Houpt, T.A. (2002). Hypothalamic NPY, AGRP, and POMC mRNA responses to leptin and refeeding in mice. Am J Physiol Regul Integr Comp Physiol *283*, R1020-1026.

Sweeney, S.T., Broadie, K., Keane, J., Niemann, H., and O'Kane, C.J. (1995). Targeted expression of tetanus toxin light chain in Drosophila specifically eliminates synaptic transmission and causes behavioral defects. Neuron *14*, 341-351.

Takashima, S., Mkrtchyan, M., Younossi-Hartenstein, A., Merriam, J.R., and Hartenstein, V. (2008). The behaviour of Drosophila adult hindgut stem cells is controlled by Wnt and Hh signalling. Nature *454*, 651-655.

Terhzaz, S., Rosay, P., Goodwin, S.F., and Veenstra, J.A. (2007). The neuropeptide SIFamide modulates sexual behavior in Drosophila. Biochem Biophys Res Commun *352*, 305-310.

Towbin, E.J. (1949). Gastric Distention as a Factor in the Satiation of Thirst in Esophagostomized Dogs. American Journal of Physiology *159*, 533-541.

Williams, E.A., Conzelmann, M., and Jekely, G. (2015). Myoinhibitory peptide regulates feeding in the marine annelid Platynereis. Front Zool *12*, 1.

Williamson, M., Lenz, C., Winther, A.M., Nassel, D.R., and Grimmelikhuijzen, C.J. (2001). Molecular cloning, genomic organization, and expression of a B-type (cricket-type) allatostatin preprohormone from Drosophila melanogaster. Biochem Biophys Res Commun *281*, 544-550.

Wood, J.D. (2004). The first nobel prize for integrated systems physiology: Ivan Petrovich Pavlov, 1904. Physiology (Bethesda) *19*, 326-330.

Wu, C.L., Xia, S., Fu, T.F., Wang, H., Chen, Y.H., Leong, D., Chiang, A.S., and Tully, T. (2007). Specific requirement of NMDA receptors for long-term memory consolidation in Drosophila ellipsoid body. Nat Neurosci *10*, 1578-1586.

Wu, Q., Wen, T., Lee, G., Park, J.H., Cai, H.N., and Shen, P. (2003). Developmental control of foraging and social behavior by the Drosophila neuropeptide Y-like system. Neuron *39*, 147-161.

Yamanaka, N., Hua, Y.J., Roller, L., Spalovska-Valachova, I., Mizoguchi, A., Kataoka, H., and Tanaka, Y. (2010). Bombyx prothoracicostatic peptides activate the sex peptide receptor to regulate ecdysteroid biosynthesis. Proc Natl Acad Sci U S A *107*, 2060-2065.

Yasothornsrikul, S., Davis, W.J., Cramer, G., Kimbrell, D.A., and Dearolf, C.R. (1997). viking: identification and characterization of a second type IV collagen in Drosophila. Gene *198*, 17-25.

Yaswen, L., Diehl, N., Brennan, M.B., and Hochgeschwender, U. (1999). Obesity in the mouse model of pro-opiomelanocortin deficiency responds to peripheral melanocortin. Nat Med *5*, 1066-1070.

Zhan, C., Zhou, J., Feng, Q., Zhang, J.E., Lin, S., Bao, J., Wu, P., and Luo, M. (2013). Acute and long-term suppression of feeding behavior by POMC neurons in the brainstem and hypothalamus, respectively. J Neurosci *33*, 3624-3632.

Zhang, Y., Proenca, R., Maffei, M., Barone, M., Leopold, L., and Friedman, J.M. (1994). Positional cloning of the mouse obese gene and its human homologue. Nature *372*, 425-432.

Zhang, Z., Li, X., Guo, J., Li, Y., and Guo, A. (2013). Two clusters of GABAergic ellipsoid body neurons modulate olfactory labile memory in Drosophila. J Neurosci *33*, 5175-5181.

Zhao, X.L., and Campos, A.R. (2012). Insulin signalling in mushroom body neurons regulates feeding behaviour in Drosophila larvae. J Exp Biol *215*, 2696-2702.

Abstract in Korean/국문초록

초파리 먹이행동에 중추적 역할을 하는 신경 네트워크와 유전자에 대한 연구

비록 먹이행동이 다양한 내•외재적 자극에 영향을 받는다 할지라도 배고픔과 배부름이라는 두 가지의 선천적으로 내장된 생리적 상태에 의해 주요하게 조절된다. 이 두 생리상태를 조절한 분자신경적 메커니즘에 대한 우리의 현재 이해도를 넓히고자, 저자는 간단한 대량적 먹이행동 측정법을 이용하여 초파리 먹이행동에 중요한 새로운 유전자와 신경을 발굴하기 위해 유전학적 스크린을 수행하였다. 총 224개의 신경특이적 GAL4 라인과 250개의 RNAi라인들을 분석하여, 저자는 두 종류의 식욕억제성 신경그룹과 먹이행동에 영향을 주는 하나의 유전자를 발굴하였다. MIP신경과 MIP유전자의 억제는 현저한 몸무게 증가를 유발하였으며, 이는 제한적 먹이공급에 의해 정상화될 수 있었는데, 이 결과는 MIP신경에 의한 먹이섭취량과 몸무게 조절이 밀접한 관련이 있음을 보여준다. 반대로 MIP신경을 활성화하면 먹이섭취량과 몸무게가 급격히 감소하였으나, 그러한 MIP신경 활성화를 멈추자마자 먹이섭취량과 몸무게가 정상으로 회복되었다.

이러한 결과는 MIP신경이 먹이섭취량과 몸무게 조절에 있어 스위치와 같은 역할을 하고 있음을 드러낸다. 두 가지의 행동실험을 이용하여 MIP신경 억제와 활성화에 따른 배부름 정도 변화를 측정한 결과, 저자는 MIP신경이 결국 배부름을 유발하여 먹이섭취량과 몸무게를 조절함을 알게 되었다. 한편 48899-GAL4에 의해 레이블되는 식욕억제성 신경의 활성이 감소되면 일련의 배고픔 반응이 유발되는데, 이는 평소에 48899 신경이 배부름을 유발하고 있음을 보여준다. 이와 일치하게도 48899신경의 활성화는 먹이섭취량을 감소시켰다. 48899-GAL4에 의해 레이블되는 신경구조 중, EB 신경이 48899에 의해 조절되는 먹이행동이 중요함을 알게 되었다. 초파리에 존재하는 다섯 종류의 세로토닌 수용체를 검정한 결과, 5-HT1A가 먹이섭취량 조절에 있어 48899신경의 억제성 인자로 작용함을 알 수 있게 되었다. 마지막으로 *misato(mst)* knockdown이 급격한 hypophagia를 보였는데. 특히 장근육 손상으로 인한 장의 부품 현상을 관찰할 수 있었다. 하지만 이러한 표현형들은 외래 *mst*를 발현시켜 주었을 때, 완벽히 정상화되는 것으로 보아 장근육과 먹이섭취량의 밀접한 관련이 있음을 보여준다. 종합해볼 때,

이러한 결과들은 먹이행동이 다양한 분자신경적 접근방법에 의해 타게팅될 수 있고, 특히 배부름 과정을 통한 먹이행동 조절에 대한 이해에 새로운 영감을 제시해준다.

주요어: 먹이행동, 배부름/식욕억제성의, MIP, 몸무게, the EB, 세로토닌 수용체, Misato, 내장 근육

학번: 2012-30083